IMAGE: A MAP OF THE STARS OF THE ORION CONSTELLATION

JournalPreview

London Journal of Research in Science: Natural & Formal

Volume 25 | Issue 5 | Compilation 1.0

Great Britain Journals Press

WWW.JOURNALSPRESS.COM

Journal Content
In this Issue

Great Britain Journals Press

M.E.M.S. for Extracting usable Electrical Power from Quantum Vacuum Energy While Remaining Compliant with Emmy Noether's Theorem

Dr. Sangouard Patrick

ABSTRACT

This theoretical work aims to explore the possibility of extracting in electrical form and in accordance with EMMY NOETHER's theorem, part of quantum vacuum energy. Cyclic deformations of an elastic piezoelectric bridge, embedded at both ends, are generated by the Casimir force (F_{CA}) between two near electrodes. This deformation of the piezoelectric bridge induces an automatic electrical charge which can in turn induce a possible Coulomb repulsive force (F_{CO}). This force F_{CO} is automatically triggered by the closing of a switch n°1 on a third electrode. The resultant force applied on the elastic piezoelectric bridge, F_{CO} - F_{CA}, straightens the bridge, imparting kinetic energy. This kinetic energy plus the deformation energy memorized in the elastic bridge is dissipated by the Casimir force F_{CA}. The force F_{CO} cancels out when a switch n°2 in series connects this third electrode to the ground shortly after closing the switch n°1. We return to the initial situation with just the Casimir force applied on the bridge. Thus, the system constantly exploits the energy of the quantum vacuum vibrates, creating peaks of usable electrical power with each vibration. This electrical could be of some microwatts per vibration depending on the chosen amplification F_{CO}/F_{CA}.

Keywords: casimir, coulomb, vacuum quantum, energy extraction, piezoelectric, mems, quantum vacuum, fluctuations, noether's theorem, energy harvesting, nano mechanics, resonant vibrations.

Classification: LCC Code: QC173.98

Language: English

Great Britain Journals Press

LJP Copyright ID: 925651
Print ISSN: 2631-8490
Online ISSN: 2631-8504

London Journal of Research in Science: Natural & Formal

Volume 25 | Issue 5 | Compilation 1.0

M.E.M.S. for Extracting usable Electrical Power from Quantum Vacuum Energy While Remaining Compliant with Emmy Noether's Theorem

Dr. Sangouard Patrick

ABSTRACT

This theoretical work aims to explore the possibility of extracting in electrical form and in accordance with EMMY NOETHER's theorem, part of quantum vacuum energy. Cyclic deformations of an elastic piezoelectric bridge, embedded at both ends, are generated by the Casimir force (F_{CA}) between two near electrodes. This deformation of the piezoelectric bridge induces an automatic electrical charge which can in turn induce a possible Coulomb repulsive force (F_{CO}). This force F_{CO} is automatically triggered by the closing of a switch n°1 on a third electrode. The resultant force applied on the elastic piezoelectric bridge, F_{CO} - F_{CA}, straightens the bridge, imparting kinetic energy. This kinetic energy plus the deformation energy memorized in the elastic bridge is dissipated by the Casimir force F_{CA}. The force F_{CO} cancels out when a switch n°2 in series connects this third electrode to the ground shortly after closing the switch n°1. We return to the initial situation with just the Casimir force applied on the bridge. Thus, the system constantly exploits the energy of the quantum vacuum vibrates, creating peaks of usable electrical power with each vibration. This *electrical could be of some microwatts per vibration depending on the chosen amplification F_{CO}/F_{CA}.*

Keywords: casimir, coulomb, vacuum quantum, energy extraction, piezoelectric, mems, quantum vacuum, fluctuations, noether's theorem, energy harvesting, nano mechanics, resonant vibrations.

Author: Retired from Ecole Supérieure Ingénieurs Electronique Electrotechnique Paris France.

I. DESCRIPTION OF THE SYSTEM

1.1: Introduction

We know that the quantum vacuum, the energy vacuum, the absolutely nothing, does not exist.
This statement has been proven multiple times and noted by:

- Lamb's shift (1947) of atomic emission frequencies: https://quantummechanics.ucsd.edu/ph130a/130_notes/node476.html)
- By the force of Van der Waals which plays a very important physicochemical role and had an interpretation quantum 1930 [London] when two atoms are coupled to the same fluctuations in vacuum:https://culturesciences.chimie.ens.fr/thematiques/chimie-du-vivant/les-forces-de-van-der-waals-et-le-gecko
- By Hawking's radiation theory, predicted in 1974 and observed on September 7, 2016. Article Observation of quantum Hawking radiation and its entanglement in an analogue black hole: https://www.nature.com/articles/nphys3863
- By the experimental verification (1958) of the existence of a force equated by Casimir in 1948. This so-called Casimir force was measured for the first time in 1997: https://arxiv.org/abs/quant- ph/9907076 https://en.wikipedia.org/wiki/Casimir_effect

The undisputed interpretation of the above effects involves an energy source coming from some kind of "nothing" or more precisely from the quantum vacuum. So, it is certain that this source of energy causing unmistakable physical manifestations exists. We will therefore choose, for the remainder of this article, a reference frame consisting of the 4-dimensional "Space-time" continuum augmented by those, still unknown, in the "quantum vacuum". In this reference frame we will try to show that the mathematical theorem of the mathematician Emmy Noether is not transgressed. This important mathematical theorem involves in other things the conservation of energy: https://fr.wikiversity.org/wiki/Outils_math%C3%A9matiques_pour_la_physique_(PCSI)/Th%C3%A9or%C3%A8me_d%27Emmy_N%C5%93ther#

In this paper we will focus essentially on presenting the detailed energy balance of a MEMS apparently capable of permanently extracting a small amount of energy from the quantum vacuum that can be used in our world. We will try to show that using a piezoelectric bridge deformed by a isotropic, atemporal , attractive, force of Casimir F_{CA} , and straightened by a very ephemeral, repulsive, but more intense force of Coulomb F_{CO} induced by this deformation , an apparent "perpetual movement" of the MEMS device is possible. The schematic of this M.E.M.S. is in figure 4 and 5

In fact, the problem is less to extract energy from the vacuum than to extract it without spending more energy that we cannot hope to recover. The attractive Casimir force is

$$F_{CA} = S_S \frac{\pi^2 c\, h}{240\, z_s^4} \qquad \text{(Eq.1)},$$

ref [1],[2],[3]. With S_S the surface of Casimir's electrodes, ~~h~~ = h/2π the reduced Planck constant, and c the speed of light, z_s the interface of Casimir's electrodes. This variation in $1/z_s^4$ of F_{CA} , would imply that a larger opposing force is provided to return to the initial position when the interface z_s is smaller.

Coulomb's force can play this role with an energy balance satisfying Emmy Noether's theorem, because -as we shall see- this force will be in $1/z_s^{10}$: In fact, we know that the fixed charges Q_F induced by a Casimir force F_{CA} - in the case of a deformation *perpendicular* to the polarization of a piezoelectric film- are proportional to the Casimir force F_{CA} and are therefore in $1/z_s^4$. We have, with z_o the initial position without any deformation of the piezoelectric film:

$$Q_F = \frac{d_{31}\, l_p}{a_p} F_{CA} \Rightarrow Q_F = \frac{d_{31}\, l_p}{a_p} S \frac{\pi^2 c\, h}{240} \left(\frac{1}{z_s^4} - \frac{1}{z_0^4} \right) \qquad \text{(Eq. (2))},$$

ref [4] [5] [6]. In this expression when $z_s = z_o$ the electric charge is null . The piezoelectric coefficient is d_{31} (CN^{-1}), l_p, a_p, are respectively length and thickness (m) of the piezoelectric bridge. Q_F does not depend on the common width bp = bs = bi of the structures (figure 4,5,6). This point is interesting and facilitates the technological realization of these structures since it limits the difficulties of their deep and straight engraving. These fixed electric and ionic charges Q_F, inside the piezoelectric bridge, have opposite signs and induce an electric field that attracts from the mass and on the two metallized faces of this bridge , mobile charges of opposite signs.

The mobile charges, for example on face 2 (Fig 4,5), of the faces of the bridge activate the insulating gates of the enriched transistors Thin Film Transistor Metal Oxide Semiconductor T.F.T. M.O.S, N and P in parallel of switch n°1 (Fig 2). It generates on these transistors a gate voltage V_G with the expression $V_g = \frac{Q_F}{C_{ox}}$ (Eq.3) . With, Cox the capacity of the grid's transistors $C_{ox} = \frac{E_0 E_{ox}}{t_{ox}} L_T W_T$ (Eq.4) and ε_o the permittivity of vacuum, ε_{ox} the relative permittivity of silicon oxide, L_T, W_T, t_{ox} the length, width and thickness of the grid of the TFT MOS . The mobile charges of the other face 1 (Fig 4,5) of the bridge

supply the sources of the T.F.T. M.O.S. N and P and can circulate to homogenize on a so-called Coulomb electrode, if the threshold voltage of the switch n°1 is exceeded. Before closing switch n°1, this Coulomb electrode was grounded by closing switch n°2, consisting of N and P M.O.S. T.F.T 's in depletion and in series. (Fig 3). It is important to note that:

1/ The threshold voltage values of these switches are V_{T_1} for switch n°1 and V_{T_2} for switch n°2, and that $|V_{T_1}|$ very slightly above $|V_{T_2}|$ with some tens of millivolts 2/ If the voltage on the insulating gates of the MOS TFTs is above their threshold voltage then: Switch n°1, changes from OFF to ON but conversely switch n°2 changes from ON to OFF (Fig 1)

1.2: description of switches n˚1 or n˚2 and autonomous electronic

1.2.1: switches electronic description

These indispensable switches are made with:

a/ Circuit n°1 (fig 2): with T.F.T. MOS P and MOS N transistors enriched and in parallel: Threshold voltage V_{TNE} and V_{TPE}

b/ Circuit n° 2 (fig 3): with T.F.T. MOS P and MOS N transistors in depletion and in series: Threshold voltage V_{TND} and V_{TPD}

An important point is that the threshold voltage values of these transistors are positioned as Figure 1.

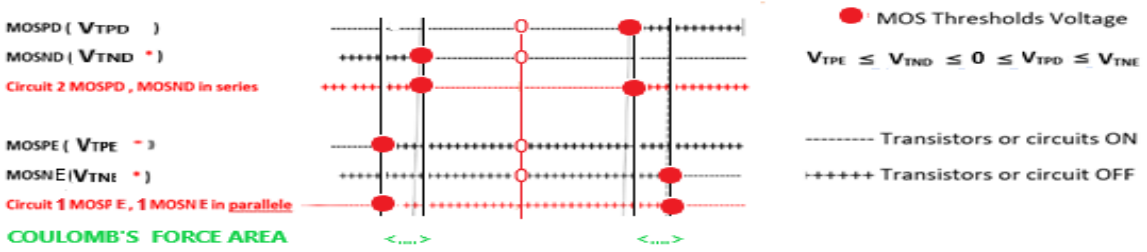

Figure 1: Distribution of the threshold voltages of enriched and depleted N and P MOS switches.

We have: $V_{TPE} < V_{TND} < 0 < V_{TPD} < V_{TNE}$. For the functioning symmetry $|V_{TPE}|$ can equal $|V_{TNE}|$ and $|V_{TPD}|$ can equal $|V_{TND}|$. Consequently, as $|V_{TND}| < |V_{TPE}|$ and $|V_{TPD}| < |V_{TNE}|$, and with a difference of their values of just some tens of millivolts , circuit switch n° 2 commute , then is open or closed *just before* circuit switch n° 1 switches respectively from closed or open (see figure n° 1, 2,3, 4, 5, 6, 18).

1.2.2: Circuit n˚1: Switch n˚ 1

Switch n°1 consists -with their threshold V_{TNE} or V_{TPE} voltage- of enriched N type TFT MOS , in parallel with an enriched P type TFT MOS (fig 1,2), as positioned in fig 2. [11]

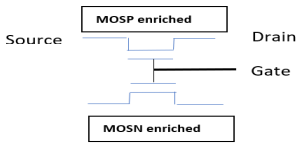

The common gates voltage of these enriched T.F.T. MOS N and P in parallel of switch n°1(figure 2), are controlled by the free charges appearing on face n°2 of the piezoelectric bridge. The N and P sources of these T.F.T. MOS are connected to face n° 1 of the bridge and the drains Coulomb's electrode. (Fig 4,5).

Fig. 2: Switch n°1

The switch n°1 is made with two types of enriched MOSPE or MOSNE transistors in parallel, to avoid the exact nature (holes or electrons) of the mobile electric charges appearing on the metal face n°1 of the piezoelectric bridge. Preferably, their thresh:old voltages are the same in absolute value $|V_{TNE}| = |V_{TPE}|$.

The input of the R.L.C circuit is connected in series between the return Coulomb electrode and the ground, the autonomous electronic n°3 in parallel (figure 4,5). This return Coulomb electrode is itself grounded via switch n°2

1.2.3: Circuit 2: Switches n°2

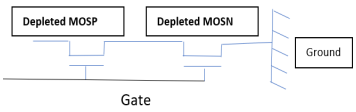

Switch n°2, consists of a P type depletion T.F.T. MOSPD in series with an N type MOSND depletion

Fig. 3: Switch n°2

(see figure 1,3 ,5). The common gates of these MOS switches are controlled by the free charges appearing on face n°2 of the piezoelectric bridge. (figure 1,4,5). The input of switch n°2 is connected to the Coulomb electrode, and its output to the RLC circuit, then to ground. Preferably, their threshold voltages are the same in absolute value $|V_{TND}| = |V_{TPD}|$. The values of $|V_{TND}| \approx |V_{TPD}|$ are lower but very close (down than 10%) of $|V_{TNE}| \approx |V_{TPE}|$

1/3: schematic and comportment of the MEMS

Thus, when it is effective (switch n°1 closed), the Coulomb return force F_{CO} is (fig 4,5,6)

$$F_{CO} = \frac{Q_F^2}{4\pi\varepsilon_0\varepsilon_r}\left(\frac{1}{z_r + z_0 - z_s}\right)^2 = \left[\frac{d_{31}\, l_p}{a_p} S_S \frac{\pi^2 c\, h}{240}\left(\frac{1}{z_s^4} - \frac{1}{z_0^4}\right)\right]^2 \left(\frac{1}{4\pi\varepsilon_0\varepsilon_r}\right)\left(\frac{1}{z_r + z_0 - z_s}\right)^2 \qquad \text{(Eq. 5)}$$

We note that F_{CO} is in $1/z_s^{10}$, with z_s = distance (time dependent) between Casimir electrodes, and z_o = initial distance between Casimir electrodes (without any electric's charges). The schematic of the sensor part of this MEMS is shown in figures (4, 5). The perpetual, isotropic and timeless Casimir F_{CA} force, resulting from quantum vacuum fluctuations, causes the deformation of a microscopic piezoelectric bridge embedded in a silicon wafer.

Casimir reflector electrodes
Piezoelectric Bridge
Recall Coulomb's electrode

*a_p, b_p and l_p , are thickness, width, and length of the piezoelectric bridge.
*a_s, b_s and l_s , are the thickness, width and length of the Casimir moving electrode .

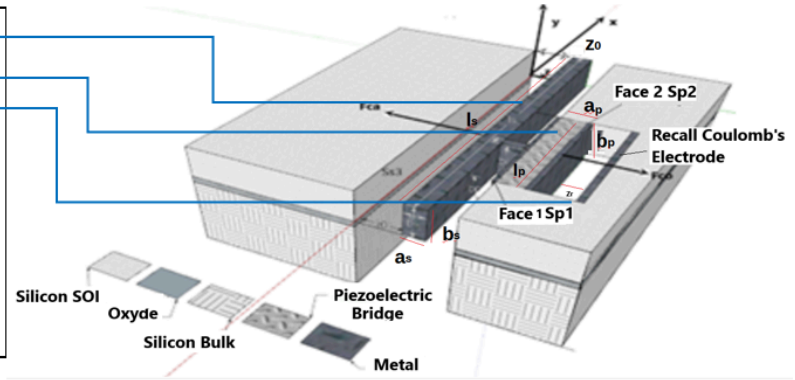

Fig. 4: Vue of the top of device, Axes, Forces, Casimir's Electrodes

*

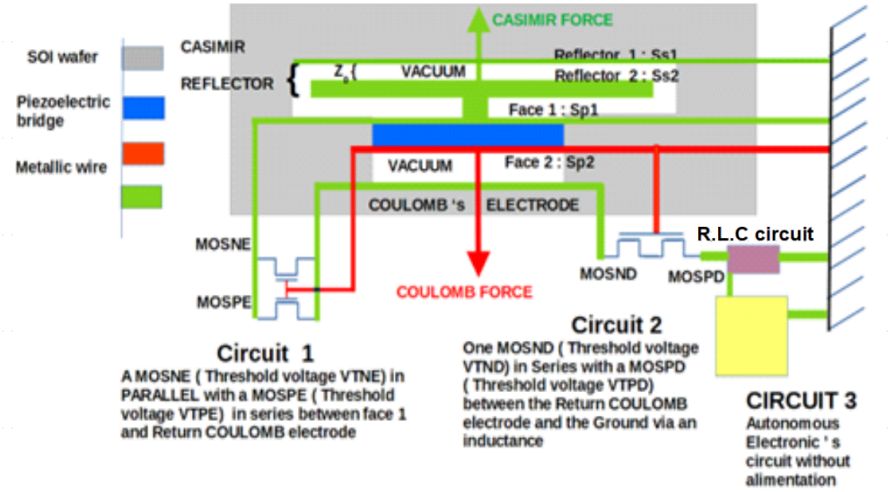

Fig. 5: General configuration of the device: MOS grid connections (Face 2 of the piezoelectric bridge: red), Source connections (Face 1 of the piezoelectric bridge: green) We remark that the Casimir force F_{CA} appearing between the reflector electrodes (green) is applied to the piezoelectric bridge (blue) via a metallic digit (green)

When the switch n°1 is open, the mobile charges of face n°1 don't move and keep on this face n°1. When the switch n°1 is closed and switch n°2 is open, the free moving electric charges must homogenize between the metallic film of face n°1 and the metallic film of Coulombs electrode (Fig 4,5). Then, as the electrical nature of mobile charges of faces n°1 and n°2 are opposite, Coulomb's force F_{CO} must appear between these two metallic electrodes. The threshold voltages of the transistors of switch n°1, technologically predetermined, impose the intensity of Coulomb's forces, which can be much greater than the force of Casimir F_{CA}. The Coulomb force's_lifespan is ephemeral, and its dissipated energy is determined by the threshold voltages of switch n°2, when it is closed to ground (Fig 1,3,4,5,6). The resulting force F_{CO} - F_{CA}, applied to the center of the piezoelectric bridge, changes direction or is zero. The piezoelectric and elastic bridge having no force to keep it deformed, necessarily returns (by the stored deformation energy + the kinetic energy) to its initial position, therefore without any deformation or electrical charges. This ephemeral Coulomb force suppresses the collapse of the two very close electrodes of the Casimir reflector and reduces, then cancels the deformation of the piezoelectric bridge, and thus its electric charges. The structure returns to its initial state and is again deformed by the timeless and isotope Casimir force F_{CA}, which always exists. (Fig 6)

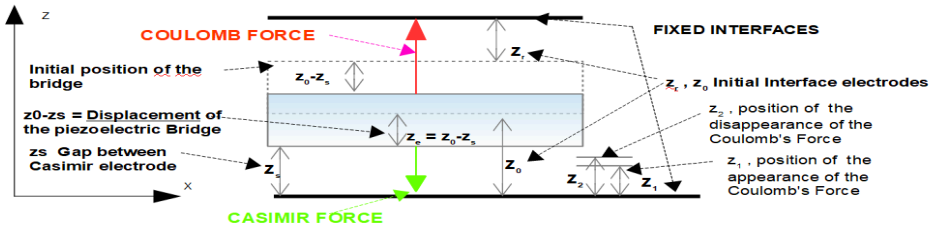

Figure 6: Axes, Forces, Casimir's Electrodes

This cycle reproduces itself and the system vibrates (Fig 8,9,10), with the vacuum energy transmitted by the F_{CA} force, as a continuous drive source for the deformation of the piezoelectric bridge and with the self-built Coulomb force F_{CO}, superior and opposed to F_{CA} as the counter-reaction force. At each cycle, the automatic switching of the integrated switches of circuits n°1 and n°2 (Fig. 1,2,3,4,5,6) distributes differently the mobile electrical charges located on face n°1 of the bridge.

Notice that initially, the Coulomb's electrode was grounded by the automatically closing of the switch n°2 (Fig 1,3)

II. CALCULATION OF THE BEHAVIOUR OF THE STRUCTURE

Let us calculate the evolution in time of the deflection of the piezoelectric bridge due to the Casimir's force which is applied between the two electrodes separated by an initial distance z_o (fig 5). We use the theorem of angular momentum for this vibrating structure.(Eq. 6).

$$\overrightarrow{\sigma^{S}_{Ax,y,z}(\ Structure)} = \overline{I^{S}_{A\,x,y,z}}\ \overrightarrow{\theta^{S}_{A\,x,y,z}} \qquad \text{(Eq. 6)}$$

With $\overrightarrow{\sigma^{S}_{Axyz}}$ the angular momentum vector of the structure, $\overline{I^{S}_{Axyz}}$ the inertia matrix of the total structure with respect to the reference (A, x,y,z) and θ^{S}_{Axyz} the rotation vector of the piezoelectric bridge with respect to the axis Ay with α the low angle of rotation along the y axis of the piezoelectric bridge

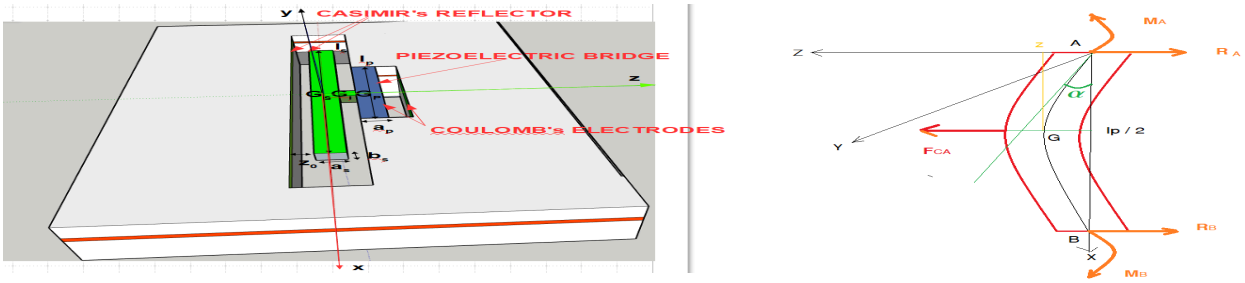

Figure 7: Piezoelectric bridge Cutting Reactions and Bending Moment, Deflection

$$\overrightarrow{\theta^{S}_{A}} = \begin{pmatrix} 0 \\ d\alpha/dt \\ 0 \end{pmatrix} \text{ with } d\alpha/dt \approx \frac{2}{l_P}\frac{dz}{dt} \text{ because } \sin(\alpha) = \sin\left(\frac{2z_s}{l_p}\right) \approx \frac{2z_s}{l_p} \text{ as } z << l_p$$

We have

Let (Gp, x, y, z), (Gi, x, y, z), (Gs, x, y, z) be the barycentric points respectively of the piezoelectric bridge, of the connecting metal finger and of the metal block constituting the mobile sole of the Casimir reflector. We have (fig 4,5):

$$\overrightarrow{AG_{P,x,y,z}} = \frac{1}{2}\begin{pmatrix} l_P \\ b_P \\ a_P \end{pmatrix} \qquad \overrightarrow{AG_{I,x,y,z}} = \frac{1}{2}\begin{pmatrix} l_P + l_i \\ b_P + b_i \\ a_P + a_i \end{pmatrix} \qquad \overrightarrow{AG_{S,x,y,z}} = \frac{1}{2}\begin{pmatrix} l_P + l_i + l_S \\ b_P + b_i + b_S \\ a_P + a_i + a_S \end{pmatrix}$$

The inertia matrix of the bridge, in the frame of reference (Gp, x, y, z) is:

$$I^{P}_{GP} = \frac{m_P}{12}\begin{pmatrix} a^2{}_P + b^2{}_P & 0 & 0 \\ & l^2{}_P + b^2{}_P & 0 \\ 0 & 0 & a^2{}_P + l^2{}_P \end{pmatrix}$$

Taking Huygens' theorem into account, this inertia matrix becomes

$$I^{P}_{A,x,y,z} = m_P \begin{pmatrix} \frac{a^2_p + b^2_p}{3} & -\frac{l_p b_p}{4} & -\frac{l_p a_p}{4} \\ -\frac{l_p b_p}{4} & \frac{a^2_p + l^2_p}{3} & -\frac{a_p b_p}{4} \\ -\frac{l_p ba}{4} & -\frac{a_p b_p}{4} & \frac{l^2_p + b^2_p}{3} \end{pmatrix}$$ (Eq (7)):

With the same reasoning we can calculate the inertia matrix of the finger $I^{I}_{A, x, y, z}$, and the inertia matrix of the reflector $I^{c}_{A, x, y, z}$ in the frame o f reference (A, x, y, z),

$$I^{I}_{A,x,y,z} = \frac{m_i}{12}\begin{pmatrix} a^2_i + b^2_i & 0 & 0 \\ 0 & a^2_i + l^2_i & 0 \\ 0 & 0 & l^2_i + b^2_i \end{pmatrix} + m_i \begin{pmatrix} \frac{(b_p+b_i)^2+(a_p+a_i)^2}{4} & -\frac{(b_p+b_i)(l_p+l_i)}{4} & -\frac{(a_p+a_i)(l_p+l_i)}{4} \\ -\frac{(b_p+b_i)(l_p+l_i)}{4} & \frac{(l_p+l_i)^2+(a_p+a_i)^2}{4} & -\frac{(b_p+b_i)(a_p+a_i)}{4} \\ -\frac{(a_p+a_i)(l_p+l_i)}{4} & -\frac{(b_p+b_i)(a_p+a_i)}{4} & \frac{(b_p+b_i)^2+(l_p+l_i)^2}{4} \end{pmatrix}$$ (Eq. (8))

$$I^{C}_{A,x,y,z} = \frac{m_s}{12}\begin{pmatrix} a^2_s + b^2_s & 0 & 0 \\ 0 & a^2_s + l^2_s & 0 \\ 0 & 0 & l^2_s + b^2_s \end{pmatrix} + m_s \begin{pmatrix} \frac{(b_p+b_i+b_s)^2+(a_p+a_i+a_s)^2}{4} & -\frac{(l_p+l_i+l_s)(b_p+b_i+b_s)}{4} & -\frac{(l_p+l_i+l_s)(a_p+a_i+as)}{4} \\ -\frac{(l_p+l_i+l_s)(b_p+b_i+b_s)}{4} & \frac{(l_p+l_i+l_s)^2+(a_p+a_i+a_s)^2}{4} & -\frac{(b_P+b_i+b_s)(a_p+a_i+as)}{4} \\ -\frac{(l_p+l_i+l_s)(a_p+a_i+as)}{4} & -\frac{(b_P+b_i+b_s)(a_p+a_i+as)}{4} & \frac{(b_p+b_i+b_s)^2+(l_p+l_i+l_s)^2}{4} \end{pmatrix}$$ (Eq. (9)

The total inertia of the structure becomes in the reference (A, x, y, z) is : $I^{s}_{A,x,y\,z} = I^{P}_{A,x,y,\,z} + I^{I}_{A,\,x,\,y,\,z} + I^{c}_{A,\,x,\,y,\,z}$ with A at the edge of the recessed piezoelectric bridge .The angular momentum theorem applied to the whole structure gives :

$$\frac{\overrightarrow{d(\sigma^{S}_{A,x,y,z})}}{dt} = \overline{I^{S}_{A,x,y,z}}\ \frac{\overrightarrow{d\theta^{s}_{A}}}{dt} \Rightarrow \overline{I^{S}_{A,x,y,z}}\ \frac{2}{l_P}\begin{pmatrix} 0 \\ \frac{d^2z}{dt^2} \\ 0 \end{pmatrix} = \sum_{A} \overrightarrow{Moments\ of\ the\ structure} =$$

$$= \overrightarrow{M_A} + \overrightarrow{M_B} + \overrightarrow{F_{CA}} \wedge \begin{pmatrix} l_P/2 \\ 0 \\ 0 \end{pmatrix} with\ \overrightarrow{F_{CA}} = \begin{pmatrix} 0 \\ 0 \\ F_{CA} \end{pmatrix}$$ Eq. (10)

The structure rotates around the Ay axis, the moments at point A are $M_{AY} = M_{BY} = - F_{CA}$ lp /8 [10], therefore the summation of Moments on the structure relative to the axe Ay = 1/4*lp * F_{CA} .

Any calculation done; we obtain:

$$\overline{I^{s}_{y}}\ \frac{2}{l_P}\ \frac{d^2z}{dt^2} = \frac{l_P}{4} F_{CA} = \frac{l_P}{4}\ S_S\ \frac{\pi^2 \hbar c}{240\ z^4}$$ Eq. (11)

with I^{S}_{y} the inertia of the structure relative to the axe Ay.

$$I^{S}_{Y} = \rho_P a_P b_P l_P \left(\frac{\left(l^2_P + a^2_P\right)}{12} + \frac{\left(l^2_P + a^2_P\right)}{4}\right) + \rho_i a_i b_i l_i \left(\frac{\left(l^2_i + a^2_i\right)}{12} + \frac{\left(l_p + l_i\right)^2 + \left(a_P + a_i\right)^2}{4}\right) + \rho_s a_s b_s l_s \left(\frac{\left(l^2_s + a^2_s\right)}{12} + \frac{\left(l_p + l_i + l_s\right)^2 + \left(a_P + a_i + a_S\right)^2}{4}\right)$$ Eq.(12)

With ρ_P , ρ_i , ρ_S , respectively the densities of the piezoelectric bridge , the intermediate finger and the mobile electrode of the Casimir reflector . By equation 6, we obtain the differential equation which makes it possible to calculate the interval between the two electrodes of the Casimir reflector as a function of time during the "descent" phase when the Coulomb forces are not present.

$$\frac{d^2z}{dt^2} = \frac{l_P^2}{8\, I_Y^S}\, S_S\, \frac{\pi^2 \hbar c}{240}\, \frac{1}{z^4} = \frac{B}{z^4} \quad with\ B = \frac{l_P^2}{8\, I_Y^S}\, S_S\, \frac{\pi^2 \hbar c}{240} \qquad \text{(Eq. 13)}$$

This differential equation unfortunately *does not have a literal solution, and we programmed it on MATLAB* to calculate the duration of this "descent" of the free Casimir electrode. This duration depends on the desired value of the coefficient of proportionality $p = F_{CO}/F_{CA}$. (See figures chapter 4).

Just at the closing switch n°1, we have $F_{CO} = p\, F_{CA}$ with p, a coefficient of proportionality defined by the threshold voltages of the MOS interrupters. Just at the end of "descent" and the start of the charge transfer , the total force F_T exerted becomes: $F_T = F_{CA}\text{-}F_{CO} = F_{CA}\,(1\text{-}p)$. The "descent" time of the free Casimir electrode will therefore stop when $F_{CO} = -\,p\, F_{CA}$. We can calculate this point z_1 where $F_{CO} = p\, F_{CA}$ We know that :

1. The Casimir force is variable in time, but its equation is (Eq. (1)):

$$F_{CA} = \frac{d(E_{CA})}{dz} = S\left(\frac{\pi^2 \hbar c}{240\, z_4^4}\right)$$

The mobile charges transiting from side 1 to the Coulomb electrode through circuit 1 variable also with time (Eq. (2)) are: $Q_{mn} \approx \frac{Q_{mn1}}{2} = \frac{d_{31}\, F_{CA}\, l_P}{2\, a_P}$ because they have the same area .

2. The Coulomb force (Eq 5), variable over time, acting in opposition to the Casimir force:

$$F_{CO} = \left(\frac{d_{31}\, l_p}{a_p}\, l_S\, b_S\, \frac{\pi^2 \hbar c}{240}\left(\frac{1}{z_s^4} - \frac{1}{z_0^4}\right)\right)^2 \left(\frac{1}{8\pi\varepsilon_0\varepsilon_r}\right)\left(\frac{1}{z_r + z_0 - z_s}\right)^2 =$$
$$p\, F_{CA} = p\, l_s b_s\, \frac{\pi^2 \hbar c}{240}\, \frac{1}{z_s^4} \qquad \text{(Eq. 14)}$$

3. So, the "descent" of the free Casimir electrode stops when the inter electrode interface z_s is such that:

$$z_S^4 \left(\left(\frac{1}{z_R + z_0 - z_S}\right)^2 \left(\frac{1}{z_s^4} - \frac{1}{z_0^4}\right)^2\right) = \frac{1920\, p\, \varepsilon_0\, \varepsilon_r}{\pi \hbar c\, S_S}\left(\frac{a_P}{d_{31}\, l_P}\right)^2 \qquad \text{(Eq. (15)}$$

See (Fig 18)

This programmable equation gives the time t_d of the "descent" of the structure submitted to the Casimir force and: a/ depend on the coefficient of proportionality p:

$$F_T = (1-p)\, F_{CA} \Rightarrow (1-p)\, S_S\, \frac{\pi^2 \hbar c}{240\, z_{sm}^4} < 0 \ \ if\ p > 1$$

b/ is calculable and will stop when the inter-electrode interface z_s has a value z_1 satisfying equation (15).

During all the phases where $0 < VT_{ND} < V_{GRIDS} \leq VT_{NE}$, or $VT_{PE} \leq V_{GRIDS} < VT_{ND} < 0$. The total force, variable over time and exerted at the center of the piezoelectric bridge, becomes:

$$F_T = F_{CA} - F_{CO} = S_S\, \frac{\pi^2 \hbar c}{240\, z_S^4} - \frac{1}{2}\left[\frac{S_S\, \pi^2 \hbar c}{240}\left(\frac{1}{z_s^4} - \frac{1}{z_0^4}\right)\left(\frac{d_{31} l_P}{a_P}\right)\right]^2 \left(\frac{1}{4\pi\varepsilon_0\, \varepsilon_r}\right)\left(\frac{1}{z_r + z_0 - z_s}\right)^2 \qquad \text{Eq. (16)}$$

The piezoelectric bridge subjected to this new force F_T rises towards a position where the Coulomb's F_{CO} disappears at the point z_2 (fig xx), because the switch n° 2 closed to ground, via a R.L.C. circuit (fig 4,5). When F_{CO} disappears, the whole moving structure (Casimir reflector electrode + finger + piezoelectric bridge) with an important masse M_t, acquires a kinetic energy E_C with $E_c = \frac{1}{2} M_t V_t^2$ and $M_t = \rho_P(a_p b_p l_p) + \rho_i(a_i b_i l_i) + \rho_s(a_s b_s l_s)$, Vt= speed of the mobile structures, ρ_p, ρ_i, ρ_s , a_p b_p l_p , a_i b_i l_i, a_s b_s l_s, respectively the volumic mass and volume of the piezoelectric bridge, finger and Casimir electrode .

Let us calculate an approximation of the duration of this "rise" of the mobile electrode Casimir's reflector + finger + piezoelectric bridge , triggered when $F_{CO} = p\, F_{CA}$. This time is approximated because when the Coulomb force F_{CO} stop (because the closing of the switch n° 2 to ground at the point z_2 between z_1 and the initial point z_o, Fig 6),_the mobile structure loses its kinetic energy E_c plus its deformation energy with the braking force provided by the Casimir force. We approximate this return time by saying that point z_2 of the loss of the Coulomb force occurs at the initial point z_o. In these conditions, to know the time taken by the structure to "go back" to its neutral position, we must solve the following differential equation:

$$\frac{d^2z}{dt^2} = \frac{l_P^2}{8 I_S^Y}\left(F_{CA} - F_{CO}\right) = \frac{l_P^2}{8 I_S^Y}\left\{\left(l_S b_S \frac{\pi^2 \hbar c}{240 z_S^4}\right) - \frac{1}{2}\left[l_S b_S \frac{\pi^2 \hbar c}{240}\left(\frac{d_{31} l_P}{a_P}\right)\left(\frac{1}{z_s^4} - \frac{1}{z_0^4}\right)\right]^2\right\}\left(\frac{1}{4\pi\varepsilon_0\varepsilon_r}\right)\left(\frac{1}{z_r + z_0 - z_S}\right)^2 \qquad \text{Eq.(17)}$$

This differential equation (17) has no analytical solution and can only be solved numerically. We programmed it on MATLAB. In these MATLAB simulations we considered that the metal of the electrodes and metal block was oxidized over a thickness allowing to have an interface between Casimir electrodes of 200 A° which modifies the mass and the inertia of the vibrating structure (See chapter 5). It turns out that the choice of aluminium as the metal deposited on these electrodes is preferable given:

1. The ratio between the thickness of the metal oxide obtained and of the metal attacked by the thermal oxidation (see chapter 6)
2. Its low density increases and optimizes the vibration frequency of the structure by minimising the inertia of the Casimir reflector and the parallelepiped block that transfers the Casimir force.

The mass $M_{structure}$ of the vibrating structure is then:

$M_{STRUCTURE} = d_{pm}(a_s b_s l_s + a_i b_i l_i) + 2\, d_{om}\, z_{of}\,(a_{so} b_{so} + b_{so} l_{so} + a_{so} l_{so}) + d_p(a_p b_p l_p)$. With d_{pm} the density of the metal, a_s, b_s, l_s the geometries of the final metal part of the Casimir electrode sole, d_{om} the density of the metal oxide, a_{so}, b_{so}, l_{so} the geometries of the oxidized parts around the 6 faces of the metal block, d_p the density of the piezoelectric parallelepiped (see figure 4,5):

III. SIMULATION OF DEVICES WITH DIFFERENT PIEZOELECTRIC BRIDGE

We present below the results of the MATLAB simulations carried out by numerically calculating the differential equations (11) and (13). These numerical calculations give the vibration frequency of the structure which, as we will see, vibrates at a frequency lower than its first resonant frequency (IV) . This vibration frequency depends on the characteristics of the structure (Nature of material, geometric dimensions, coefficient of proportionality $p = F_{CO} / F_{CA}$ ...)) . With its low density of 2.7 g cm^{-3} and its high oxidation power, the metal chosen for the Casimir reflector block is aluminum.

3.1 / PMN-PT piezoelectric materials for the piezoelectric bridge

To increase the density of electric charges at the terminals, piezoelectric material PMN-PT can be used. It can be deposited by RF-magnetron sputtering with a composition, for example: PMN-PT= (1-x) $\mathbf{P}_b$ (1/3 $\mathbf{M}_g$– 2/3 $\mathbf{N}_b$) O_3- x $\mathbf{P}_b\mathbf{T}_iO_3$; with piezoelectric coefficient d_{31} = 1450. 10^{-12} C / (kg. m. s^{-2}) and a Young's modulus Ep = 150 .10^9 Kg M^{-1} T^{-2}.

With MATLAB simulation, and for an interval between Casimir electrode z_o= 200 Angstroms, we obtain the evolution over time of the Casimir and Coulomb forces as well as the F_{CO} / F_{CA} ratio of figures 8 to 22 below. For a ratio p= F_{CO}/F_{CA} of 1000, the maximum current I delivered by the vibrating structure, the threshold voltage of the MOSE and the vibration frequency of the structure are respectively: I=1.2 10^{-4} A, Vt = 3.2 V and 957000 Hertz

3.1.1 / Evolution of the Casimir interface as a function of time during two periods: PMN-PT

The F_{CO} / F_{CA} ratio = 10000 induces a period of 3.85 10^{-6} s and a rise time of 21.3 10^{-9} s with a deflection of the bridge of 105 A°. The structure vibrates at 259.7 kHz. Due to inertia, at the rise sequence, the structure exceeds the initial 200 A° by 20 A° (Fig 28).

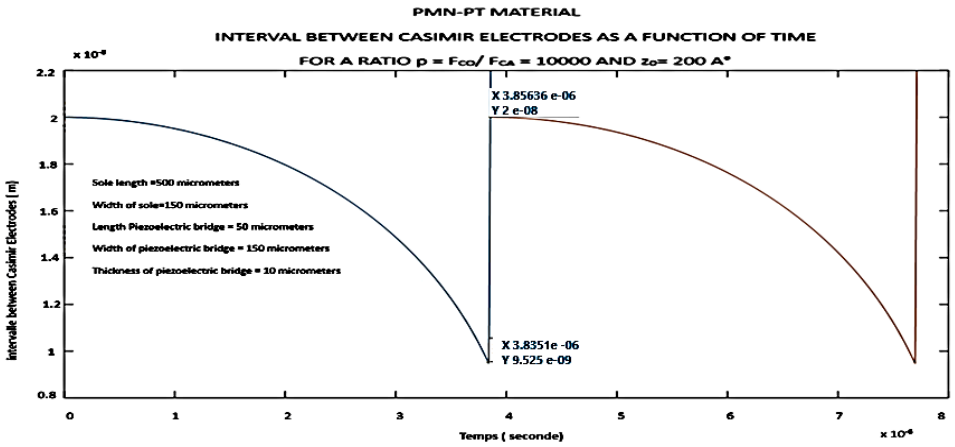

Figure 8: Axes, Forces, Casimir's Electrodes

A ratio F_{CO} / F_{CA} = 1000 induces a period of 2.96 10^{-6} s and a rise time of 44.5 10^{-9} s with a deflection of the bridge of 50 A ° The structure vibrates at 337.8 kHz: (fig 29).

For this ratio of 1000 we notice a vibration amplitude of 50A°, a period of 2.96 10^{-6} s, with the faster rise of the mobile electrode producing a slight rebound of 5A, because of the inertia of the structure.

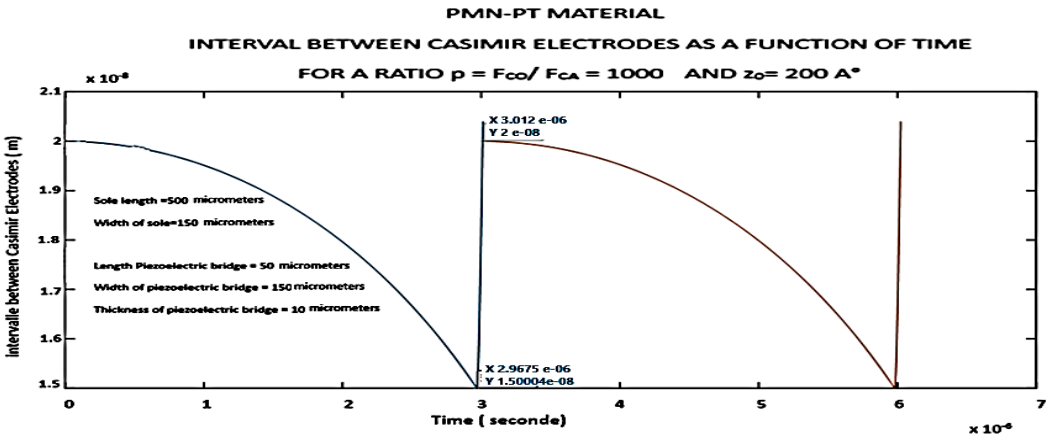

Figure 9: plot of the evolution of the Casimir inter-electrode interval as a function of time over two periods and Fco / Fca Ratio = 1000: Casimir inter-electrode interface = 200 A°

For the ratio F_{CO} / F_{CA} = 2 (figure 30) a vibration amplitude of just 0.27 A° and a period of 1.8610^{-7} s is obtained This low deformation of the PMN-PT piezoelectric bridge is mainly due to the extremely high piezoelectric coefficient d_{31} of 1450 (pC/N) of PMN-PT compared to 120 (pC/N) for PZT. We observe the weak overshoot of the initial interface.

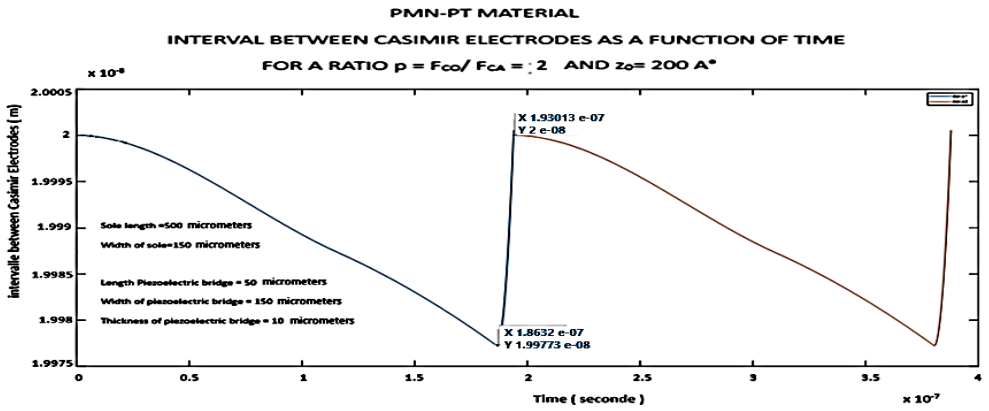

Figure 10: Plot of the evolution of the Casimir inter-electrode interval as a function of time over two periods and a Ratio Fco / Fca = 2. Casimir inter-electrode interface = 200 A

3-1-2 / Evolution of the forces of Casimir and Coulomb: PMN-PT

We obtain:

1/ The evolution of the Casimir and Coulomb forces as a function
a / of the inter-electrode interface (figure 11) and
b/ over time (figure 12)
2/ The F_{CO} / F_{CA} ratio as a function of time for an entire period (figures 13).

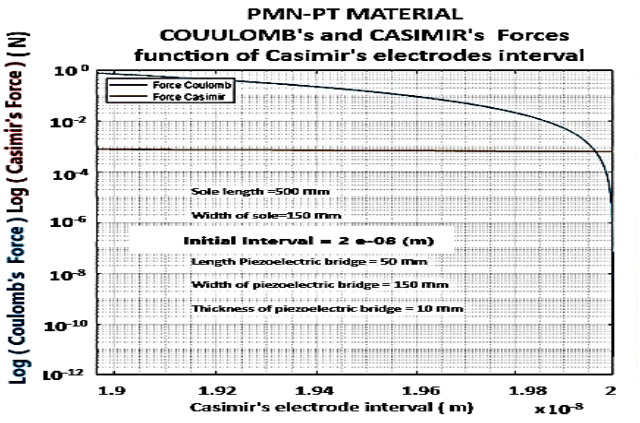

Figure 11: Materials = PMN-PT: Coulomb and Casimir force as a function of the inter-electrode interface. Start interface = 200A°

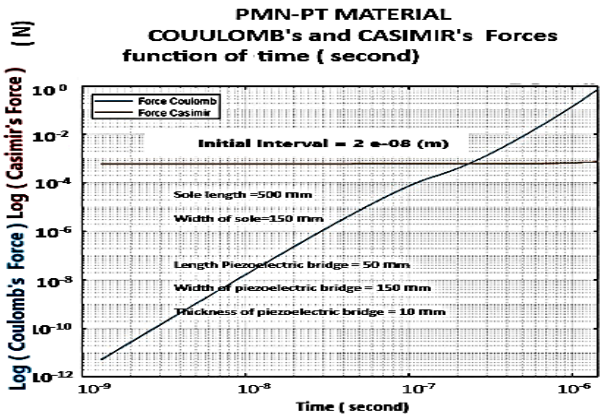

Figure 12: Materials = PMN-PT: Coulomb and Casimir force as a function of time. Start interface = 200A°

It is observed (Fig. 13) that the Coulomb return force is less important for an initial inter-electrode gap zr = 400A° than for z_r= 200A°.

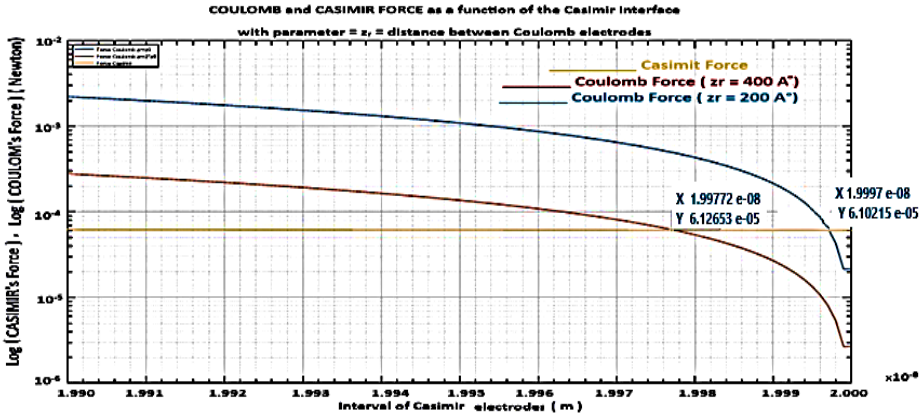

Figure 13: Materials = PMN-PT: Coulomb force for z_r = 200 A° (Blue) and z_r = 400 A° (Red) and Casimir force (Yellow, z0 =200 A°) as a function of the inter-electrode interface Starting interface = 200 A

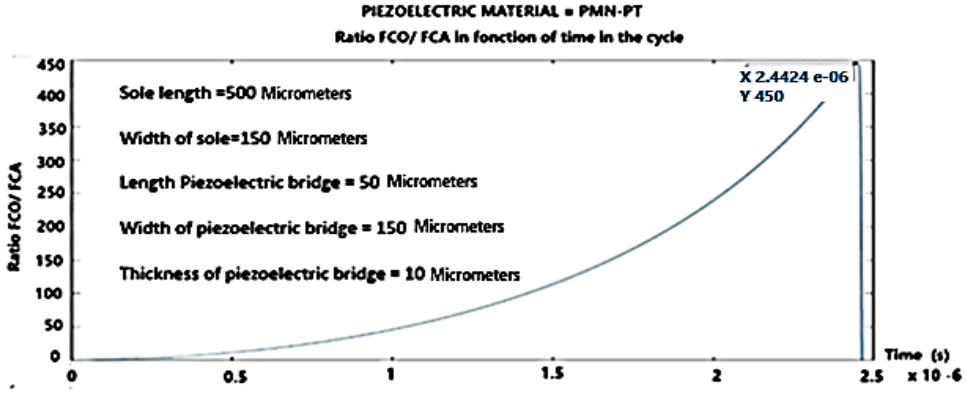

Figure 14: Materials = PMN-PT: Ratio p = F_{CO} / F_{CA} as a function of time, during a period of vibration. Start interface = 200A°, Maximum ratio chosen = 450

The break circuits n°1 triggered at time t = 2.44 10^{-6} s suddenly induce a rise of the mobile electrode, therefore a sudden decrease in electric charges and grids voltages. We observe the gradual evolution towards the chosen ratio of 450 and then the sudden drop in this ratio as the electrodes regain their initial position (Fig. (34)).

3.1.3 / Threshold voltage according to the desired Ratio F_{CO} / F_{CA}: PMN-PT

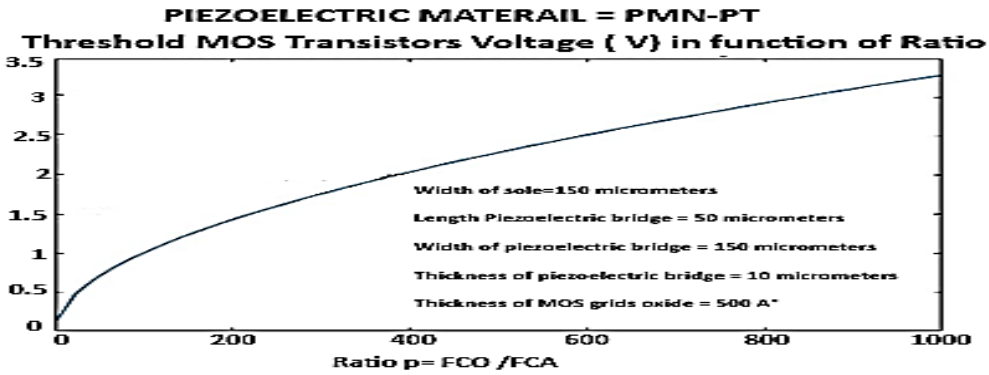

Figure 15: Materials = PMN-PT: Threshold voltage of the Enriched or Depleted MOS according to the F_{CO} / F_{CA} Ratio. Start interface = 200A°

It can be seen (Fig. 15) that we must increase the threshold voltage of the TFT MOS of switch n°1 up to 3.5V if we desire to obtain a ratio FCO/FCA of 1000.

.1.4 / Vibration frequency as a function of the F_{CO} / F_{CA} ratio and peak current as a function of the itial Casimir interval chosen: PMN-PT.

ote (fig 16), that for an initial interface z_o = 200 A°, and for a ratio F_{CO} / F_{CA} = 2, the maximum ibration frequency of the structure is 3.50 MHz. It falls to 750 kHz for a ratio of 1000. These requencies are still lower than the first resonance of the structure, which is of the order of 7.94 egahertz. This vibration frequency of the Casimir structure approaches that of the first resonance for eaker interfaces below 200 A°.

or a ratio F_{CO} / F_{CA} = 500, the maximum current delivered by the structure falls as a function of an ncrease in the initial Casimir interval (Fig 17).

t seems that the piezoelectric material PMN-PT coupled with a conductor like aluminium is an nteresting couple for our vacuum energy extraction structure.

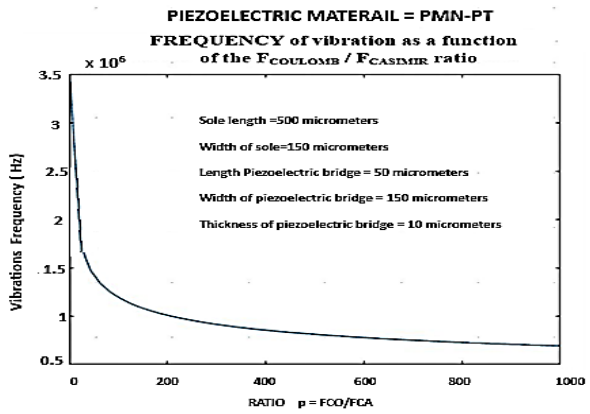

Figure 16: Materials = PMN-PT: Vibration frequency as a function of the F_{CO} / F_{CA} Ratio. tart interface = 200A ° Start interface = 200A°

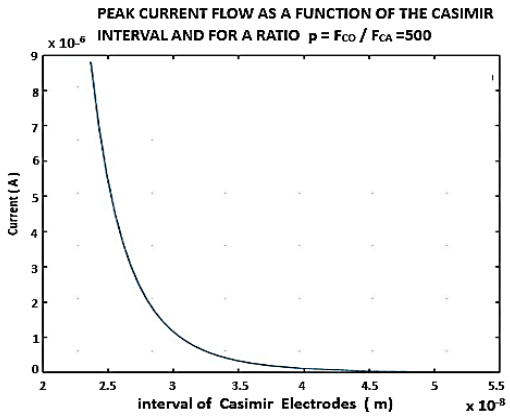

Figure 17: Materials = PMN-PT: Current peak across the 2 . 10^{-4} H inductance as a function of the starting interval between Casimir electrodes. Start interface = 200A°

IV. MEMS ENERGY BALANCE

n this part, we will try to make a detailed and exhaustive assessment of the behavior of the MEMS uring one vibration. Firstly, we will focus on the first half of this vibration, which we will call the "go" hase, so from the initial position z_o to the position z_1 where the switch n°1 commutes from OPEN to LOSE. Secondly, we will focus on the second half of the vibration, which is to say the "return" phase , o from the position z1 to zo passing throw the position z2 where the switch n°2 commute from OPEN o CLOSE and put the Coulomb's electrode to the ground canceling the F_{CO} force. Let us recall that the iezoelectric bridge is perfectly elastic, which implies, as with any elastic structure, that the energy xpended by a mechanical deformation of the positions from 0 to 1 is integrally restored when eturning. The conditions of use of the piezoelectric bridge (vibrations amplitude) are in the purely lastic domain and we never enter in the domain of plasticity.

n the following we propose to put into equations the energy balance of «go» then in "return "steps.

< VT_{PD} < VT_{NE}, and VT_{PE} < VT_{ND} < 0 and F_{CO} / F_{CA}< p. With p the chosen amplification F_{CO} / F_{CA}. We ote V_{T1}= abs (VT_{NE} or VT_{PE}) and V_{T2}= abs (VT_{ND} or VT_{PD}), and call V_G the voltage due to the mobiles harge on the face 2 of the piezoelectric bridge and appearing on the gate of all the TFT MOS ransistors. [11]

4/1 MEMS energy balance during the phase "going " from z_0 to z_1

a/_0 < V_G < abs (V_{T2})< abs(V_{T1}). and F_{CO} / F_{CA}< p: switch n°1 OFF, Switch n°2 ON. (Fig 1)

At the start, in the beginning conditions of the "go" phase, we have very small deformations applied to the piezoelectric bridge. Consequently, very small electrical charges are present on it, so the electrical voltages V_G on the grid of the enriched and parallel TFT MOS N and P of switch N°1 is lower than their threshold voltage V_{T1}. This witch n°1 is open and in the OFF position. On the other hand, as $V_G < V_{T2}$, switch N°2 consisting of two TFT MOS N and P in series, operating in depletion mode is closed and in the ON position to ground. In these conditions the so-called Coulomb electrode is to the ground, thus eliminating the Coulomb force F_{CO}.

b/ 0 < abs (V_{T2})< V_G < abs (V_{T1}). and F_{CO} / F_{CA}< p: switch n°1 OFF, Switch n°2 OFF. (Fig 1)

No moving electric charge appears on the return side of the Coulomb electrode, which is connected to ground by switch 2, which is ON, and isolated from the piezoelectric bridge by switch 1, which is OFF. The Casimir force begins to deform the piezoelectric bridge more significantly. Consequently, the mobiles charge on face 1 and 2 of the piezoelectric bridge therefore the voltage V_G on the gates of transistors of switch n° 1 and n° 2 increases. This voltage V_G still lower than the threshold voltage V_{T1}, exceeds now V_{T2} of switch n°2 which opens and switches OFF.

The structure being assumed to be perfectly elastic and the amplitudes of the vibrations being extremely low, we will see that the mechanical energy losses by an increase of temperature in the device are negligible.

1/ Note also that the mobile parallelepiped metal electrodes of the Casimir electrodes remain parallel to each other and that the mobile metal Casimir electrode does not deform. It simply transmits its movement to the piezoelectric bridge which deforms but therefore does not heat up. (Fig 4,5)

2/ The expulsion of entropy ΔS from the vibrating structure of Casimir is transmitted to the piezoelectric bridge. It causes an extremely slight increase ΔT in its temperature and expels this heat to the outside. Let us calculate an order of this magnitude ΔT. We note ΔQ_{vib} the heat transmitted by the vibrations of the piezoelectric bridge. In first approximation, we can use the well-known formula ΔQ_{vib} = ΔS. ΔT, with ΔS= entropy variation (J °K^{-1}) and Δ T = temperature variation (° K)

However, we know that: $\Delta Q_{vib} = \frac{M_{Bridge}\left[2\pi f_{vib}\right]^2}{2} z_1^2$ Eq. (18) [10] With: fvib= Vibration frequencies of the piezoelectric bridge, M_{Bridge} = mass of this bridge, which is the only one to deform because the Casimir electrodes are simply in translations. We note z_1 the maximum deflection of the bridge (Fig 6) .

This heat expended at the level of the piezoelectric bridge causes its temperature to increase. As a first approximation we can say: ΔQ_{vib} = $M_{Structure}$.Cpiezo ΔT. With: C_{piezo} = Specific heat capacity of the piezoelectric bridge (J Kg^{-1} °K^{-1}), ΔT = Temperature variation (°K).

Consequently $\Delta T = \frac{2\left[\pi f_{vib}\right]^2}{C_{piezo}} z_1^2$ = Temperature variation of the bridge. Eq. (19)

For example, for a PMN-PT piezoelectric film: C_{piezo} = C_{PMN-PT} = 310 (J Kg^{-1} °K^{-1}), $f_{vib} \approx 10^6$ Hz, $z_e \approx 100*10^{-10}$ m, we then obtain: $\Delta T \approx 10^{-3}$ °K.

The expulsion of entropy from the vibrating Casimir Electrode is negligible.

We note that simply half of this expended heat occurs in the "go", the second part occurs in the "return" phases of the vibration. During a cycle from z_0 to z_1, to deform the elastic piezoelectric bridge during the

displacement "go" of the vibration, the quantum energy $E_{CASIMIR}$, given by the quantum vacuum, is used for four different energies:

1/ The mechanical energy for the deformation of the elastic bridge: W_{DEFCA}
2/ The energy to create the fixed Q_F charges in this piezoelectric structure: W_{BRIDGE}
3/ The energy for the simple displacement of the point of application of the Casimir force in the middle of the bridge: $W_{CASIMIR}$
4/ The expulsion of entropy $\Delta S/2$ energy, expended in heat due to the friction of the atoms in the half of the vibration of the bridge heat: $\Delta\ Q_{vib}/2$

We can write that to deform the piezoelectric bridge from the start position z_0 to the position z_1:

$$E_{CASIMIR1} = W_{DEFCA1} + W_{BRIDGE1} + W_{CASIMIR1} + \Delta\ Q_{vib}/2, \qquad \text{(Eq 8).}$$

This quantum vacuum energy $E_{CASIMIR1}$ is bigger than the simple translation energy WCASIMIR1. The energies W_{DEFCA} and W_{BRIDGE} are store in the deformed piezoelectric bridge as a potential energy.

1/ The translation energy of the Casimir force is:

$$WCASIMIR1 = \int_{z0}^{z1} FCAdz = \int_{z0}^{z1} S\ \frac{\pi^2\ h\ c}{240\ zs4} dz_S = S\left(\frac{\pi^2\ h\ c}{720}\right)\left[\frac{1}{z_1^3} - \frac{1}{z03}\right]. \qquad \text{(Eq 20)}$$

The $W_{CASIMIR1}$ energy represents the translation of the Casimir force F_{CA} from z_0 to z_1 without considering that this force also deforms an elastic and piezoelectric structure from z_0 to z_1.

Now, let's calculate the deformation energy W_{DEFCA} of the piezoelectric bridge fixed at both ends. We know that the deformation energy of an elastic system is the energy that accumulates in the solid body during its elastic deformation. Yet, all Material Resistance book says that the deformation energy W_d of an embedded elastic bridge and for a constant force F is: $W_d = ½\ z_e\ F$ with $z_e = z_o - z_s$, the deflection (arrow) acquired by the elastic bridge subjected to the constant force F . In the case of our piezoelectric bride the force F being the Casimir force, varies in $1/z^4$, with the distance z.

So, for a differential deflection dz of the bridge under the force F(z) we can write:

$$d(W_d) = 1/2\ F(z)\ dz. \Rightarrow W_d = \frac{1}{2} W_{DFCA}(z_s) = \frac{1}{2} S \frac{\pi^2\ h\ c}{240} \int_{z_0}^{z_s} \frac{1}{z^4}\ dz = \frac{1}{6} \frac{\pi^2\ h\ c}{240} \left[\frac{1}{z_s^3} - \frac{1}{z03}\right] \qquad \text{(Eq. 21)}$$

This energy W_{DEFCA} is stored in the elastic bridge as a potential energy. The position of the mobile Casimir electrode reaches the limit z_1 when the grid voltage V_G on switch n°1 reaches its threshold voltage V_{T1}. This reached position z_1 is unstable because the Casimir force increases with its position. As a result, the mobile Casimir electrode can collapse. But, when the Casimir electrode is in position z_1 , the switch n°1 switches to ON. The charges present on the metallic face n°1 of the piezoelectric bridge must homogenize with the metallic Coulomb electrode, which was previously grounded by the closing of switch n°2. Note that, when switch n°1 switches, switch n°2 is still open because the voltage of the TFT MOS of switch n°2 are in depletion $V_G > V_{T2}$ (Fig 1,4,5,6).

The energy stored in the bridge through its deformation is in

$$z_1\ W_{DFCA1} = \frac{1}{6}\ S\ \frac{\pi^2\ h\ c}{240}\ \left[\frac{1}{z_1^3} - \frac{1}{z03}\right] \qquad \text{Eq 22,}$$

At position z_2 of the structure, the memorized elastic energy is

$$W_{DFCA2} = \frac{1}{6} S \frac{\pi^2 h c}{240} \left[\frac{1}{z_2^3} - \frac{1}{z03}\right] \quad \text{Eq23 .}$$

We notice that $W_{DEFCA} > 0$ and that the numerical value of W_{DEFCA1} is a little smaller than the expression calculated when $F_{CA}(z_1)$ was constant: Wd= ½ ze*$F_{CA}(z_1)$.

2/ During the displacement "go" the energy $E_{CASIMIR}$ is also used to generate a potential energy W_{BRIDGE} accumulated in the capacity of this piezoelectric bridge which follows the equation: $d(W_{BRIDGE}) = Q_F\, d(V_{PIEZO})$ with V_{PIEZO} = Voltage between the two metallic faces of the piezoelectric bridge, with $Q_F = C_{PIEZO}\ V_{PIEZO} \Rightarrow W_{BRIDGE1}$ = potential energy at the position z_1

$$W_{BRIDGE1} = \int_0^{Q_1} \frac{Q_F}{C_{PIEZO}} d(Q_F) = \left[\frac{Q_F^2}{2\, C_{PIEZO}}\right]_0^{Q_1} = \frac{a_P}{2\, l_P b_P \epsilon_0 \varepsilon_{PIEZO}} \left(\frac{d_{31}\, l_p}{2\, a_P}\right)^2 F_{CA}^2 = \left(\frac{a_P}{2\, l_P b_P \epsilon_0 \varepsilon_{PIEZO}}\right)\left(\frac{d_{31}\, l_p\, l_s b_s \pi^2 c\, h}{480\, a_P}\right)^2 \left[\frac{1}{z_1^4} - \frac{1}{z_0^4}\right]^2$$

Eq. (24)

We notice that $W_{BRIDGE1} > 0$, similarly when the structure reaches position z_2, the same memorized elastic energy occurs. To get $W_{BRIDGE2}$ for position z_2 of the bridge, we simply swap z_1 for z_2. In these equations, we use $d(Q_F) = C_{PIEZO}\, d(V_{PIEZO})$, with C_{PIEZO} = electrical capacity of the piezoelectric bridge,

$$C_{PIEZO} \frac{\epsilon_0 \varepsilon_{PIEZO}}{a_P} b_P l_P \quad \text{Eq.25 .}$$

We know (Eq2) that the creating fixed charges on this piezoelectric structure is $Q_F = \frac{d_{31} l_P}{a_P} F_{CA}$. We have $Q_e = - Q_F$ = the accumulated mobile charges, coming from the mass, on the surface of the metallic film. This part W_{BRIDGE} of $E_{CASIMIR}$ is stored in the piezoelectric bridge as potential energy and contributes to the usable energy $W_{ELECTRIC}$ appearing during a cycle.

So, during the phase "going " from z_0 to z_1 the total energy coming from the vacuum = $E_{CASIMIR}$ is used:

1/to deform the piezoelectric bridge W_{DEFCA},
2/ to produce the electrical charges as potential energy$W_{BRIDGE1}$,
3/Translate the point of application of the Casimir Force $W_{CASIMIR}$,
4/ produce a heat of the structure by the entropic transfer $\Delta\ Q_{vib}/2$.

We have:

Energy produced by vacuum = $E_{VACUUM} = W_{DFCA} + W_{CASIMIR} + W_{BRIDGE} + \Delta\ Q_{vib}/2 = W_{GOING}$ (Eq 26)
W_{DEFCA} and W_{BRIDGE} are potential energies that will be used when the elastic bridge returns to its equilibrium position, that is to say without deformation.

4/2: MEMS energy balance during the "return" phase from z_o to z_1", switch n°1 ON, Switch n°2 OFF: 0 < abs (V_{T2}) < V_G < =abs (V_{T1}). and Ratio F_{CO} / F_{CA}> = p: (Fig 1)

Figure 15 page 10 above, shows the F_{CO}/F_{CA} ratio obtained by the choice - defined during the technological realization of the MEMS- of the threshold voltage V_{T1} of switch n°1.

Now, the voltage on the grids of switch n°1 exceeds its threshold voltage and switch commute ON. The switch n°2 is till OFF, so the Coulomb's electrode is opened. The free charges Q_{m1}, stored on the metal electrodes of face 1 (Fig 1,4 ,5), passing through one of the MOSE transistors, are uniformly distributed on the Coulomb metal electrode of the surface for example S_{C1} = lp*bp.

If $S_{C1} = S_{P1}$, this metallic Coulomb's electrode therefore has approximately a mobile charge Q_{mn} $S_{C1}/ S_{P1} = Q_{mn}/2$. This homogenization is obligatory because there is no electric field in a perfect metallic conductor. The free charges Q_{m2}, stored on face 2 and on all the isolated grids TFT MOS don't move. So, the grid's electrodes and return electrode have opposite free charges. (Fig 4,5,15). A Coulomb force F_{CO} then appears between these two electrodes during the very short time when switch no. 2 is still open, isolating the Coulomb electrode from the ground. The resulting force $F_R = F_{CO}-F_{CA}$ is now applied to the piezoelectric bridge. This force F_R, is opposite to the force F_{CA} or null. In presence of this force F_R the deformations of the bridge and its electrical charges, so the grid's voltage are necessarily reduced. Since the threshold voltage V_{T2} of switch n°2 is lower but very close to V_{T1} (we choose $V_{T1} - V_{T2} = 50$ mV), the time duration during which this Coulomb force is exerted is very small (a few nanoseconds).

Very quickly, the switch n°2 commutes from OFF to ON, grounding the Coulomb electrode via an R.L.C. circuit, (Fig 23). The Coulomb force vanishes quickly after its appearance at position z_2.. The values of V_{T2} and V_{T1} impose that z_2 is very close to z_1. So , the energy $W_{COULOMB} = \int_{z_1}^{z_2} F_{CO} dz$ expanded by the Coulomb force remains low, even if this force is several times that of Casimir in intensity.

The time of existence of F_{CO} is of the order of a few tens of nanoseconds (fig 1,5). The position z_1 of appearance of this force F_{CO} is such that $F_{CO} = p\, F_{CA}$ and is numerically calculated by MATLAB(fig. 18).

$$F_{CO}=pF_{CA} \Rightarrow \frac{Q_F\, Q_F}{8\pi\varepsilon_0\varepsilon_r}\left(\frac{1}{z_r+z_0-z_s}\right)^2=\left[\frac{d_{31}\,l_p}{a_p}S_S\frac{\pi^2 c\,h}{240}\left(\frac{1}{z_s^4}-\frac{1}{z_0^4}\right)\right]\left(\frac{1}{4\pi\varepsilon_0\varepsilon_r}\right)\left(\frac{1}{z_r+z_0-z_s}\right)^2=p\,S\frac{\pi^2 c\,h}{240\,z_s^4} \qquad \text{Eq 27}$$

We note that the position z_1 depends on the values of the interface's z_o of Casimir's electrodes and of Coulomb's electrodes z_r.

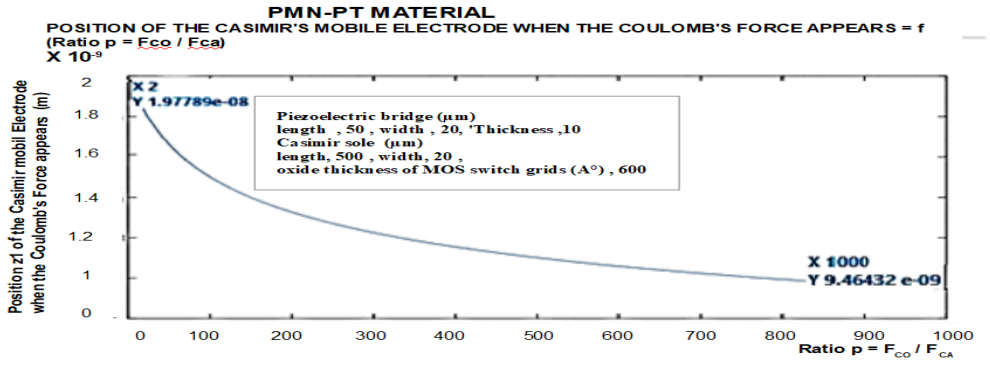

Fig. 18: Position of the mobile Casimir electrode z_1 where the Coulomb force occurs: $z_r = z_o$ =200A°, ls = 500 µm, bs = 20 µm, lp = 50µm, bp =20µm, ap = 10µm

The $F_R = F_{CO}-F_{CA}$ force is now applied to the mobile structure. This resulting force is at least zero or has a greater intensity than the Casimir force F_{CA}. It contributes with the energy stored in the elastic bridge to straighten the structure and to give it kinetic energy. This F_{CO} force exists as long as switch n°2 has not switched to ground, canceling its existence by the dispersion of charges on the Coulomb electrode. We describe below the energy dispensed in the cycle of the piezoelectric bridge positions. We hope to show

that a usable energy $W_{ELECTRIC}$ is possible and not due to any electrical energy applied but by the dissipation of the mobile electric charges to the mass throw the switch n°2 and an R.L.C. circuit. (Fig 21)

There are two phases for this return to from z_1 to z_0 (returning phase):

1. From z_1 to z_2 where the Coulomb's force F_{CO} exist and contribute to straighten the elastic structure and to give it kinetic energy,
2. From z_2 to z_0 where this acquired kinetic energy, and the remaining energy still stored in the structure which will be dissipated by the energy spent by the Casimir force.

4.2.1 Calculation of energies between z_1 and z_2.

As soon as switch n°1 has switched to homogenize the electric charges between face 1 of the bridge and the Coulomb electrode, the resulting force F_{CO} -F_{CA} straightens this bridge and the electric charges drop. The electric voltage on the grids falls below the threshold voltage of this switch n°1 which commutes again very quickly. The energy $W_{COULOMB}$ is write:

$$WCOULOMB = WFC0 = \int_{z2}^{z1} FC0dz = \left\{ S_S . \frac{\pi^2 h c}{240} . \frac{d_{31} l_p}{a_p} \right\}^2 \left(\frac{1}{8 \pi \epsilon_0 \epsilon_r} \right) . \int_{z2}^{z1} \left[\left(\frac{1}{z_s^4} - \frac{1}{z_0^4} \right) \left(\frac{1}{z_r + z_0 - z_s} \right) \right]^2 dz_s \qquad \text{Eq28}$$

This energy exists only between the very close positions z_1 and z_2. The literal formulation of $W_{COULOMB}$ energy is possible but its expression is not convenient because it is too complex. We prefer to calculate by MATLAB its numerical value between the value z_1 and z_2.

The position z_2 of commutation of switch n°2 is deduced from the chosen threshold value V_{T2} of switch n°2. We note that we can minimize the value of the energy spent by $W_{COULOMB}$, by choosing a value of the threshold voltage V_{T2} close but slightly lower than V_{T1} of switch n°1. For example $V_{T2} = V_{T1}$- 0.05 (V).

We use MATLAB to find position z_2 of commutation of circuit 2 to cancel the Coulomb's Force F_{CO}, see (Eq 22) and figure 18. We have, at position z2 of the bridge, the electric charge in the TFT MOS. $Q_2 = \frac{d_{31} l_p}{a_p} S_S \frac{\pi^2 c h}{240} \left(\frac{1}{z_2^4} - \frac{1}{z_0^4} \right)$ with

$$Q_2 = Cox\, V_{T2} \text{ . So } z_2 = \frac{1}{\sqrt[4]{\left[\frac{240\, a_p C_{ox}}{d_{31} l_p \pi^2 c h S_S} V_{T2} + \frac{1}{z_0^4} \right]}} \qquad \text{(Eq .29).}$$

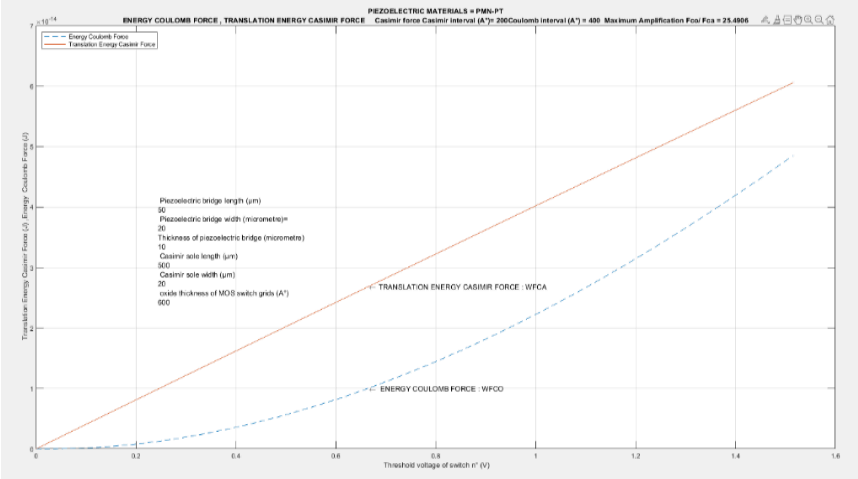

Fig 19: Energy of translation of Casimir Force and energy of Coulombs 'Force between its apparition in the position z_1 and its disappearance in position z

We present in figure 21 the curve representing the translation energy of the Casimir force as well as the Coulomb's force the time when the structure is between the positions z and z, which represents a few nanoseconds. We can calculate the energy spent in the first part of return of the structure (from z_1 to z_2) Fig 6, by simply calculating the kinetic energy W_{CIN} acquired by the structure when it reaches the position z_2 upon its return.

We know that the variation of the kinetic energy W_{CIN} is equal to the sum of all the energies supplied or spent on the moving structure. Thus, as we know the numerical value of all these participants in the variation of this kinetic energy W_{CIN}, we can write equation Eq.25 which allows us to calculate W_{CIN} because all the terms of this equation are known.

$$W_{CIN} = (W_{DFCA1} + W_{BRIDGE1}) - (W_{DFCA2} + W_{BRIDGE2}) + W_{COULOMB} - (W_{CASIMIR1} - W_{CASIMIR2}) \qquad \text{(Eq. 30)}$$

and fig 20. All the terms of the equation are known , so we now know the kinetic energy acquired by all the mobile systems in z_1 and know when the Coulomb force disappears. All calculations done, we obtain : $W_{CIN} = \frac{1}{6} S \frac{\pi^2 h c}{240} \left(\frac{1}{z_2^3} - \frac{1}{z_1^3} \right) + W_{COULOMB}$ We know now the kinetic energy acquired in z_1 and know when the Coulomb force disappears.

The structure must now spend this energy which gives it inertia. The braking energy provided by the Casimir force will cancel this kinetic inertia plus that stored in the elastic energy. Let us calculate the final ascent position z_f of the mobile structure. It has an inertia provided by the kinetic energy W_{CIN}, a stored elastic energy W_{DFCA} but is slowed down by the energy provided by the Casimir force.

We can write

$$W_{CIN} + \frac{1}{6} S \frac{\pi^2 h c}{240} \left(\frac{1}{z_2^3} - \frac{1}{z_f^3} \right) = \frac{1}{3} S \frac{\pi^2 h c}{240} \left(\frac{1}{z_2^3} - \frac{1}{z_f^3} \right) \Rightarrow W_{CIN} = \frac{1}{6} S \frac{\pi^2 h c}{240} \left(\frac{1}{z_2^3} - \frac{1}{z_f^3} \right).$$

We deduce of this equation that the final position zf of the bridge is

$$z_f = \frac{1}{\sqrt[3]{\left[\frac{1}{z_2^3} - \frac{1440\, W_{CIN}}{\pi^2 h c} \right]}} \qquad \text{Eq 31 .}$$

We can see in Figure 22 that depending on the acquired inertia, which depends on the energy provided by the Coulomb force, zf can slightly exceed its initial position. We will use this property at the end of this article in order to increase usable energy.

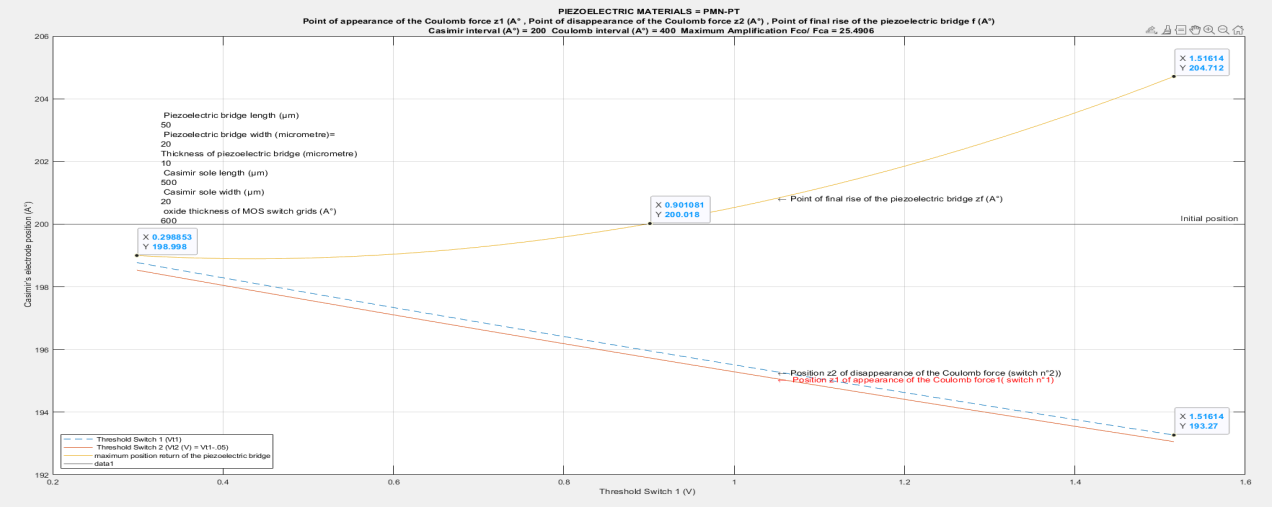

Fig 20: Positions of: 1/ The final rise z_f of the structure, 2/ of the point z_2 of disappearance of the Coulomb force depending on the threshold voltage V_{T2} of switch n°2, 3/ of the point z_1 of appearance of the Coulomb force depending on the threshold voltage V_{T1} chosen for switch n°1

It is easy to calculate the damping energy $W_{CASIMIR2}$ that appears between the intermediate position z_2 and the final position z_f.

$$\text{We have } WCASIMIR2 = \int_{z2}^{zf} FCAdz = \int_{z2}^{zf} S\,\frac{\pi^2\,h\,c}{240\,zs4}dz_S = S\left(\frac{\pi^2\,h\,c}{720}\right)\left[\frac{1}{z_f^3} - \frac{1}{z23}\right] \qquad \text{(Eq 32)}$$

As, at position z_2 the switch n° 2 commutes to ON and puts the Coulomb electrode to ground through the RLC circuit below (Fig 21). The electrical charges present on the Coulombs electrode flow towards the ground, creating a current and a power which remains to be evaluated.

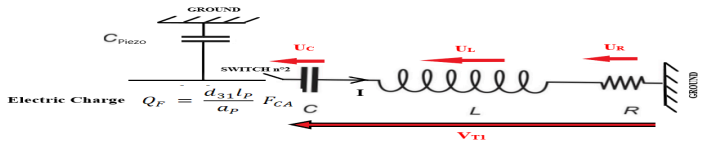

Fig 21: RLC circuit to power the autonomous electronics for converting power peaks into direct voltage

We now evaluate this usable current flowing to ground. We put in the circuit an adjustment capacitance C in series with C_{PIEZO}. We call $C_E = \frac{C_{PIEZO}\,C}{C_{PIEZO}+C}$ the equivalent capacity of the two capacities in series. When the switch n°2 commutes, we have the equation $U_C+U_L+U_R = C_{PIEZO} / Q_F = V_{T1}$ (fig 21) , with U_R= R I, U_L=L dI /dt and Q_F =U_C C_{PIEZO}. With R a resistance, L an inductance and C a capacity. After rearranging we have the following equation $\frac{d^2U_C}{dt^2} + \frac{R}{L}\frac{dU_C}{dt} + \frac{U_C}{LC} = 0$ Eq 33.

This differential equation has solutions that depend on the value of its determinant. We choose the values of R, L, C in such a way that the determinant $\Delta = \sqrt{\left(\frac{R}{L}\right)^2 - \frac{4}{LC}} = 0$ of this equation is positive

or vanishes. So, if $\Delta=0$ the solutionis: $x_1 = \frac{R}{2L}\left(-1 + \sqrt{1 - \frac{4L}{CR^2}}\right) = -\frac{R}{2L}$ and $x_2 = \frac{R}{2L}\left(-1 - \sqrt{1 - \frac{4L}{CR^2}}\right) = -\frac{R}{2L}$ then we have $x_1 = x_2 = -\frac{R}{2L}. < 0$ Considering the initial conditions, we obtain :

$$u_c = \frac{V_{T1}}{x_1 - x_2}\left[x_1\, exp(x_2 t) - x_2\, exp(x_1 t)\right] \quad \text{Eq 34}$$

$$i_c = C\frac{du_C}{dt} = C\frac{V_{T1}\, x_1 x_2}{x_1 - x_2}\left[exp(x_2 t) - exp(x_1 t)\right] \quad \text{Eq 35}$$

The peak of current is given when $d(i_c)/dt = 0$ so at the time

$$t_{imax} = \frac{Ln\left(\frac{x_2}{x_1}\right)}{x_1 - x_2} = \frac{Ln\left(\frac{1+\sqrt{1-\frac{4L}{CR^2}}}{1-\sqrt{1-\frac{4L}{CR^2}}}\right)}{\frac{R}{L}\sqrt{1-\frac{4L}{CR^2}}} \quad \text{Eq 36}$$

Replacing t by t_{imax} in the equation 34 and 35 we obtain the expression for the maximum of the voltage is $u_{cmax} = V_{T1}$ and of the maximum current i_{cmax};

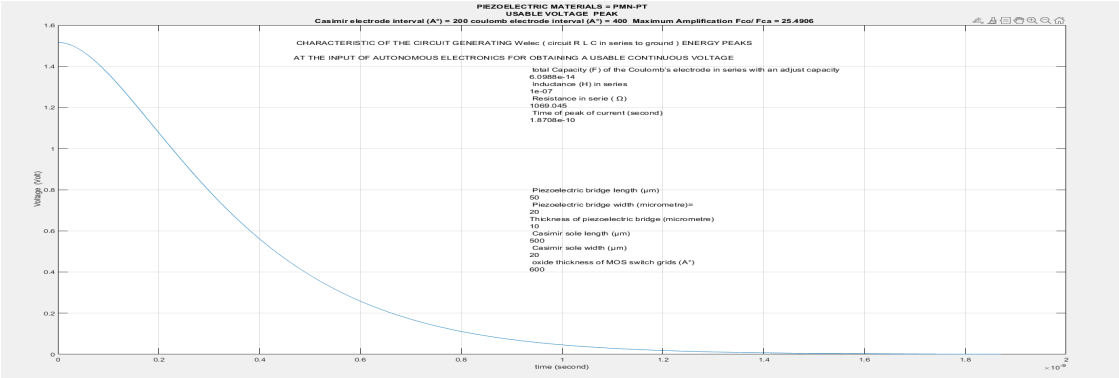

Fig 23: The electric current flowing through the capacitance C in series with the capacitance of the Coulomb electrode

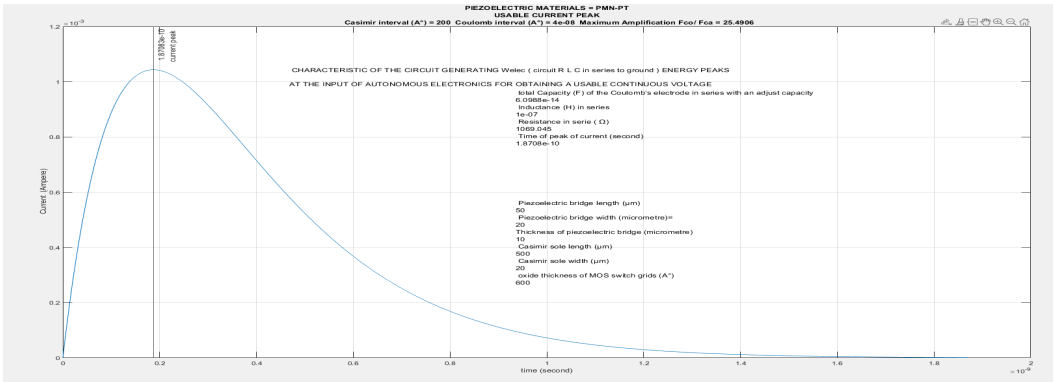

Fig 23: The electric current flowing through the capacitance C in series with the capacitance of the Coulomb electrode

The electrical power of the signal is:

$$P(t) = u_c\, i_c = \left(\frac{V_{T1}}{x_1 - x_2}\right)^2 C\, x_1 x_2 \left[\, exp(x_2 t) - exp(x_1 t)\right]\left[x_1\, exp(x_2 t) - x_2\, exp(x_1 t)\right] \qquad \text{Eq 37}$$

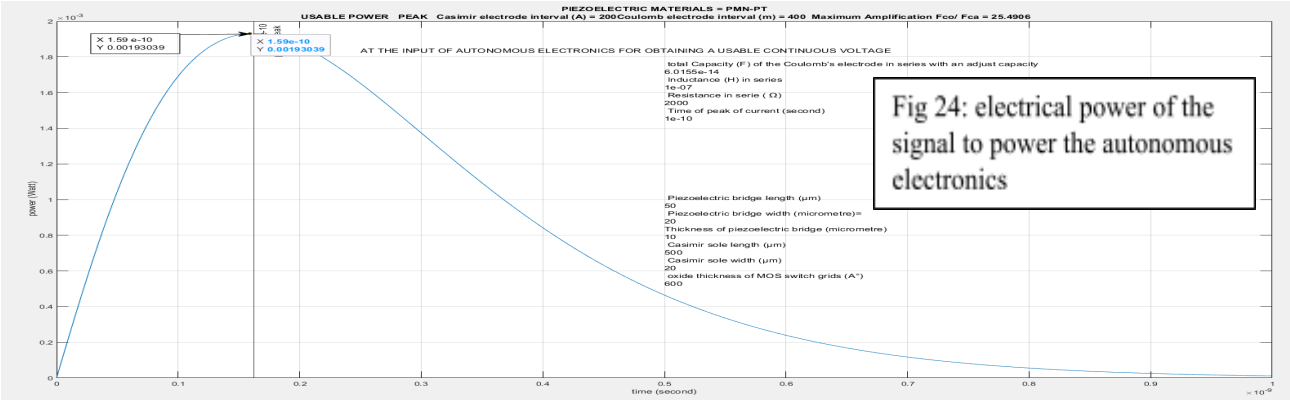

Fig 24: electrical power of the signal to power the autonomous electronics

Fig 24: Electrical power of the signal to power the autonomous electronics

We note on Fig 23 and 24 that the maximum t_{imax} = 1.87 10^{-10} (s) for the peak current is different than those t_{pmax} = 3.03 10^{-10} s for the peak power P(t). The peak power of 1.93 mW is sufficient to power the autonomous electronics of fig 30,31 and obtain a useful voltage of several volts in a few milliseconds. The period of a vibration being (fig 10) of 0.2 µs for an F_{CO} /F_{CA} of simply 2, the average power over a period is then approximately ≈ 0.3 µW.

We deduce that the power provided by the system in 1 second is of the order of 3e-7 / 2e^{-7} ≈ 1.5 W.

Knowing the electrical power P(time) we can numerically evaluate this finale and usable energy, by MATLAB.We obtain $W_{ELECTRIC}$ in fig 25.

$$W_{ELECTRIC}(t) = \int_0^{10^* t_{max}} u_c\, i_c\, dt = \left(\frac{V_{T1}}{x_1 - x_2}\right)^2 C\, x_1 x_2 \int_0^{10^* t_{max}} \left[\, exp(x_2 t) - exp(x_1 t)\right]\left[x_1\, exp(x_2 t) - x_2\, exp(x_1 t)\right] dt$$

Eq38

The energy balance is completed for the "return" phase to its initial position of the structure.

$$\text{We have } W_{RETURNING} = W_{CIN} + W_{ELECTRIC} + W_{DFCA2} + W_{BRIDGE2} - W_{CASIMIR2} + \Delta Q_{vib}/2 \qquad \text{(Eq 39)}$$

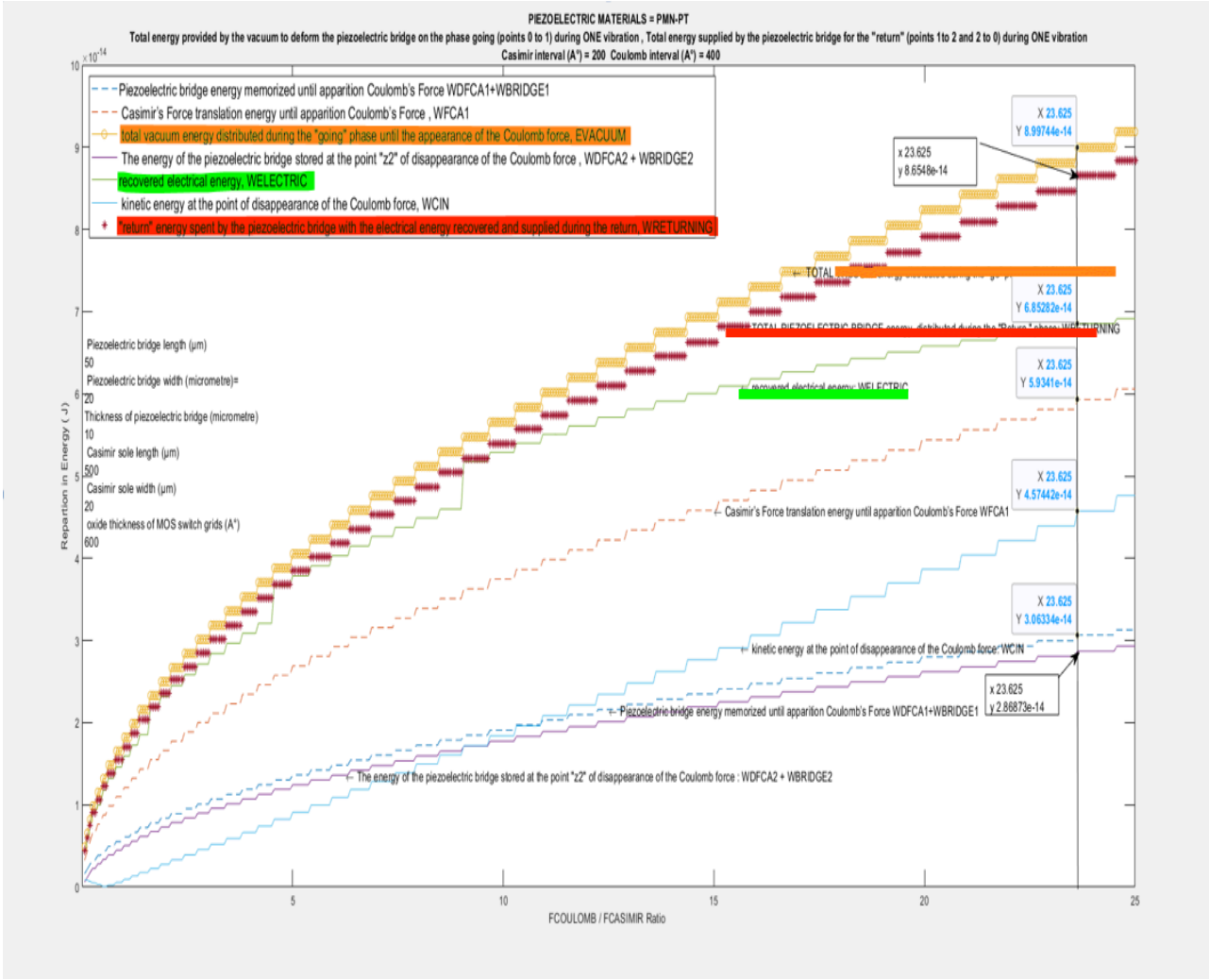

Fig 25: Balance of the energies of the "go" and "return" phases for the proposed MEMS which seems to be able to "extract energy from the quantum vacuum."

With Figure 25, we can make the energy balance of the energies provided by the quantum vacuum in the "going" and "returning" phases. The constant energy provided by the quantum vacuum ocean in the "go" phase simply changes its nature and subdivides into other energies in the "return" phase of vibrations. One of these energies in this "return" phase can be used by creating a little electrical energy.We note that the energy necessary for the perpetual maintenance of these vibrations is constantly provided by the isotropic and timeless energy of the quantum vacuum and that it is possible to extract from this gigantic ocean of energy of "nothing" a small electrical and exploitable energy. Whatever the F_{CO}/F_{CA} amplification factor, we note that $W_{RETURNING}$ is always slightly lower than E_{VACUUM}, thanks to the choice of $W_{ELECTRIC}$

We observed that in the referential of our 4 dimensions Space-Time plus the Quantic Vacuum, the energy is conserved which is consistent with Noether's theorem.This very important theorem of 1905 explains why, as Monsieur de Lavoisier said, "Nothing is created, nothing is lost, everything is transformed."

Remember that energy is defined as the "physical quantity that is conserved during any transformation of an isolated system. However, the system constituted by simply the MEMS device in space is not an isolated system while the system constituted by the MEMS device plus the space plus the energy vacuum seems an isolated system. The part of the MEMS energy sensor vibrates at frequencies

depending on the size of the structure and operating conditions, but with an amplitude of just a few Angstroms. These vibrations aren't perpetual motion; they can be continuously powered by vacuum energy from the Casimir force.

The following diagram summarizes the operation of this presented MEMS (Fig 26 and Fig 27)

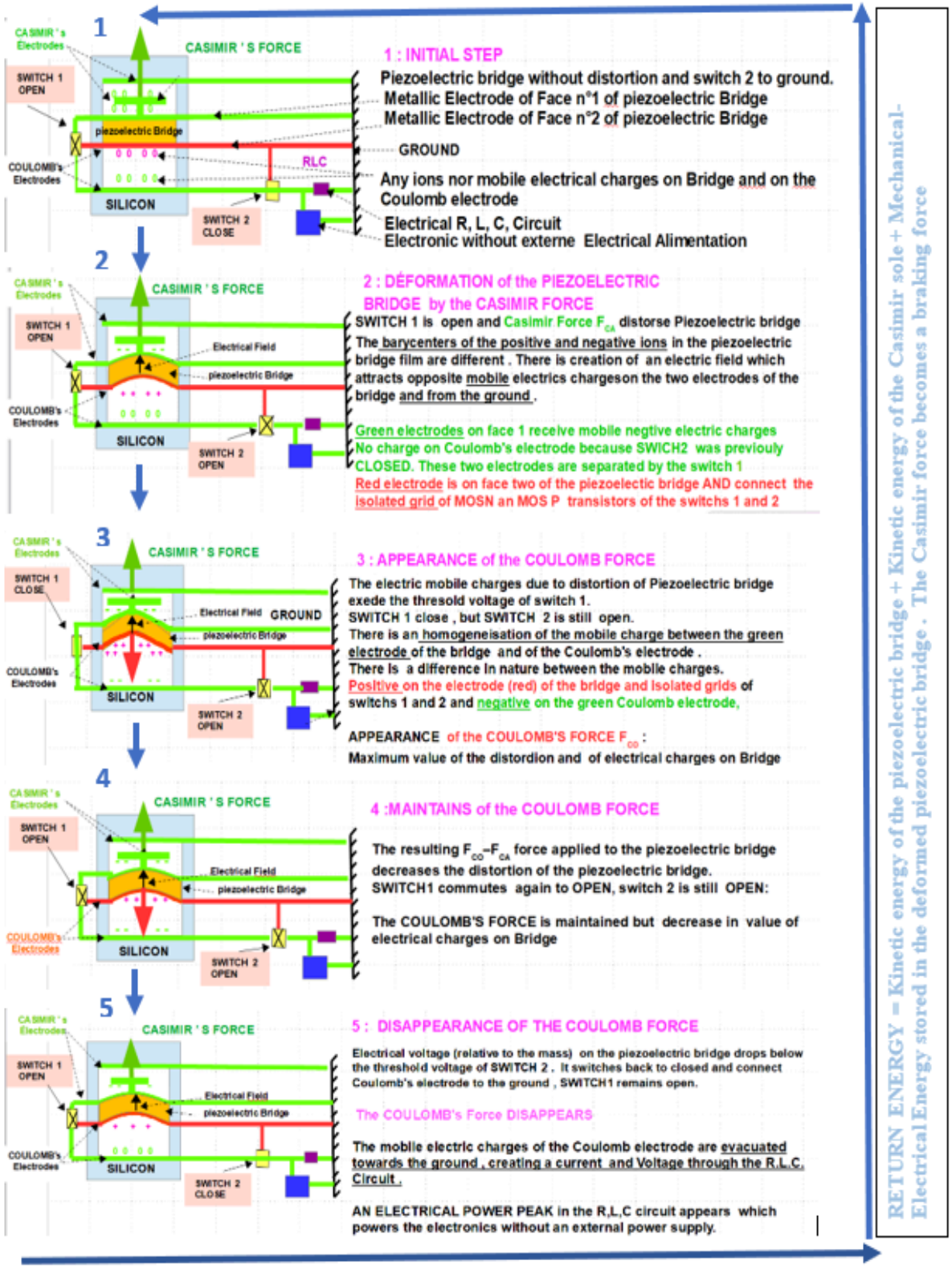

Fig. 26: Overview of the 5 successive and repetitive steps of the M.E.M.S.

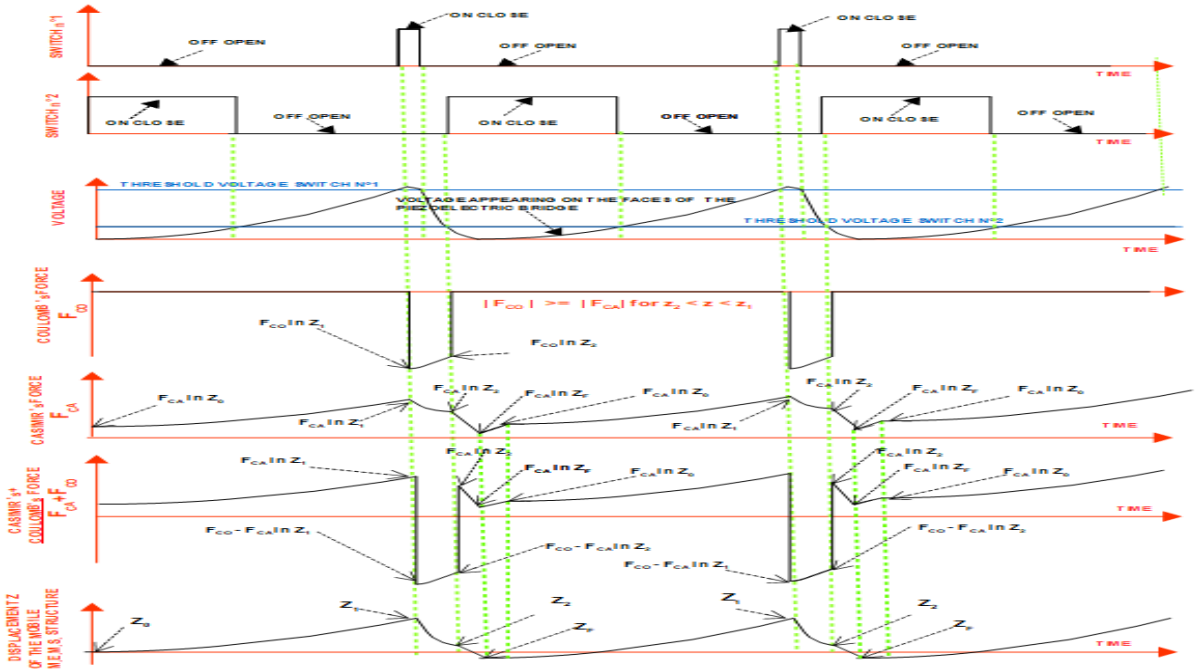

Fig. 27: Shape of the curves representing 1/ The switching of the two switches 2/ The electrical voltage on face 1 of the piezoelectric bridge 3/ The Casimir forces F_{CA} 4/ The coulomb forces F_{CO} 5/ the energies W_{FCO}, W_{FCA} , W_{FCO} -W_{FCA} 6/ The maximum elevation z_f of the moving part

We notice in the previous pages that the piezoelectric bridge could reach a position z_f which exceeds its initial position z_o. We can take advantage of this observation by modifying the moving part of this MEMS to provide the RLC circuit with the two signs of current peak and voltage emitted by the sensor. This modification should increase the continuous electrical voltage on the capacitive output of the autonomous electronic circuit whose role is to transform the signals from the quantum vacuum energy sensor(fig 28)

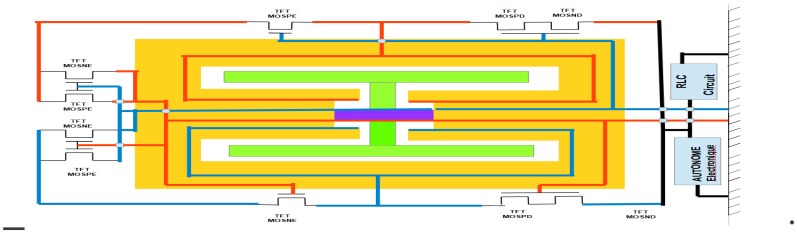

Fig. 28: Shape of the MEMS circuit making it possible to double the direct voltage at the output of the autonomous electronic circuit, by providing it with consecutive voltage and current peaks of opposite sign.

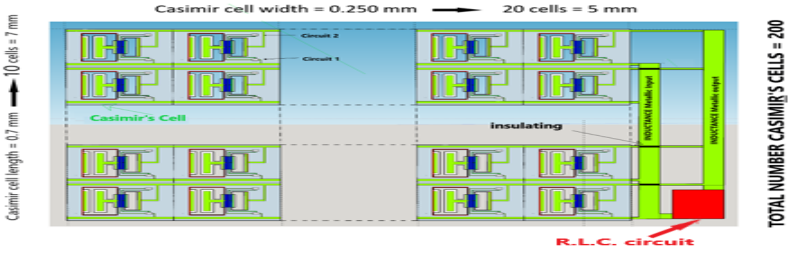

Figure 29: Positioning of 20 Casimir cells in parallel and 10 in series. Total of Casimir cells delivering a periodic current during a small part of the vibration frequency of the devices = 200. Total des cellules = 200, Width = 5mm, Length = 7 mm

In order to obtain a current peak greater in intensity, the Casimir cells can be positioned in a series and parallel network at the 2 terminals of a single and as described RLC circuit for example, 20 Casimir cells can be placed in parallel and 10 in series, (Figure 29).Important increase in current intensity, time duration of the peak, as of the voltage peak. This work on the energy balance of a M.E.M.S., which appears to be able to extract energy from a new, totally unexploited source, was carried out completely alone and without the help of any organization, by an old retiree. It seems that - unless there is always a possible error - the fundamental theorem of EMMY NOETHER from 1905 is not contradicted. In the event of a theoretical confirmation by specialists, the supreme and definitive judgement will be the realization of a prototype, and I will be happy to participate in this development.

V. AUTONOMOUS ELECTRONICS TO TRANSFORM THE CYCLIC POWER PEAKS FROM THE R.L.C CIRCUIT

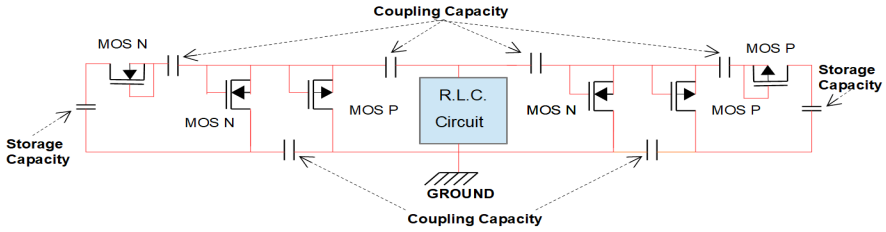

Figure 30: Principle of the single-stage doubler without power supply electrical diagram. All the MOS are isolated from each other by etching on an S.O.I wafer, and their threshold voltage is as close as possible to ground

The circuit of the figure 30 is an autonomous device operating without any electrical power source. It rectifies and accumulates the repetitive peak power delivered to the terminals of the RLC circuit in the figure 4 and 5 and transforms them into a usable direct voltage source.

The impedance of the output of this autonomous circuit must be important.

We note the extreme weakness of the electrical power required at the start of the conversion of the power peaks (60 nW) and at the end (2 pW). This transformation require 4

The circuit of the figure 30 is an autonomous device operating without any electrical power source. It rectifies and accumulates the repetitive peak power delivered to the terminals of the RLC circuit in the figure 4 and 5 and transforms them into a usable direct voltage source. The impedance of the output of this autonomous circuit must be important .

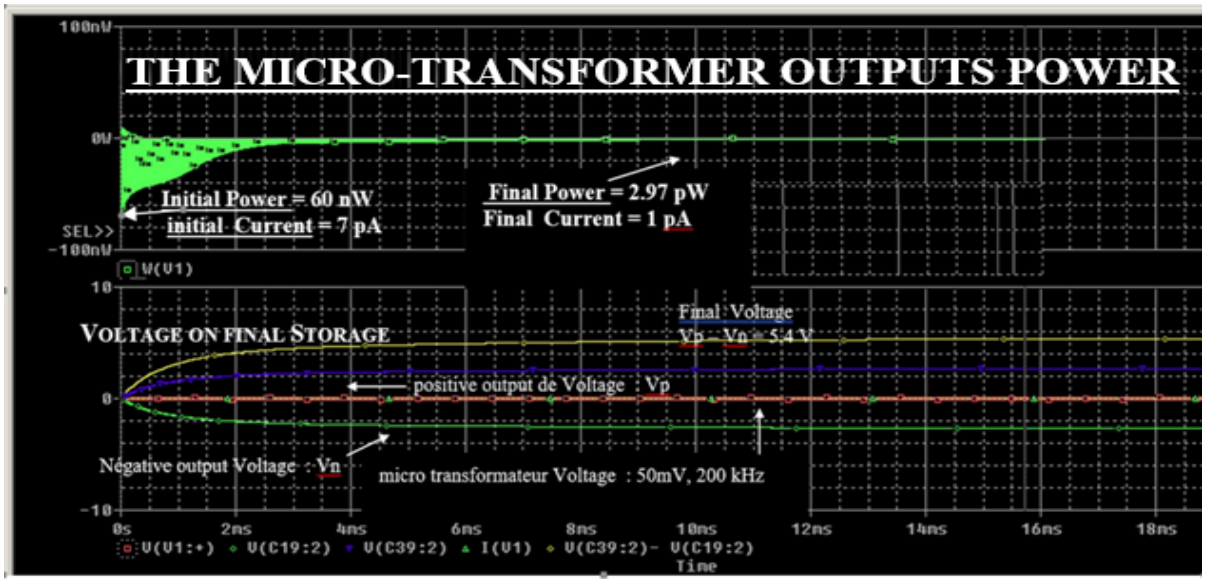

Figure 31: SPICE simulations of voltages, current, power consumed by the autonomous electronics for the transformation into direct voltage (5.4 V) of an alternating input signal of 50 mV, frequency = 150 kHz, number of stages = 14, coupling capacities = 20 pF, storage capacity = 10 nF.

We note the extreme weakness of the electrical power required at the start of the conversion of the power peaks (60 nW) and at the end (2 pW). This transformation require 4 milliseconds

Table 1: Output Continuous voltage, with current and power consumed by the autonomous electronic in function of two input cyclic voltage parametrized with the number of stages

CHARACTERISTICS OF OUTPUT VOLTAGES (V), POWERS (nW) CURRENTS (nA)
AS A FUNCTION OF THE NUMBER OF STAGES
INPUT SIGNAL FREQUENCY = 150 kHz OUTPUT VOLTAGE MEASUREMENT FOR t = 50 ms

	Vg=50mV					Vg=100mV				
number of stages	Output Voltage	Current (nA) start	Current (nA) end	Power (nW) start	Power (nW) end	Output Voltage	Current (nA) start	Current (nA) end	Power (nW) start	Power (nW) end
2 *3	550mV	300nA	26nA	15nW	1.3nW	1.1v	800nA	46nA	75nW	5nW
2 *6	1	300nA	29nA	13nW	1.3nW	2V	700nA	67nA	60nW	6.5nW
2 *14	2.2v	300nA	40nA	14nW	2.6nW	4,5v	700nA	50nA	65nW	4.8nW
2 *21	2.8v	250nA	38nA	13nW	860pw	6v	600nA	80nA	60nW	2.7nW
2 *30	3.3	250nA	43nA	12nW	1.2nW	6.5V	750nA	85nA	61nW	4nW
2 *39	3.5v	250nA	45nA	12nW	900pW	7.5V	750nA	95nA	64nW	3.5nW
2 *48	3.6v	250nA	46nA	12nW	1nW	7.6V	750nA	100nA	60nW	4.2nW
2 *60	3.8	270nA	47nA	12nW	1.1nW	7.9V	700nA	90nA	65nW	4.2nW
2 *61	3.8	270nA	48nA	12.1nW	1.3nW	8V	700nA	90nA	65nW	42nW

The interesting points for the presented electronics' device are:

1. The low alternative input voltages required to obtain a continuous voltage of several volts at the output
2. The low power and current consumed by this conversion and amplification circuit on the source which in this case is only R.L.C. circuit, supplied by the current peaks generated by the autonomous vibrations.
3. The rapid time to reach the DC voltage (a few tens of milliseconds)

The technology used to fabricate the TFT (Thin Film Transistors) [11] MOSNE and MOSPE transistors with the lowest possible threshold voltages, is CMOS on intrinsic S.O.I. and each element are isolated from each other on independent islands. This technology, represented in the following figure 54, strongly limits the leakage currents.

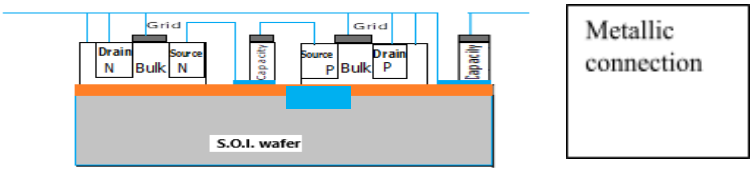

Figure 32: S.O.I technology for making the elements of the "doubler"

We note that the coupling capacities of 20 pF of this electronic, like that of storage of the order of 10 nF, have relatively high values. To minimize the size of these capacitor we propose to use of titanium dioxide as insulator, with a relative permittivity of the order of 100 which is one of the most important for a metal oxide, then the size of the capacity passes to 33 µm for a thickness of TiO2 = 500 A °, which is more reasonable.

IV. TECHNOLOGY OF REALIZATION OF THE CURRENT EXTRACTOR DEVICE USING THE FORCES OF CASIMIR IN A VACUUM

For the structures presented above, the space between the two surfaces of the reflectors must be of the order of 200 A °, ... which is not technologically feasible by engraving. *Yet it seems possible to be able to obtain this parallel space of the order of 200 A ° between Casimir reflectors, not by etching layers but by making them thermally grow.* Indeed, the S_{S3} and S_{S2} surfaces of the Casimir reflector must;

- Be metallic to conduct the mobile charges
- insulating as stipulated by the expression of Casimir's law who established for surfaces without charges.
- This should be possible if we grow an insulator in the z direction of the structure, for example Al_2O_3 or TiO_2 or other oxide metal which is previously deposited and in considering the differences in molar mass between the oxides and the original materials.

For example, silicon has a molar mass of 28 g/mol and silicon dioxide SiO2 of 60 g/mol. It is well known that when a silicon dioxide SiO2 grows by one unit, a silicon depth of about 28/60 = 46.6%. This means that the fraction of oxide thickness "below" the initial surface is 46% of the total oxide thickness according to S.M. Sze. [9] The same must happen, for example for thermal growth of alumina. The molecular masses of Alumina and aluminium are M_{Al2O3} = 102 g/mole and M_{Al} = 27 g/mole. We obtain an aluminium attack ratio of 27/102 = 26%, which implies that the original surface of this metal has shifted by 26% so that 74% of the alumina has grown out of the initial surface of the aluminiu. As regards the technological manufacture of electronics and structure, it therefore seems preferable:

For electronics to choose Titanium Oxide because of its high relative permittivity ε_r =114 allowing to minimize the geometries required for the different capacities.

For the Casimir structure, the choice of aluminium, because its low density increases the resonant frequency of the structure and that 74% of the Alumina Al2O3 is outside the metal, allowing to reduce the interface between Casimir electrodes. A simple calculation shows for example that for aluminium gives:

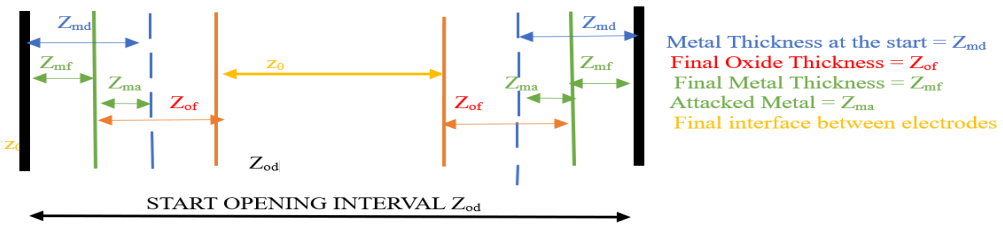

Figure 33: distribution of thicknesses

$$z_{od} = 2(z_{md} + z_{of} - z_{ma}) + z_o = 2[z_{md} + (1-0.26)\, z_{of} + z_o \Rightarrow z = z_{od} - 2(z_{md} + 0.74\, z_{of})$$

For example, we start from an opening z_{od} = 3 µm. We deposit a metal layer of aluminium that is etched leaving a width z_{md} = 1 µm on each side of the reflector. Then an Alumina Al_2O_3 can grow, the thickness of which is precisely adjusted, simply by considerations of time, temperature, and pressure to increase a necessary thickness to have the desired interface z_o. For example, if z_o = 200A °, z_{od} = 3 µm, z_{md} = 1 µm, then z_{of} = 0.662 µm. So, we obtain a Casimir interface of 200 A°. The final remaining metal thickness will be z_{mf} = 0.338 µm and will act as a conductor under the aluminium oxide.

Obviously, the growth of this metal oxide between the electrodes of the Casimir reflector modifies the composition of the dielectric present between these electrodes, therefore of the mean relative permittivity of the dielectric Let: ε_o be the permittivity of vacuum and ε_o. ε_r the metal oxides one (ε_r = relative permittivity ≅ 8 in the case of Al_2O_3), z_{of} the final oxide thickness on one of the electrodes and z the thickness of the vacuum present between electrode, (initially we want z = z_o).

Then the average permittivity e_{om} of the dielectric is:

$$\varepsilon_{Om} = \frac{z_{qf}\,\varepsilon_0\,\varepsilon_r + z_0\,\varepsilon_0 + z_{qf}\,\varepsilon_0\,\varepsilon_r}{(2\,z_{qf} + z_0)} = \varepsilon_0 \frac{(2\,z_{qf}\,\varepsilon_r + z_0)}{(2\,z_{qf} + z_0)} \simeq \varepsilon_0\,\varepsilon_r$$, because z_o is << z_{of}...

For example, z_{of} = 6620 A° is large compared to z <= 200A ° therefore ε_{om} ≅ 8 * ε_o in the case of Al_2O_3.

We have considered this change in permittivity in the preceding simulations.

VII. STEPS FOR THE REALIZATION OF THE STRUCTURE AND ITS ELECTRONICS

We use an SOI wafer with an intrinsic silicon layer: The realisation start with voltage "doubler" is obtained by using CMOS technology with 8 ion implantations on an SOI wafer to make:

1 /The sources, drains_of the TFT MOSNE, MOSND of the "doubler" and of the Coulomb force trigger circuits and of the grounding

2 / The source, drains of the MOSPE, MOSPD of the "doubler" and of the Coulomb force trigger circuits

3 / The best adjust the zero-threshold voltage of the MOSNE of the "doubler" circuit

4 / The best adjust the zero-threshold voltage of the MOSPE of the "doubler" circuit

To define the threshold volta e of the MOSNE of the circuit n°1

7 / To define the threshold voltage of the MOSND of the circuit n°2

8 / to define the MOSPD threshold voltage of the circuit n°2

This electronic done, we take care of the vibrating structure of CASIMIR

9 / engrave the S.O.I. silicon to the oxide to define the location of the Casimir structures (figure 34)

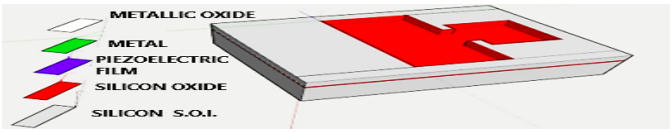

Figure 34: 9/ Etching of S.O.I silicon

10/ Place and engrave a protective metal film on the rear faces of the S.O.I wafer (figure 35)

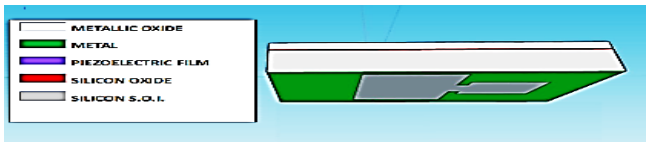

Figure 35: 10/ Engraving of the protective metal rear face of the S.O.I. silicon

11 / Deposit and engrave the piezoelectric layer (figure 36)

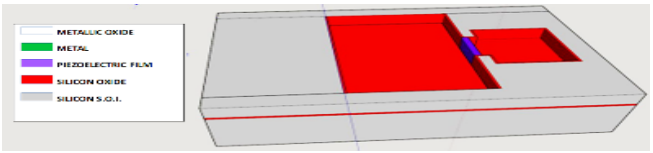

Figure 36: 11/deposition and etching of the piezoelectric layer deposition and etching of the piezoelectric layer

12/ Depose and etch the metal layer of aluminium (figure 37).

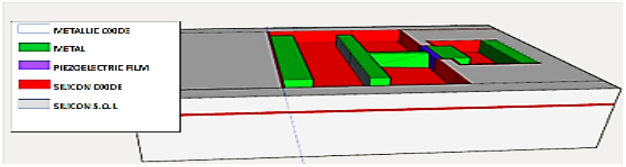

Figure 37: 12/ Metal deposit, Metal engraving etching of the piezoelectric layer

13 /Plasma etching on the rear side the silicon of the Bulk and the oxide of the S.O.I wafer protected by the metal film to free the Casimir structure then very finely clean both sides (figure 38)

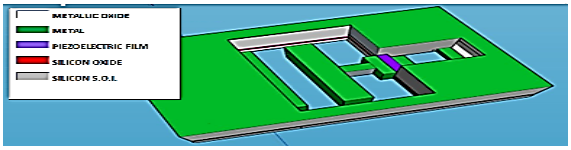

Figure 38: 13/ view of the Casimir device on the rear face, engraving on the rear face of the structures.

14 /Place the structure in a hermetic integrated circuit support box and carry out all the bonding necessary for the structure to function.

15 /Carry out the thermal growth of aluminium oxide Al_2O_3 with a measurement and control of the circuit under a box. The electronic circuit should generate a signal when the interface between the Casimir electrodes becomes weak enough for the device to vibrate ... and then stop the oxidation. (Figure 39)

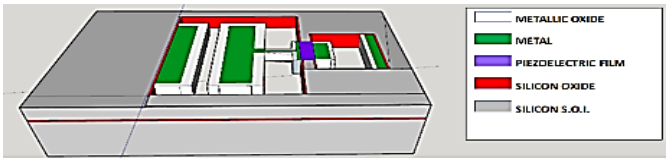

Figure 39: 14 /Adjusted growth of metal oxide under the electronic control, front view of the Casimir device

16 /Create a vacuum in the hermetic box

In the case where the 2 metal electrodes of Casimir, adhere to one another, they can be separated by the application of an electrical voltage on the Coulomb's electrodes.

VIII. CONCLUSION

The theoretical results of this project seem sufficiently encouraging to justify the development of prototypes. While theoretical results indicate promising potential, further experimental validation is necessary to confirm the feasibility of harnessing quantum vacuum energy. Future work will focus on developing prototypes and refining the theoretical models to address practical implementation challenges. Of course, if these theoretical predictions are confirmed, it will trigger a scientific, technical and human revolution, because the quantum vacuum could be used as a new source of energy both on Earth and in space with a considerable commercial market. As an inventor who has kept some details confidential, I would like to collaborate in its development after signing a contract with the potential investor

In the universe, everything is energy, everything is vibration, from the infinitely small to the infinitely large" Albert Einstein. "A person who has never made mistakes has never tried to innovate." Albert Einstein

BIBLIOGRAPHY

1. Fluctuations du vide quantique : Serge Reynaud Astrid Lambrecht (a), Marc Thierry Jaekel (b) a/ Laboratoire Kastler Brossel UPMC case Jussieu F Paris Cedex 05, b/Laboratoire de Physique Théorique de l'ENS 24 rue Lhomond F 75231 Paris Cedex 05, Juin 2001.
2. On the Attraction Between Two Perfectly Conducting Plates. H.B.G. Casimir, *Proc. Kon. Nederl. Akad. Wet.* 51 793 (1948)
3. Casimir force between metallic mirrors | Springer Link. E.M. Lifshitz, *Sov. Phys. JETP* 2 73 (1956); E.M. Lifshitz and L.P. Pitaevskii, *Landau and Lifshitz Course of Theoretical Physics: Statistical Physics Part 2* Ch VIII (Butterworth-Heinemann, 1980)

4. Direct measurement of the molecular attraction of solid bodies. 2. Method for measuring the gap. Results of experiments B.V. Deriagin (Moscow, Inst. Chem. Phys.), I.I. Abrikosova (Moscow, Inst. Chem. Phys.)Jul, 1956 B. V. Deriagin and I.I. Abrikosova, *Soviet Physics JETP* 3 819 (1957)
5. Techniques de l'Ingénieur 14/12/2012: l'expertise technique et scientifique de référence « Applications des éléments piézoélectriques en électronique de puissance » Dejan VASIC : *Maître de conférences à l'université de Cergy-Pontoise, Chercheur au laboratoire SATIE ENS Cachan,* François COSTA: Professeur à l'université de Paris Est Créteil, Chercheur au laboratoire SATIE ENS Cachan
6. Wachel, J. C., and Bates, C. L., "Techniques for controlling piping vibration failures", ASME Paper, 76-Pet-18, 1976.
7. Jayalakshmi Parasuraman, Anand Summanwar, Frédéric Marty, Philippe Basset, Dan E. Angelescu, Tarik Bourouina «Deep reactive ion etching of sub-micrometre trenches with ultra-high aspect ratio Microelectronic Engineering» Volume 113, January 2014, Pages 35-39
8. F. Marty, L. Rousseau, B. Saadanya, B. Mercier, O. Français, Y. Mitab, T. Bourouina, «Advanced etching of silicon based on deep reactive ion etching for silicon high aspect ratio microstructures and three-dimensional micro- and nanostructure» Microelectronics Journal 36 (2005) 673–677.
9. Semiconductor Devices, Physics' and Technology S. M. SZE Distinguished Chair Professor College of Electrical and Computer Engineering National Chiao University Hsinchu Taiwan, M.K. LEE Professor Department of Electrical Engineering, Kaohsiung Taiwan
10. (M. BARTHES, M. Colas des Francs SOLID MECHANICAL VIBRATIONAL PHYSICS, ESTP: (Special School of Public Works)
11. Modélisation de transistors polysilicium en couches minces sur isolants: conception et réalisation d'écrans plats à cristaux liquides et matrices actives, Auteur Patrick Sangouard, Thèse de doctorat Paris 11, Soutenance en 1987, président du jury René Castagné https://theses.fr/1987PA112461

Pharmacognostic Standardization and Quality Profiling of *Mangifera indica* Bark Powder for Comprehensive Analysis of Alzheimer Disorder

Shivani Agarwal, Rahul Chauhan, Shivam Kumar Gupta, Neha Saxena, Sonam & Ajay Kumard

ABSTRACT

The therapeutic efficacy of medicinal plants is attributed to polyphenolic chemicals, which are essential bioactive components. The bark of the mango plant, Mangifera indica, is a rich source of polyphenols that have antibacterial, anti-inflammatory, and antioxidant properties. For plant-derived products to be consistent, effective, and quality controlled, however, thorough phytochemical standardisation is necessary. The purpose of this research is to provide a comprehensive phytochemical profile by utilising High-Performance Liquid Chromatography (HPLC) to analyse and interpret the polyphenolic content of Mangifera indica bark powder.Mangifera indica bark powder methanolic extracts were made and then separated chromatographically using HPLC in conjunction with photodiode array (PDA) detection. Acetonitrile and aqueous formic acid were used as the mobile phase in a gradient elution technique using a reverse-phase C18 column. Major polyphenolic components, such as Mangifera, quercetin, gallic acid, catechin, and ellagic acid, were identified and quantified using standard reference compounds using UV detection at 280 nm. The structural identity and fragmentation patterns of the identified polyphenols were further confirmed by LC-MS analysis.According to the study,Mangifera is the main component of Mangifera indica bark, which is a strong source of polyphenolic chemicals. Researchers studied the pharmacognostic characteristics of Mangifera indica's bark.

Keywords: *Mangifera indica*, HPTLC, quality control, polyphenols, m*angiferin*, flavonoids, phytochemical standardization.

Classification: LCC Code: HC110.E5

Language: English

Great Britain Journals Press

LJP Copyright ID: 925652
Print ISSN: 2631-8490
Online ISSN: 2631-8504

London Journal of Research in Science: Natural & Formal

Volume 25 | Issue 5 | Compilation 1.0

Pharmacognostic Standardization and Quality Profiling of *Mangifera indica* Bark Powder for Comprehensive Analysis of Alzheimer Disorder

Shivani Agarwal[α], Rahul Chauhan[σ], Shivam Kumar Gupta[ρ], Neha Saxena[Ↄ], Sonam[§] & Ajay Kumar[ν]

ABSTRACT

The therapeutic efficacy of medicinal plants is attributed to polyphenolic chemicals, which are essential bioactive components. The bark of the mango plant, Mangifera indica, is a rich source of polyphenols that have antibacterial, anti-inflammatory, and antioxidant properties. For plant-derived products to be consistent, effective, and quality controlled, however, thorough phytochemical standardisation is necessary. The purpose of this research is to provide a comprehensive phytochemical profile by utilising High-Performance Liquid Chromatography (HPLC) to analyse and interpret the polyphenolic content of Mangifera indica bark powder.Mangifera indica bark powder methanolic extracts were made and then separated chromatographically using HPLC in conjunction with photodiode array (PDA) detection. Acetonitrile and aqueous formic acid were used as the mobile phase in a gradient elution technique using a reverse-phase C18 column. Major polyphenolic components, such as Mangifera, quercetin, gallic acid, catechin, and ellagic acid, were identified and quantified using standard reference compounds using UV detection at 280 nm. The structural identity and fragmentation patterns of the identified polyphenols were further confirmed by LC-MS analysis.According to the study,Mangifera is the main component of Mangifera indica bark, which is a strong source of polyphenolic chemicals. Researchers studied the pharmacognostic characteristics of Mangifera indica's bark. Organoleptic studies of the air-dried bark powdered rind revealed character like brown colour, sweet odour and unique flavour taste. The physicochemical characteristics, which include drying loss, values for total ash, acid-insoluble ash, water-soluble ash, swelling index, and foaming index, were analyzed. Investigate the solubility and extractive value of various solvents, such as methanol, ethanol, hydroalcohol, ethyl acetate, petroleum spirit, water and hexane. The ethanol solvent was found to have a higher extractive value. Flavonoids were found in the aqueous extract according to a preliminary phytochemical investigation.

Keywords: *Mangifera indica*, HPTLC, quality control, polyphenols, m*angiferin*, flavonoids, phytochemical standardization.

Author α σ ρ: Moradabad Educational Trust Group of Institutions Faculty of Pharmacy, Moradabad, 244001.
Ↄ §ν: Moradabad Institute of Technology College of Pharmacy, Moradabad, 244001.

London Journal of Research in Science: Natural & Formal

Graphical Abstract

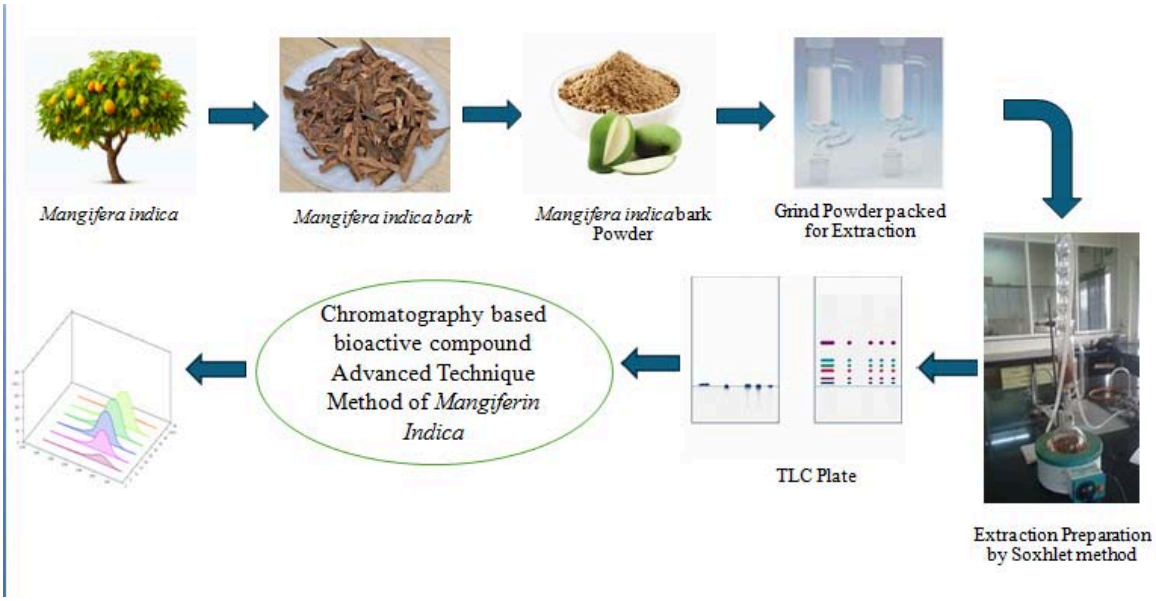

Figure 1: Graphical representation of extraction of *Mangifera indica* bark powder extract with advanced spectroscopic techniques.

I. INTRODUCTION

A vital source of compounds used as food additives, agrochemicals, medications, flavourings, aromas, colours, and biopesticides, plants produce secondary metabolites, which are biosynthetically produced from primary metabolites. The medicinal plants shown a wide variety of pharmacological and therapeutic effects, according to recent papers (1-6). Protein, carbohydrates, glycosides, phenol, volatile oil, alkaloids, flavonoids, phlobatannins, terpenoids, tannins, and resins were all detected by phytochemical screening of *Mangifera indica*. Immunomodulatory, cardiovascular, hypolipidemic, anti-obesity, anti-cancer, antidiabetic, reproductive, dermatological, antioxidant, hepatoprotective, nephroprotective, CNS and neuro-protective, gastrointestinal, anti-anemic, and anti-snake venom activity were just a few of the many pharmacological actions of *Mangifera indica*. The purpose of this review was to highlight *Mangifera indica's* pharmacological action and chemical components (7). In terms of export volume, the three most traded tropical fruits worldwide in 2021 were pineapple, avocado, and mango, according to the Food and Agriculture Organisation of the United Nations (FAO) (8). With 2.3 million tonnes exported that year, mangoes made up 29% of the total among mangos, mangosteen, and guava, representing a 1.9% increase over the previous year (8).That indicates the economic significance of fruits in the market. Postharvest losses result in financial losses for farmers, distributors, and the agricultural sector because of the fruit's perishable nature, microbial deterioration, issues with transportation, marketing, and overall unfavourable handling circumstances (9,10,11,12). Based on FAO estimates, worldwide (13), "With the exception of the retail stage, 13.8% of the food produced in 2016 was lost from the farm.which fruits and vegetables make up nearly 21%. Dehydration is used as a conservation technique because of the fruit's market value and inherent propensity to deteriorate (14). is significant because it makes it possible to produce fruit that keeps better for longer than fresh fruit (15). This reduces losses in terms of money and goods. Fruit preservation is difficult, though, because conventional methods of dehydration, like convective hot air drying, can change the fruit's physicochemical characteristics, nutritional value, and sensory qualities, such as colour, texture, flavour, and perfume(9). by causing the fruit to lose volatile and heat-sensitive substances due to exposure to high temperatures (16); additionally, airflow drag can transfer substances that dissolve in the media from the solid (17).

Hence, it is necessary to determine the distinctions between products dehydrated using convective hot air drying and alternatives such freeze-drying and the reactance window.

Freeze-drying process operates in ultra-vacuum with the use of pre-frozen substance (18), water from which is extracted through the sublimation of ice into steam and not through its liquid phase (19).According to the Spanish original, "it is based on the use of water as the main means for power transfer" (20). Reactance window technology uses radiating hot water through a transparent sheet to transfer heat that comes into interaction with the food that will be dried under atmospheric pressure. The film in question is a Mylar® film (21).

In light of this, the study's objective is to assess several methods of dehydrating mango (Mangifera indica) using a Systematic Literature Review (SLR) in order to ascertain how they affect the fruit's physicochemical, nutritional, and sensory qualities, which act as quality indicators (22). It also aims to analyse bibliographic information, such as pertinent keywords, authors, years of publication, products, fields of use, and mango varieties used.

Because they now have a broad guideline to assess which technology is best considering the process's operating conditions and the intended qualities of the final productthis paper seeks to be beneficial to entrepreneurs and industrialists.

A **B**

Figure 2: (A) Whole plant of *Mangifera indica* (B) *Mangifera indica*Bark

II. ROLE OF *MANGIFERA INDICA* IN NEURODEGENERATIVE DISEASE

Neurodegenerative illnesses like Huntington's disease (HD), Parkinson's disease (PD), Alzheimer's disease (AD), multiple sclerosis (MS), and amyotrophic lateral sclerosis (ALS),Thus make a characterized of a pathologies group by separate etiologies with pathophysiological characteristics and unique morphological characteristic.There are many pieces of evidence that indicate the multifactorial conditions which encompass (a) aberrant protein dynamics with impaired protein aggregation and degradation, (b) oxidative stress and free radical production, (c) mitochondrial dysfunction and dysfunctional bioenergetics, and (d) metal toxicity and pesticide exposure as potential etiologies of these disorders (23).

Mangiferin, quercetin, and gallic acid are bioactive compounds found in mangos (Mangifera indica) that have neuroprotective properties. According to research, these substances may be able to stop oxidative stress, inflammation, and β-amyloid aggregation—all of which are major contributors to neurodegenerative illnesses including Parkinson's and Alzheimer's. Mango extracts may be a natural treatment for neurodegenerative diseases since they have been demonstrated to enhance cognitive function and prevent neuronal damage(23).

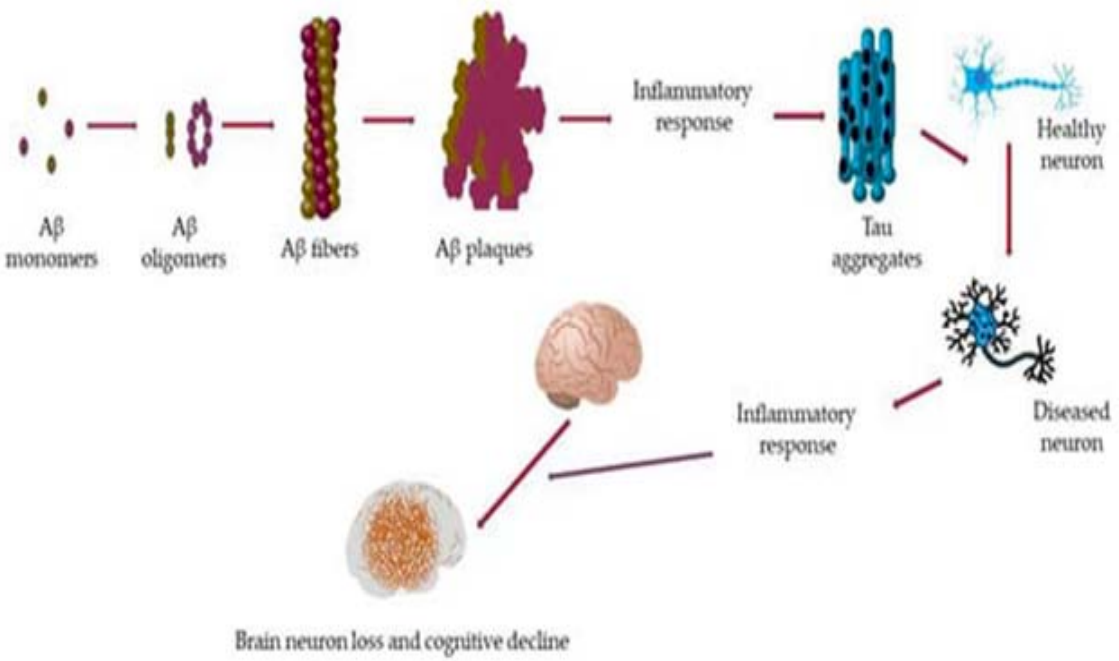

Figure 3: Role of *Mangifera Indica*in Neurodegenerative Disease

III. NEURODEGENERATIVE DISORDER TYPES

A. *Alzheimer's Disease [AD]*

A progressive neurological disease, Alzheimer's disease causes β-amyloid plaque buildup, memory loss, and cognitive impairment. It results in impaired brain function with an impact on daily activities and quality of life.

B. *Parkinson's Disease [PD]*

A neurological condition that impairs mobility, Parkinson's disease causes bradykinesia (slow movement), stiffness, and tremors. Motor and cognitive impairment are brought on by the brain's dopamine-secreting neurones degenerating.

C. *Huntington's Disease [HD]*

Parkinson's disease is a neurodegenerative condition that impacts movement, resulting in tremors, stiffness, and bradykinesia (slow movement). It is caused by the degeneration of dopamine-secreting neurons in the brain, which produces motor and cognitive dysfunction.

D. *Amyotrophic Lateral Sclerosis [ALS]*

The long-term, steadily worsening neurodegenerative disease known as amyotrophic lateral sclerosis (ALS) damages nerve cells in the brain and spinal cord. Muscle weakening, paralysis, and ultimately the loss of voluntary movement are the results. Motor neurone degeneration causes the condition, which hinders the brain's capacity to connect with muscles. There is presently no cure for ALS, which over time significantly impairs breathing and mobility.

E. *Multiple Sclerosis [MS]*

Multiple sclerosis (MS), a chronic autoimmune disease, affects the central nervous system and causes damage. nerves and interferes with brain-body communication. Muscle weakness, exhaustion, eyesight impairments, and coordination problems are some of its symptoms. The

illness affects everyday living and mobility and advances in an unpredictable manner with relapse and remission phases (24).

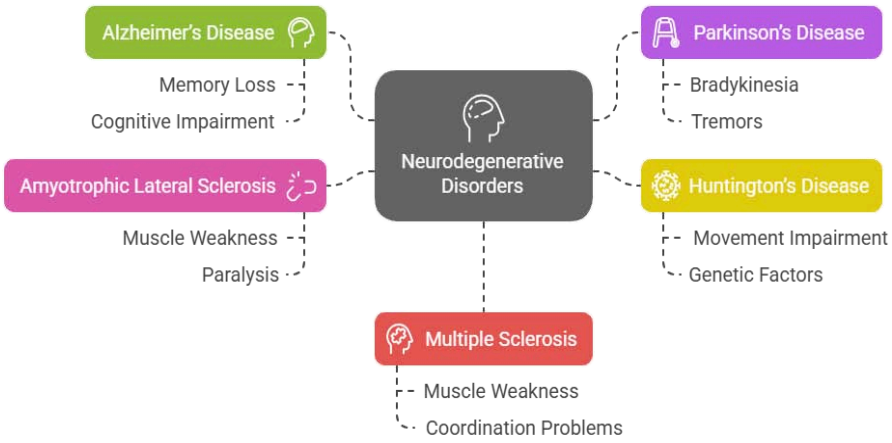

Figure 4: Neurodegenerative Disorder Types

IV. MATERIALS AND METHODS

4.1 Apparatus and Instrument

The Camag HPTLC system consists of a Linomat 5 applicator, a Camag TLC scanner 3, and WinCATS software. The Shimadzu HPLC system consists of an LC AT10 VP pump, an SPD M10 AT VP detector, and CLASS M10A software. A Jasco V-560 UV/Vis spectrophotometer is also employed.

4.2 Chemical

Chemical such as ethanol, methanol, ethyl acetate, and petroleum ether purchased from Bio Liquid Research Pvt Ltd. We conducted the remaining phytochemical tests in our pharmacognosy lab at the MET Faculty of Pharmacy, which is part of the Moradabad Educational Trust Group of Institutions.

4.3 Plant Material

Mangifera indica Barkpowder,which is dark brown incolour, was obtainedfrom the Herbal Garden MITGI, Faculty of Pharmacy, and identified Herbarium of Hindu college Moradabad.

4.4 Preparation of Mangifera indica Bark Powder

The plant material (bark) of *Mangifera indica* were taxonomically identified and authenticate with and collected at local market of Moradabad.

4.5 Yield Calculation

By computing the percentage weight (w/w) ratio between the produced extract and the simplicia utilised, the yield is determined (25).

V. CRUDE EXTRACT EXTRACTION FROM BARK POWDER

5.1 Crude extracts are extracted using the cold maceration process from bark powder

The extraction process for the selected plant parts is described below. Plants Active components were tracked using the cold extraction method (26).

Method:	Cold Maceration
Principle:	Cold Percolation
Apparatus:	Iodine Flask
Temperature Maintained:	25 – 30°C
Quality of Plant Bark Powder Used:	Fine Grand Powder
Volume of Each solvent used:	500 ML
Period of Extraction with Each Solvent:	3 – 4 days.

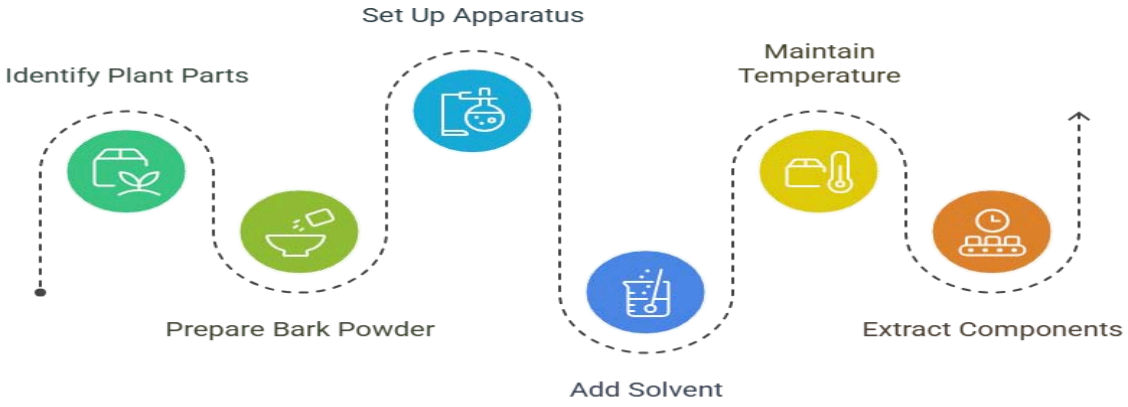

Figure 5: Cold Maceration Extract Process

5.2 Extraction of Crude Extracts from bark powder by Soxhlet Extraction method

Collect *Mangifera indica* bark, wash it to remove any debris, and air-dry it.Grind the dried bark into a fine powder to maximize the surface area, which enhances extraction efficiency.

Method:	Successive extraction
Principle:	Continuous hot percolation
Apparatus:	Soxhlet extractor
Temperature maintained:	35 – 40°C
Quality of Plant Powder Used:	Fine Grand Powder
Volume of Each Solvent Used:	500 ML
Period of Extraction with Each solvent:	3 days

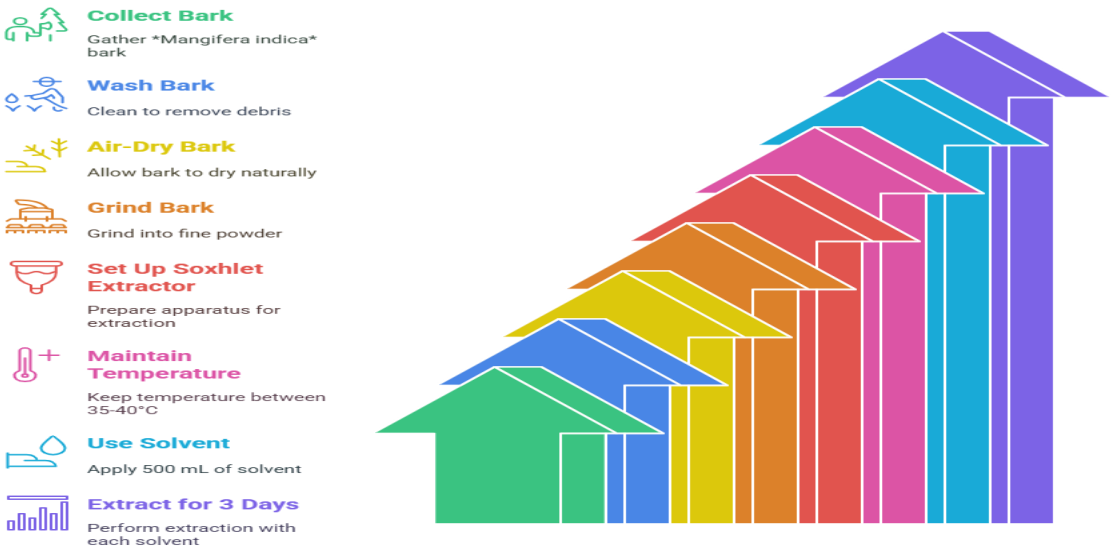

Figure 6: Soxhlet Extraction Process

Powdered crude drug was separately extracted by solvents of ascending polarity such as methanol, water, hydro-alcohol, ethanol, ethyl acetate, and petroleum spirit. The extraction yields were considerably different, the maximum being obtained by ethanol with a yield of 86.9%. The process of extraction was done step by step with continuous hot percolation using Soxhlet apparatus.

5.3 Macroscopic Studies of Mangifera indica bark

Macroscopic examination of *Mangifera indica*(mango) bark shows its scaly, fissured, and rough outer surface with dark brown to greyish-brown color. The inner bark is reddish-brown, fibrous, and emits a faint astringent smell when cut. It possesses a moderately hard texture with a bitter flavour. The bark is frequently lenticel-marked and ridged, which gives it a rugged look.

5.4 Microscopic study of Mangifera indica bark

Microscopic examination of Mangifera indica bark shows a distinct periderm, cortex, and phloem with clear mechanical and functional features. The occurrence of stone cells and resin ducts indicates its protective and defensive function. These anatomical features are responsible for the medicinal nature of the bark, which makes it a good source for pharmacological applications.

5.5 Physicochemical Parameters Mangifera indica bark Powder

Table 2 presents the physicochemical characterization of *M. indica* bark powder. The assessment of physical constants of medications is a crucial factor in identifying adulteration or poor management of pharmaceuticals. The leaf had a moisture content of merely 7.5%, hence inhibiting bacterial and fungal proliferation. Acid-insoluble ash, water-soluble ash, and totalash were the three different ways we measured the ash value. With 1.5% acid-insoluble ash and 1.5% water-soluble ash, we calculated that the total ash content was 9.6%. Calculate the 12% values for the foaming index and swelling index. Table 1 shows the bark of M. indica's extractive value. We observed the highest extraction value in methanol solvent, and the lowest in petroleum ether. We assessed the solubility of the methanol extract of *M. Indica*bark in six solvents of differing polarity. The extract exhibited high solubility in ethanol and methanol but reduced solubility in non-polar solvents (Table 3).

5.6 Phytochemical Examination of Mangifera indica Powdered Bark

Phytochemical analysis of *Mangifera indica* bark powder detects the bioactive molecules like tannins, flavonoids, alkaloids, and saponins responsible for its medicinal activities. Phenolic molecules and glycosides are also present with antioxidant and antimicrobial activity. Secondary metabolites like steroids and terpenoids are found to be present in abundance in the bark, verifying its use in traditional medicine.

VI. RESULT AND DISCUSSION

Advanced Phytochemical Analysis of Mangifera indica Bark Powder

Table 1: Macroscopic Studies of *Mangifera indica* bark: The colour, texture, thickness, odour, taste, moisture content and bulk density of the powdered drug were studied [14].

Colour	Greyish brown to dark powder
Texture	Smooth
Thickness	Around 0.1 to 1.5 cm
Odour	Slightly astringent
Taste	Bitter and astringents
Moisture Content	Low moisture content
Bulk density	Depending on an particle size and storage conditions.

Table 2: Standardization Parameters: *Mangifera indica* bark Powder

S. No	Specifications	%W/V
1.	Moisture Content	7.5 %
2.	Acid Insoluble Ash	1.5 %
3.	Total Ash Value	9.6 %
4.	Water Soluble Ash	12 %
5.	Swelling Index	5.5 %
6.	Foaming Index	4mm
7.	Foreign Index	No Foreign Index

Table 3: Extractive Value of *Mangifera indica* bark Powder

Solvent extraction yields vary significantly: Ethanol produces highest yield at 86.9%.

S. No	Types of Solvent	% Yield (W/V)
1.	Ethyl acetate	67.2%
2.	Petroleum Sprit	0.8%

3.	Methanol	15.2%
4.	Ethanol	86.9%
5.	Hydroalcohol	9.6%
6.	Water	4.8%

Table 4: Screening of *Mangifera indica* Bark Powder Phytochemically

To identify the bioactive components, photochemical screening was performed on *Mangifera indica* bark powder.

Tests	Decoction
Flavonoids	+
Alkaloids	+
Saponins	+
Tannins	+
Terpenoids	-
Glycosides	+
Steroids	-
Phenols	+
Carbohydrates	+
Proteins	-

VII. DETERMINATION OF MAXIMUM ABSORPTION WAVELENGTH

The spectrophotometer UV-Vis is used to determine the maximum absorption wavelength (Figure 1). As a result, *Mangiferin Indica*has an absorbance of 0.601 with a maximum absorption wavelength of 320 nm.

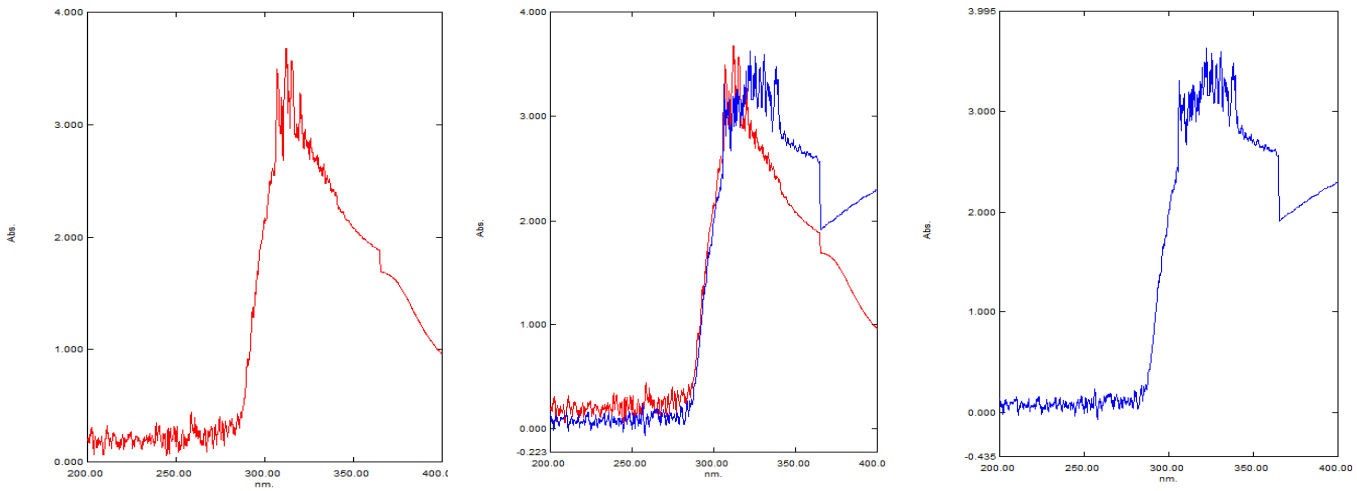

(A) *Mangiferin Indica* (B) Mixture of Qurectine and *MI* (C) Qurectinr Standard

Figure 7: UV Spectrum of *Mangiferin Indica* 10 µg/mL Ethanol

VIII. ULTRAVIOLET SPECTROSCOPY

8.1 Preparation of Standard solution

Following carefully weighing 50 mg of pure *Mangiferin Indica*, it was put in a 50 mL volumetric flask and diluted with methanol to the appropriate level. It was then diluted until it created a solution with 100 µg/mL, 200 µg/mL, 300 µg/mL, 400 µg/mL, and 500 µg/mL concentrations (27).

8.2 Determination of Maximum absorption wavelength

A 100 µg/mL pure *Mangiferin Indica* solution is pipetted up to 1 mL, after which it was moved to a 10 mL volumetric flask and filled with the proper amount of methanol. The spectrophotometer UV-Vis is then used to identify the dilution's peak absorption wavelength, which is between 200 and 400 nm (28).

HPTLC: A reliable analytical technique used for the separation and identification of phytochemicals in powdered *Mangifera indica* bark is High-Performance Thin-Layer Chromatography (HPTLC).HPTLC yields high-resolution chromatographic fingerprints, which facilitate qualitative and quantitative evaluation of bioactive compounds. The technique guarantees accurate identification, reproducibility, and validation of plant-derived constituents.

8.3 Preparation of Standard Stock Solution of Marker

10 mg of *Mangiferin Indica* were transferred into a 10 ml standard flask and dissolved in 1 ml of methanol to achieve a concentration of 1000µg/ml.and then adding more methanol to get the volume up to 10 ml. Among the stock solutions mentioned above, one containing 100 µg/ml of the final concentrations were set at 200, 400... 1200 ng/spot once the marker was created.HPTLC and solutions ranging in concentration from 0.2 to 0.4 to 1 g/ml were made forHPLC examination.

8.4 Standardization by HPTLC

In the current study the HPTLC fingerprinting analysis and standardization was conducted on *Mangifera indica* extract. Different organic solvents such as petroleum ether, chloroform and methanol in order of their increasing polarity were employed in preparing the selected plant extract and methanol to extract the formulation. Optimized mobile phase system employed was ethyl acetate:methanol: Ethanol: water, 10:1:1:0.5 % v/v/v/v. The stationary phase on which separation was done was pre-coated plates with silica gel $60F_{254}$ on aluminium sheets. 310nm was the wavelength used for fingerprinting and standardization.

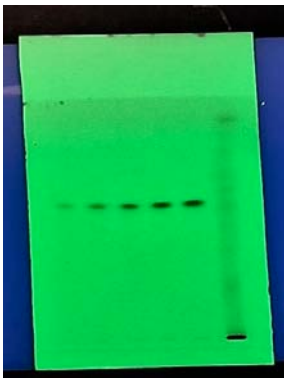

Figure 8: HPTLC Platecontaining optimized mobile phase system employed was ethyl acetate: methanol: Ethanol: wate

8.5 Recording of the HPTLC Chromatogram

50µl of each of the solution of the *Mangifera indica* extracts and its formulation were used with CAMAG semiautomatic applicator on to individual plates and chromatograms were developed. The plates were photo-metrically analyzed according to detection technique and chromatograms were taken. The fingerprinting of extracts was taken and the different. The Rf values achieved were recorded. The Rf values achieved in the respective extracts (plant as well as its formulation extracts) corresponding to respective marker is detected in the plant extracts and their formulations that correspond to the marker, the peak areas of the detected component (*Mangiferin Indica*) are recorded. The marker's calibration graph is used to determine the quantity of component present.

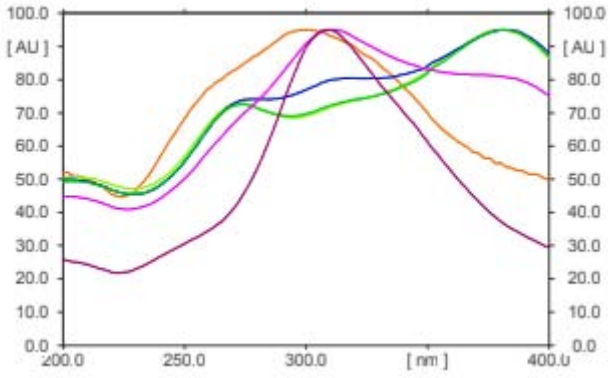

Figure 9: The calibration graph at different wavelengths in HPTLC

Table 5: Quercetin spectrum on all Tracks of different wavelength

S. No	Rf	Substance	Max @
1.	0.58	Quercetin	309 nm
2.	0.57	Quercetin	311 nm
3.	0.57	Quercetin	383 nm
4.	0.57	Quercetin	381 nm
5.	0.57	Quercetin	380 nm
6.	0.55	Quercetin	300 nm

8.6 Validation

A number of factors, including linearity, accuracy, limit of detection (LOD), limit of quantification (LOQ), intraday and interday precision, sample application and measurement repeatability, stability evaluations, and selectivity, were taken into consideration when calibrating the HPTLC processes for the selected marker.

8.7 Range andLinearity

Markers were developed in different concentrations and tested using HPTLC methods. For HPTLC linear regression, data is observed to have a good linear relationship overa range of Y = 295.9 + 3.309 * Xr = 0.97543sdv = 11.96.

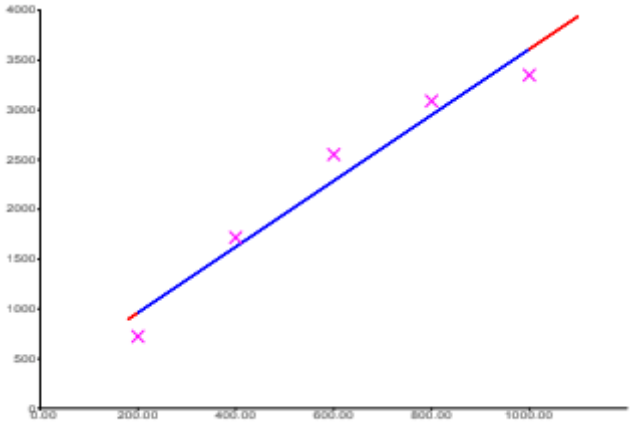

Figure 10: Linearity and Range

S. No	Vial	Rf	Amount	Area
1.	1	0.58	200.00 µg	720.63
2.	1	0.57	400.00 µg	1711.34
3.	1	0.57	600.00 µg	2547.95
4.	1	0.57	800.00 µg	3083.15
5.	1	0.57	1000.00 µg	3343.94
6.	2	0.55		389..03<180.00 µg MI Extract

Different HPTLC Chromatogram at various wavelength of standard markers with sample Extract

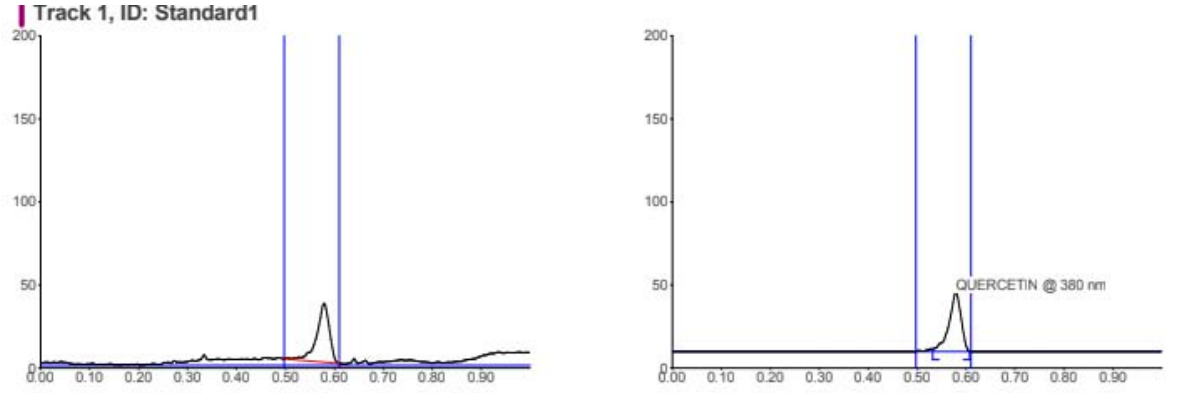

Peak	Start Rf	Start Height	Max Rf	Max Height	Max %	End Rf	End Height	Area	Area %	Assigned substance
1	0.53	1.5	0.58	35.4	100.00	0.61	0.1	720.6	100.00	QUERCETIN

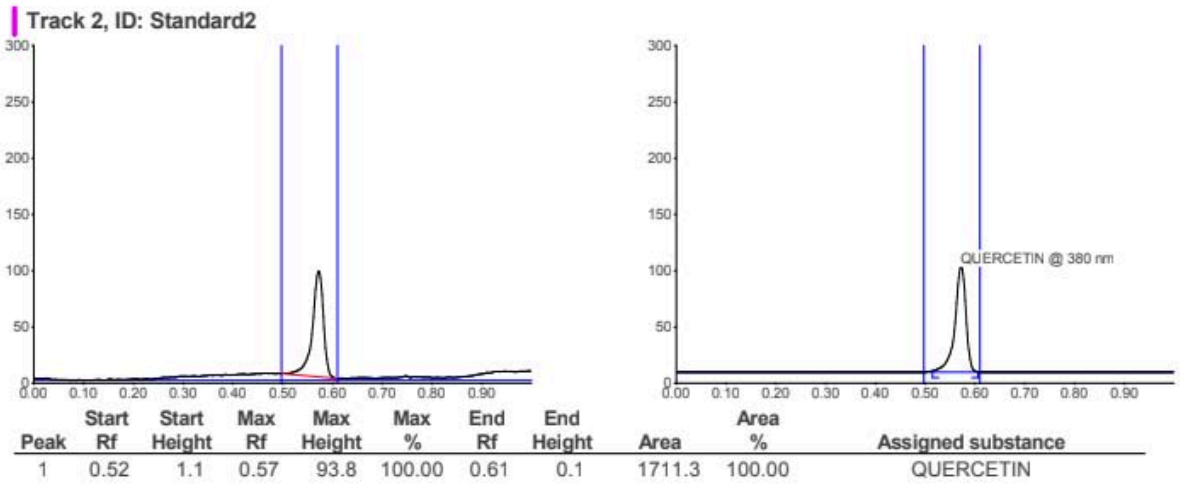

Peak	Start Rf	Start Height	Max Rf	Max Height	Max %	End Rf	End Height	Area	Area %	Assigned substance
1	0.52	1.1	0.57	93.8	100.00	0.61	0.1	1711.3	100.00	QUERCETIN

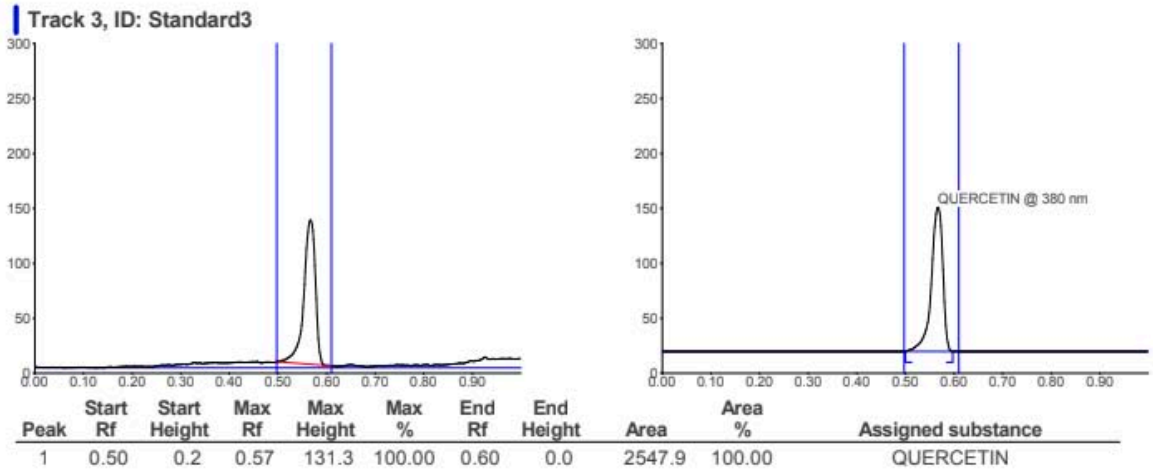

Peak	Start Rf	Start Height	Max Rf	Max Height	Max %	End Rf	End Height	Area	Area %	Assigned substance
1	0.50	0.2	0.57	131.3	100.00	0.60	0.0	2547.9	100.00	QUERCETIN

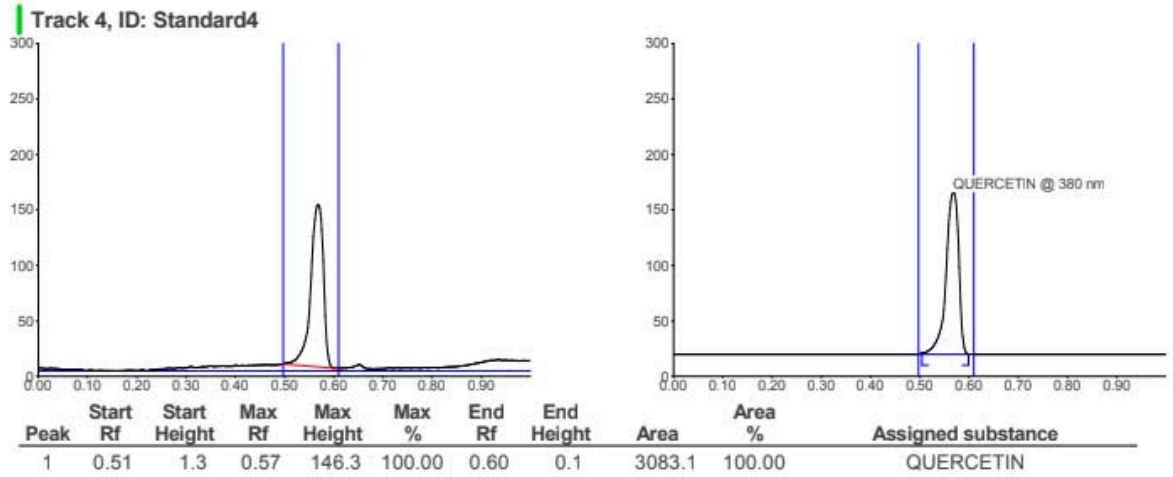

Peak	Start Rf	Start Height	Max Rf	Max Height	Max %	End Rf	End Height	Area	Area %	Assigned substance
1	0.51	1.3	0.57	146.3	100.00	0.60	0.1	3083.1	100.00	QUERCETIN

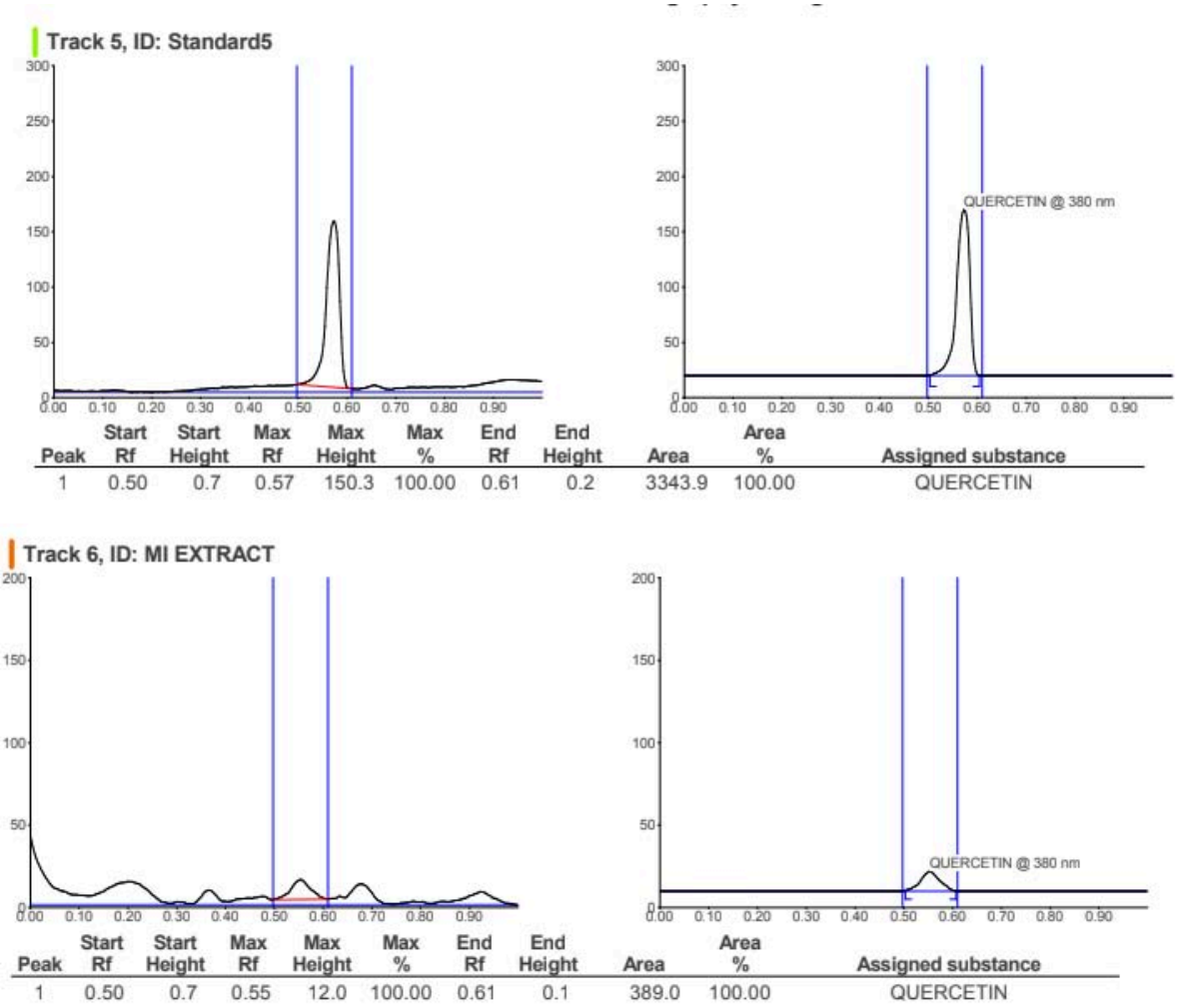

Figure 11: Different HPTLC Fingerprint of Methanolic Extract

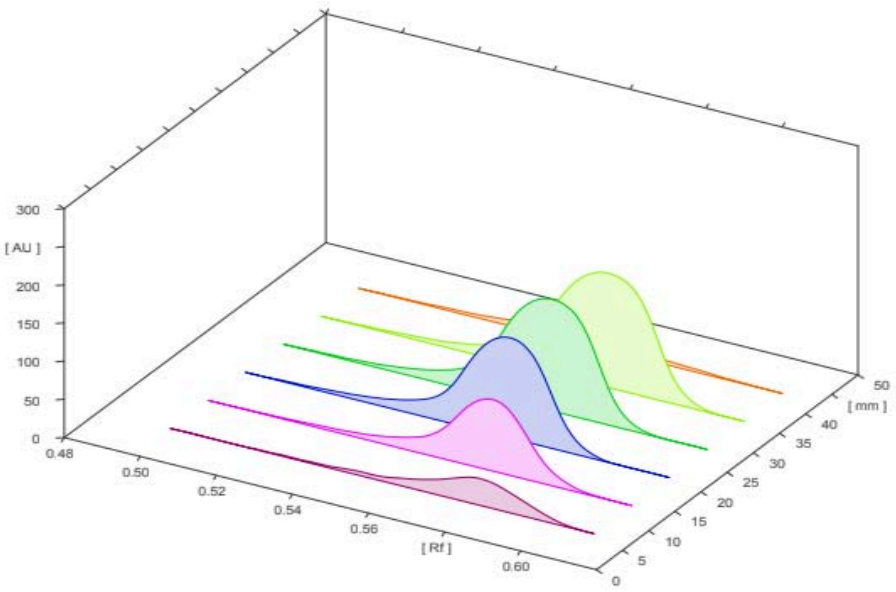

Figure 12: Overall Different HPTLC Fingerprint of Methanolic Extract

S. No	Appl. Position	Appl. Volume	Viral#	Sample ID	Active
< 1.	6.8 mm	0.4 µl	1	Quercetin Std.	Yes
< 2.	14.0 mm	0.8 µl	1	Quercetin Std.	Yes
< 3.	21.2 mm	1.2 µl	1	Quercetin Std.	Yes
< 4.	28.4 mm	1.6 µl	1	Quercetin Std.	Yes
< 5.	35.6 mm	2.0 µl	1	Quercetin Std.	Yes
< 6.	42.8 mm	3.0 µl	2	*MI* extract	Yes

Polydispersity Index and Particle size: Polydispersity Index (PDI) is an important parameter to assess the homogeneity of particle size distribution in *Mangifera indica* bark powder. It reflects the homogeneity of the sample, and lower values represent a more homogeneous dispersion. PDI is an important factor in deciding the stability and consistency of pharmaceutical and herbal products.

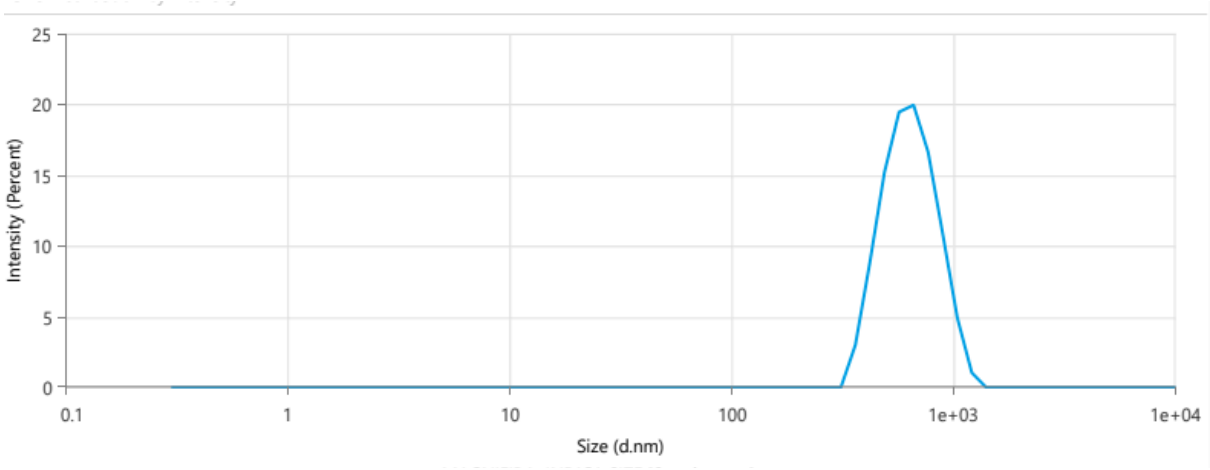

Figure 13: Polydispersity Index and Particle size *Mangifera indica*

Name	Mean	Standard Deviation	RSD	Minimum	Maximum
Z – Average (nm)	671.4	-	-	671.4	671.4
Polydispersity Index (PI)	0.2835	-	-	0.2835	0.2835
Intercept	0.8449	-	-	0.8449	0.8449

IX. CONCLUSION

In summary, pharmacognostic standardization and quality profiling of Mangifera indica bark powder reveal crucial information regarding its prospective therapeutic use, particularly in neurological disorder management. Through a detailed examination of its macroscopic and microscopic characters and Physico-chemical attributes, it has been proven that Mangifera indica bark contains a multifaceted profile of bioactive constituents, which may contribute to its neuroprotective actions. The availability of vital phytochemicals like alkaloids, flavonoids, and terpenoids, along with its proven antioxidant and anti-inflammatory properties, indicates its potential application in the management of diseases like Alzheimer's disease, Parkinson's disease, and other neurodegenerative diseases. In addition, the development of strong standards for the quality of the bark powder guarantees its reliability and consistency for therapeutic purposes. The results highlight the necessity for additional in-depth

research, such as clinical trials, to comprehensively assess the safety and efficacy of Mangifera indica bark in neurological use. As research evolves, this plant is promising as a valuable natural resource for integrative strategies in managing neurological health. The pharmacognostic profile further highlights the significance of quality control and standardization of herbal medicine to ensure that patients are administered safe and effective treatments from natural sources.

Future Aspects

The potential of the pharmacognostic standardization and quality profiling of Mangifera indica bark powder as an antidote against neurological disorders is immense. With further development in research, one of the primary regions of interest will be the complete isolation and characterization of bioactive molecules within the bark, employing novel methods such as high-throughput screening and liquid chromatography-mass spectrometry. These investigations will unveil new molecules with neuroprotective effects. Additionally, clinical trials are important to confirm the effectiveness, safety, and ideal dosage of Mangifera indica bark for neurological disorders to ensure that the plant can be made a part of mainstream treatment approaches. More studies on how it affects neurobiological pathways, especially on how it acts upon them, will also be important in determining its application in fighting neurodegenerative diseases.

Conflicting Interests

The authors acknowledge their individual contributions to the study and declare that they have no financial or other conflicts of interest.

Contribution of the Authors

All authors participate in the conception and design of the study. Shivani Agrwal and Rahul Chauhan conducted the material preparation, data collecting, and analysis. Shivani Agarwal and Rahul Chauhan composed the initial draft of the book, and all writers reviewed and endorsed the final version.

Funding

None

Availability of data and material

The authors atleast that the information in the article supports the study's conclusions.

ACKNOWLEDGEMENTS

For their assistance with this study project, the authors would like to thank the MET Faculty of Pharmacy Moradabad. Additionally, they disclose that they worked together to obtain the graphical abstract.

REFERENCES

1. Al-Snafi AE. Pharmacological and therapeutic importance of Hibiscus sabdariffa- A review. International Journal of Pharmaceutical Research 2018; 10(3): 451-475.
2. Salehi B, Krochmal, Marczak B, Skiba D, Patra JK, Das SK Das G, Popović Djordjević JB, Kostić AZ, Kumar NV, Tripathi A, Al, Snafi AE, Arserim, Uçar DK, Konovalov DA, Csupor D, Shukla I, Azmi L, Mishra AP, Sharifi‐Rad J, Sawicka B, Martins N, Taheri Y, Fokou BVT, Capasso R and Martorell M. Convolvulus plant- A comprehensive review from phytochemical composition to pharmacy. Phytotherapy Research 2019;1–14

3. Al-Snafi AE. The pharmacology of Anchusa italica and Anchusa strigosa- A review. International Journal of Pharmacy and Pharmaceutical Sciences 2014; 6(4): 7-10.
4. Al-Snafi AE. The pharmacological importance of Anethum graveolens- A review. International Journal of Pharmacy and Pharmaceutical Sciences 2014; 6(4): 11-13.
5. Al-Snafi AE. Chemical constituents and pharmacological activities of Milfoil (Achillea santolina) - A Review. Int J Pharm Tech Res 2013; 5(3): 1373-1377.
6. Al-Snafi AE. The Pharmaceutical importance of Althaea off icinalis and Althaea rosea: A Review. Int J Pharm Tech Res 2013; 5(3):1387-1385.
7. The plant list, *Mangifera indica*, http://www.theplantlist.org/tpl/record/kew-2362842
8. Food and Agriculture Organization of the United Nations (FAO). *Major Tropical Fruits: Market Review 2021*; FAO: Rome, Italy, 2022.
9. Alzamora, S.M.; Guerrero, S.N.; Nieto, A.B.; Vidales, S.L. Conservación de Frutas y Hortalizas Mediante TecnologíasCombinadas: Manual de Capacitación; Food and Agriculture Organization of the United Nations (FAO): Rome, Italy, 2004.
10. Mendoza, E.; Calvo, C. Bromatología: Composición y Propiedades *de Los Alimentos*; McGraw-Hill: México, Italy, 2010.
11. Quintero, V.C.; Giraldo, G.G.; Lucas, J.A.; Vasco, J.L. Physicochemical characterization of the common mango (*Mangifera indica* L.) during ripening process. *Biotecnología* 2013, *11*, 10–18.
12. Atoche-Chauca, L.S.; García-Siu, M.W. Aprovechamiento de ResiduosAgroindustriales (Cáscara de Mango) para la Formulación de Cupcakes. Bachelor's Thesis, Universidad Nacional del Santa, Nuevo Chimbote, Peru, 2017.
13. Food and Agriculture Organization of the United Nations (FAO). The State of Food and Agriculture 2019: Moving forward on Food Loss and Waste Reduction; FAO: Rome, Italy, 2019.
14. Singh, S.; Kawade, S.; Dhar, A.; Powar, S. Analysis of mango drying methods and effect of blanching process based on energy consumption, drying time using multi-criteria decision-making. *Clean. Eng. Technol.* **2022**, *8*, 100500.
15. Nguyen, T.V.L.; Nguyen, Q.D.; Nguyen, P.B.D. Drying kinetics and changes of total phenolic content, antioxidant activity and color parameters of mango and avocado pulp in refractance window drying. *Pol. J. Food Nutr. Sci.* **2022**, *72*, 27–38.
16. Basulto, J.; Moñino, M.; Farran, A.; Baladia, E.; Manera, M.; Cervera, P.; Romero-de-Ávila, M.D.; Miret, F.; Astiasarán, I.; Bonany, J.; et al. Recomendaciones de manipulacióndoméstica de frutas y hortalizas para preservarsuvalornutritivo. *Rev. Esp. Nutr. Hum. Diet.* **2014**, *18*, 100–115.
17. Hernández-Ruíz, Y.N. Deshidratación de Manzanas Tipo Granny Smith en Ventana Refractiva con Pretratamiento de Deshidratación Osmótica y Campo Eléctrico Moderado. Bachelor's Thesis, Universidad Técnica Federico Santa María, Valparaíso, Chile, 2017.
18. Díaz-Urbano, C.E. Evaluación de Tecnologías de Secadoen las Propiedades Fisicoquímicas del Banano (Cavendish Valery). Bachelor's Thesis, Universidad Nacional Abierta y a Distancia (UNAD), Bogotá, Colombia, 2018.
19. Chakraborty, R.; Saha, A.K.; Bhattacharya, P. Modeling and simulation of parametric sensitivity in primary freeze-drying of foodstuffs. *Sep. Purif. Technol.* 2006, *49*, 258–263.
20. Nindo, C. Novel drying method for vegetables, fruits, herbs, and aquatic resources. In Proceedings of the CSBE/SCGAB Annual Conference, Vancouver, BC, Canada, 13–16 July 2008.
21. Carrascosa-Morelló, A. Obtención de Aperitivos de Manzana con Efecto Probiótico Mediante Impregnación con Lactobacillus Paracasei. Bachelor's Thesis, Universitat Politècnica de València, Valencia, Spain, 2019.
22. Torres, R.; Montes, E.J.; Pérez, O.A.; Andrade, R.D. Relación del Color y del Estado de Madurez con las PropiedadesFisicoquímicas de FrutasTropicales. *Inf. Tecnol.* **2013**, *24*, 51–56.
23. Saba Sheikh safiaEjazul Haque, and Snober S. Mir Neurodegenerative Diseases:Multifactorial Conformational Diseases and Their Therapeutic Interventions Hindawi Publishing Corporation

Journal of Neurodegenerative Diseases Volume 2013, Article ID563481,8 pages http://dx.doi.org/10.1155/2013/563481
24. Johannes C.M. Schlachetzki, Soraya Wilke Saliba, Antonio Carlos Pinheiro de Oliveira Studying neurodegenerative diseases in culture models Revista Brasileira de Psiquiatria. 2013;35:S92–S100 2013 Associac¸a˜o Brasileira de Psiquiatria doi:10.1590/1516-4446-2013-1159.
25. Departemen Kesehatan RI. Farmakope Herbal Indonesia. Jakarta: Kementerian Kesehatan Republik Indonesia, 2008.
26. Jayaprakasam R, Ravi TK. HPTLC and RP-HPLC methods for the estimation of Mangiferin in Mangifera indica extract and its formulation.
27. Harmita. Petunjuk Pelaksanaan Validasi dan Cara Penggunaannya. MajalahIlmuKefarmasian, 2004; 1(3): 117–135.
28. Lai L, Lin L, Lin J, Tsai T. Pharmacokinetic Study of Free Mangiferin in Rats byMicrodialysis Coupled with Microbore High-Performance Liquid Chromatography andTandem Mass Spectrometry. Journal of Chromatography, 2003; 987: 367–374.

Visibility of Websites of Agricultural Research Institutes in Nigeria

Ovuorie, R.A. & O.M. Adesopend

University of Port Harcourt

ABSTRACT

The study focused on the visibility of websites of agricultural research institutes in Nigeria. A purposive sampling technique was employed to select 34 agricultural research institutes. The specific objectives were to assess the online visibility of these websites and identify the types of agricultural activities showcased. Secondary data were collected using webometric tools such as SEO tools, Moz, Similarweb, and Ahrefs. The research adopted a mixed-method approach, incorporating both quantitative and qualitative data analysis. Quantitative data were analyzed using IBM SPSS (Statistical Package for the Social Sciences), while qualitative data were analyzed using Atlas.ti version 8. The results revealed that the websites of ARMTI, CIFOR, NAERLS, NSPRI, WARDA, FRIN, IFPRI, ICRISAT, NIFOR, NAPRI, NIFST and ICRAF agricultural research institutes had high visibility. The most frequently mentioned words included "research," "food," "capacity," and "development," reflecting the key activities of some agricultural research institutes. Additionally, the coefficient of global rank showed a positive correlation with website visibility, while visit duration and bounce rate exhibited negative correlations. The study concluded that the high and moderate levels of website visibility were associated with the sharing of links and content, as well as maintaining an active presence on social media platforms. It recommended that agricultural research institutes leverage social media platforms such as Twitter, Facebook, and LinkedIn to promote website content and drive traffic, thereby enhancing online visibility and engagement.

Keywords: website visibility, agricultural research institutes, webometrics, digital presence.

Classification: LCC Code: S494.5.I5

Language: English

Great Britain Journals Press

LJP Copyright ID: 925653
Print ISSN: 2631-8490
Online ISSN: 2631-8504

London Journal of Research in Science: Natural & Formal

Volume 25 | Issue 5 | Compilation 1.0

Visibility of Websites of Agricultural Research Institutes in Nigeria

Ovuorie, R.A[α]. & O.M. Adesope[σ]

ABSTRACT

The study focused on the visibility of websites of agricultural research institutes in Nigeria. A purposive sampling technique was employed to select 34 agricultural research institutes. The specific objectives were to assess the online visibility of these websites and identify the types of agricultural activities showcased. Secondary data were collected using webometric tools such as SEO tools, Moz, Similarweb, and Ahrefs. The research adopted a mixed-method approach, incorporating both quantitative and qualitative data analysis. Quantitative data were analyzed using IBM SPSS (Statistical Package for the Social Sciences), while qualitative data were analyzed using Atlas.ti version 8. The results revealed that the websites of ARMTI, CIFOR, NAERLS, NSPRI, WARDA, FRIN, IFPRI, ICRISAT, NIFOR, NAPRI, NIFST and ICRAF agricultural research institutes had high visibility. The most frequently mentioned words included "research," "food," "capacity," and "development," reflecting the key activities of some agricultural research institutes. Additionally, the coefficient of global rank showed a positive correlation with website visibility, while visit duration and bounce rate exhibited negative correlations. The study concluded that the high and moderate levels of website visibility were associated with the sharing of links and content, as well as maintaining an active presence on social media platforms. It recommended that agricultural research institutes leverage social media platforms such as Twitter, Facebook, and LinkedIn to promote website content and drive traffic, thereby enhancing online visibility and engagement.

Keywords: website visibility, agricultural research institutes, webometrics, digital presence.

Author α: Department of Agricultural Extension and Development Studies.
σ: University of Port Harcourt, Port Harcourt, Rivers State, Nigeria.

I. INTRODUCTION

Website visibility is an indicator of how visible a website is in the organic search results when queries are entered into search engines. It refers to the ease and effectiveness with which a search engine crawler can find and index a webpage (Weideman 2009). Ojokoh and Akinola (2017) stated that visibility considers two parameters: number of external links and number of referring domain. Weideman (2009) stated that external links are hyperlinks on webpage B, linking to webpage A, where webpage A is the one currently under consideration. Many external links from other websites in the same community makes a positive contribution to website visibility. A webpage coder has very little control over the quantity and quality of external links, but the website owner could canvass for external links from other high-quality websites. The referring domains (ref. domain) are pages on different websites that points to resources in the target domain. It is a domain for links that redirect visitors to the target website. One referring domain can have more than one link to different pages on a website, for example a link in a referring domain to Postgraduate School of University of Port Harcourt, and another link in the same domain to School of Sciences of the same Institution. Ahrefs and Majestic, having a weighted score of 50%, can be used to determine the visibility of websites (Kunosic et al. 2019).

According to Patel (2015), one important aspect of visibility is search engine optimization (SEO). SEO is the process of improving the quality and quantity of website traffic by increasing the visibility of a website or a web page in a search engine's unpaid results. This can be achieved through a combination of on-page and off-page optimization techniques, such as keyword research, meta tags, and backlink building. Also, another important aspect of visibility is the use of social media. Social media can be used to promote a website and increase its visibility through the sharing of links and content, it can be used to engage with users and build a community around a website, which can also help to increase visibility.

Website visibility is important for several reasons, including increasing website traffic and improving search engine rankings. When a website has good visibility, it means that it appears high in search engine results, making it more likely for users to find and visit the site. This can lead to an increase in website traffic, which can in turn lead to more sales, leads, and conversions. Again, websites that are visible on search engines are more likely to be considered reputable and credible by users. Website visibility is also important for businesses because it can help to improve brand awareness and reputation. When a website is visible on search engines, it can help to establish the business as a leader in its industry, which can help to build trust and credibility with potential customers. Furthermore, visibility can help to generate interest and engagement from potential customers and help to build relationships with them. In addition, website visibility can also affect how users perceive the website. A website that is visible on search engines is often seen as more professional, reliable, and trustworthy than a website that is not. This can have a positive impact on the user's experience and increase the likelihood that they will return to the site in the future (Rosario, 2021).

II. STATEMENT OF THE PROBLEM

The insufficient number of change agents or development facilitators assisting millions of development beneficiaries serves as a clear indication of the need for media help. According to Davis et al. (2019), Nigeria has a workforce of over 7,000 public agents, with an extension agent to farmer ratio of between 1:5,000 and 1:10,000. Using a website is unavoidable if any progress is to be made quickly, and the web presence of agricultural research institutes play an essential role for all key actors. Like university websites that attracts students, academics, funding, and make these institutions widely known through E-learning programs and open access initiatives, while spreading knowledge beyond physical boundaries (Razak et al., 2019), websites of agricultural research institutions should be visually appealing, polished, and professional to reflect the institutions' services and mandates. It should help users' complete tasks quickly through on-site search and keep them engaged by suggesting relevant content, while minimizing dead ends. The websites should be fast, correct, and perform as intended, and should be built to web standards, rigorously proofed, and regularly tested for speed or functionality issues. But most of the agricultural research institutes have dormant websites, the few that are not dormant, are not visible enough. This agrees with Ogege (2011) who stated that Nigeria is well recognized for having abandoned websites, and among parastatals, agencies, and ministries, only a select few have an amazing record in building websites that are really useful, while numerous others merely have websites that maintain static home pages. At such, the required collaboration is not there, for instance, between the academia, the industries, government, societies, professional associations, etc. These websites of the agricultural research institutes are not visible enough to reflect the true image of the various research going on in the research stations. The study therefore examines the visibility of agricultural research institutes in Nigeria.

III. OBJECTİVES OF THE STUDY

This study aimed to address the following objectives:

i. Ascertain the online visibility of the websites of agricultural research institutes.
ii. Identify the types of agricultural activities that are visible on the websites of the agricultural research institutes.

Hypothesis of the Study

H_0: Webometric indexes do not influence the online visibility of the websites of agricultural research institutes.

IV. METHODOLOGY

This study employed a descriptive research design. This type of research design was employed because the nature of the study required the collection of quantitative and qualitative data from the entire population on webometric factors using webometric tools and the result would provide a detailed understanding of each sample in the entire population of the study. The study was undertaken in Nigeria. Between the latitudes of 4° and 14° and the longitudes of 3° and 14° is where Nigeria is found in West Africa. It covers 923,768 square kilometers in total. The Republics of Niger and Chad border it to the north; the Republic of Benin borders it to the west; and the Republic of Cameroun borders it to the east all the way to the Atlantic Ocean's coastlines, forming the southern limits of Nigerian Territory (Akinwale et al. 2023).

The study's population comprised of 34 national and international agricultural research institutes drawn from the six (6) geopolitical zones in Nigeria. Purposive sampling technique was employed to select the 34 national and international agricultural research institutes in Nigeria.

The study employed secondary data collection. The secondary data for the study were collected through the use of webometric tools such as SEO (Search Engine Optimization) tools, Moz, Similarweb, and Ahrefs. These webometric tools can be accessed online through their URL links.

The researcher designed a research brief and employed the following procedures:

Step 1: Access the link online for Ahrefs: https://www.ahrefs.com.

Step 2: Enter the institute's URL into the accessed link in step 1.

Step 3: Retrieve the required information for the institutes.

V. RESULTS AND DISCUSSION

5.1 Visibility of Websites of Agricultural Research Institutes in Nigeria

Table 1 shows the extent of visibility of the websites of agricultural research institutes in Nigeria. The websites of ARMTI, CIFOR, NAERLS, NSPRI, WARDA, FRIN, IFPRI, ICRISAT, NIFOR, NAPRI, NIFST and ICRAF agricultural research institutes had high visibility with scores ranging from 63% to 86%. The websites of CRIN, IAR, IITA,ILRI, NIHORT, NVRI, NRCRI, NCAM, NACGRAB, NIOMR, NISS, NIFFR, CIMMYT and CIP agricultural research institutes had moderate visibility with scores ranging from 39% to 62%. The websites of IART, LCRI, NWRI and RMRDC agricultural research institutes had low visibility with scores ranging from 15% to 38%.

The high and moderate extent of visibility could be as a result of positive user experience and continuous website updates with new research findings, trainings, trends, and events. This agrees with

the findings of Pant & Pant (2017) who reported that websites with larger number of engaging pages are associated with higher visibility. Also, the high and moderate extent of visibility can be associated with sharing of links and contents, as well as maintaining an active presence on social media platforms such as facebook, twitter, linkedIn, youtube, instagram, etc., thereby building links and generating traffic to the websites. This agrees with the findings of Zhang & Cabage, (2016) who claimed that social media can be a useful tool for generating traffic quickly and that link building and social media both increase website traffic and profitability. The high and moderate extent of visibility suggests that when agricultural information users such as the government decision-makers, agricultural policymakers, planners, researchers, educators, students, program managers, field staff, and farmers make queries for information on search engines, only the visible websites will appear on search engine result page. For example, when a user is looking for information on the use of fertilizers in maize production, they may use keywords such as "maize," "fertilizer application," and "yield improvement." An agricultural research institute that has conducted research on the use of fertilizers in maize production and uses these relevant keywords in their content strategically or have RSS field on their website and social media handles with notifications being sent on every content uploaded and updated, search engines are more likely to display the website in the search results, increasing its visibility to the users, and the website can also attract organic traffic from such users and establish themselves as a reliable source of information on the subject.

Table 1: Extent of Visibility of Website of Agricultural Research Institutes

S/N	URL	Visibility Score (%)	Remark
1	www.armti.gov.ng	75	High
2	www.crin.gov.ng	60	Moderate
3	www.cifor.org	85	High
4	www.frin.gov.ng	67	High
5	www.iar.gov.ng	46	Moderate
6	www.iart.gov.ng	30	Low
7	www.iita.org	55	Moderate
8	www.ilri.org	60	Moderate
9	www.ifpri.org	71	High
10	www.icrisat.org	71	High
11	www.lcrimaid.gov.ng	15	Low
12	www.nihort.gov.ng	55	Moderate
13	www.nwrikd.edu.ng	38	Low
14	www.napri.gov.ng	69	High
15	www.nvri.gov.ng	55	Moderate
16	www.nrcri.gov.ng	55	Moderate
17	www.ncamng.org	50	Moderate
18	www.nacgrab.gov.ng	45	Moderate
19	www.niomr.gov.ng	55	Moderate
20	www.nifor.gov.ng	69	High
21	www.niss.gov.ng	50	Moderate
22	www.nifst.org	71	High
23	www.naerls.gov.ng	75	High
24	www.nspri.gov.ng	75	High

S/N	URL	Visibility Score (%)	Remark
25	www.niffrng.org	60	Moderate
26	www.rmrdc.gov.ng	38	Low
27	www.africarice.org	75	High
28	www.worldagroforestry.org	71	High
29	www.cimmyt.org	55	Moderate
30	www.cipotato.org	56	Moderate

Source: Researcher, 2023 Low (15-38), Moderate(39-62), High (63-86)

*Data were available for only 30 Agricultural Research Institutes

5.3 Activities on the Websites of Agricultural Research Institutes

Figure 1 shows the word cloud depicting the activities of the agricultural research institute. The size of the word determines how frequently it was mentioned. The boldest of all the words is the most mentioned word indicating the most prominent activity. “Research” was the most mentioned word for CIP, FIIRO, FRIN, IART, IAR, IFPRI, IITA, NCRI, NAPRI, NRCRI, NSPRI, and NVRI agricultural research institutes. In the case of WARDA and ICRISAT “development” was the most mentioned word. “Food” was the most mentioned word for CIMMYT and NIFST agricultural research institutes. “Capacity” was the most mentioned word for CRIN, while “livestock” was the most mentioned word for ILRI. “Agricultural”, “genetic”, “fish”, “palm”, “marine”, “soil”, and “production” were the most mentioned words for NAERLS, NACGRAB, NIFFR, NIFOR, NIOMR, NISS, and NIHORT respectively. Findings revealed that “research” was the most mentioned word for CIP, FIIRO, FRIN, IART, IAR, IFPRI, IITA, NCRI, NAPRI, NRCRI, NSPRI, and NVRI agricultural research institutes, demonstrating that research is an important part of their activity. In the case of WARDA and ICRISAT, “development” was the boldest word. This implies that these institutes main focus is agricultural development, which entails enhancing and advancing agricultural methods and technologies. Also, the word tag for CIMMYT and NIFST agricultural research institutes was “food”, this suggests that these institutions are engaged in research and initiatives concerning food production, food security, and food technology.

Furthermore, ARMTI was associated with the word tag “management”. This suggests that ARMTI concentrates on studies and initiatives pertaining to agricultural management, which could entail things like agricultural policy, resource management in the agricultural sector, farm management methods, and agribusiness management. The use of the word "management" underlines the institute's focus on efficient and effective management procedures in agriculture. Also, the word tag for CRIN was “capacity”, which implies that CRIN focuses on strengthening the abilities and knowledge of farmers, researchers, and agricultural practitioners as a way of building capacity in the agricultural sector. The word tag for ILRI was “livestock”. This demonstrates the expertise of ILRI in research and activities pertaining to raising livestock, including animal health, breeding, and production. The word tag for NAERLS was “agricultural”, which implies that NAERLS works on several facets of agriculture, including agricultural policy, extension services, and rural development. The most mentioned word for NACGRAB was “genetic”. This suggests that NACGRAB engages in genetic research as well as projects including crop improvement, genetic resources, and plant breeding. Furthermore, the most mentioned word for NIFFR was “fish”. This implies that NIFFR focuses on studies and initiatives pertaining to fisheries, aquaculture, and aquatic resources. The most mentioned word for NIFOR was “palm”. This demonstrates that NIFOR concentrates on studies and initiatives pertaining to the growth of palm trees, the production of palm oil, and palm-derived goods. The most mentioned word for NIOMR was “marine”. This implies that NIOMR focuses on studies and initiatives pertaining to the management of marine ecosystems, marine biology, and marine resources. For NISS, the most mentioned word was

"soil", which suggests that NISS concentrates on studies and tasks pertaining to soil science, soil fertility, and soil preservation. In the same vein, the most mentioned word for NIHORT was "production", which demonstrates that NIHORT focuses on studies and initiatives pertaining to the cultivation of horticulture crops, such as fruits, vegetables, and ornamental plants. The most mentioned word for RRIN was "rubber", which implies that RRIN focuses on studies and initiatives concerning rubber production, rubber tree cultivation, and rubber processing. The institute's work focuses on generating novel rubber tree kinds, enhancing rubber tree farming practices, researching rubber processing techniques, and addressing issues unique to the rubber industry.

Although the word cloud might reveal some of the most significant activity taking place within agricultural research institutes, it does not indicate that these activities are open to the public. According to Clement et al., (2021), the visibility of agricultural research institutes operations is affected by several factors, including their communication plans, outreach initiatives, publishing of research results, interaction with stakeholders, and information distribution through their websites, conferences, journals, and other platforms. Agricultural research institutes can effectively drive traffic to their websites by making the most mentioned words keywords for their websites' contents, thus, increasing their online visibility.

ARMTI

CIP

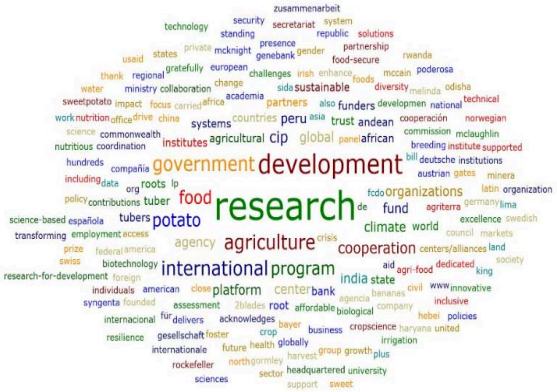

WARDA

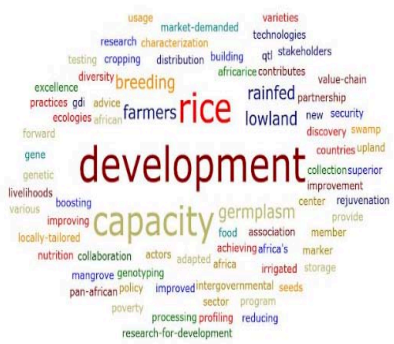

CIMMYT

CRIN

FIIRO

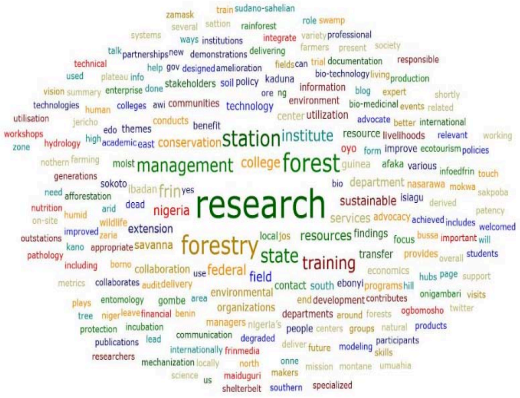

FRIN

IART

IAR

ICRISAT

IFPRI

IITA

ILRI

LCRI

NAERLS

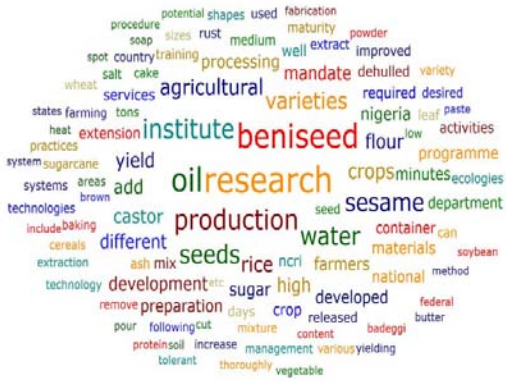

NCRI

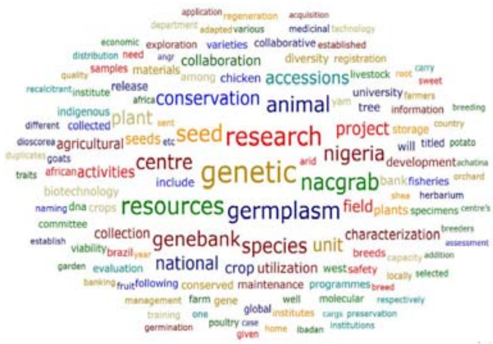

NACGRAB

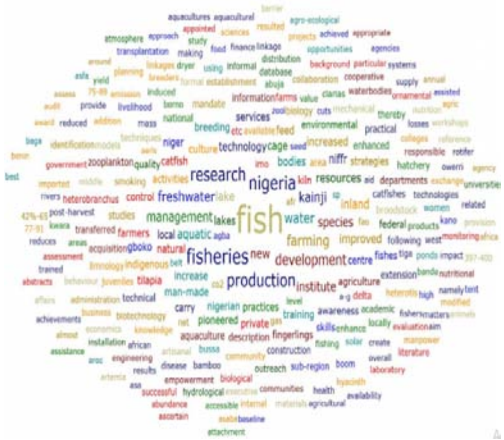

NIFFR

NAPRI

NIFST

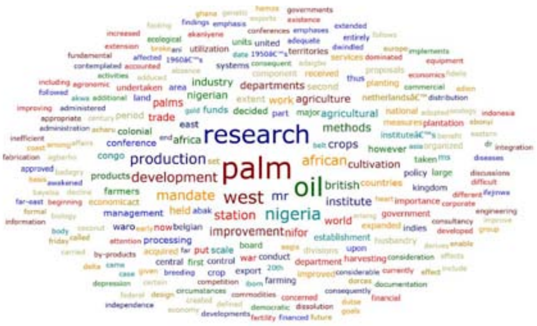

NIFOR

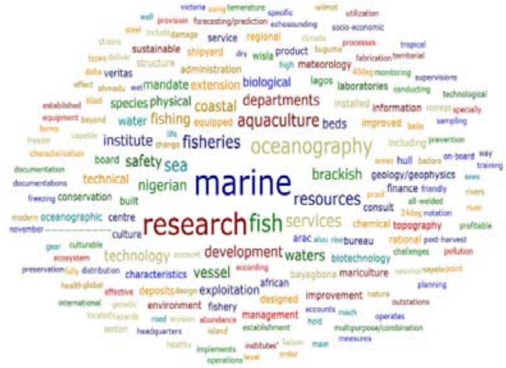

NIOMR

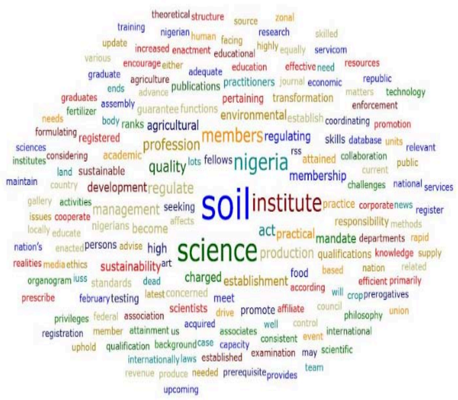

NISS

NIHORT

NRCRI

NSPRI

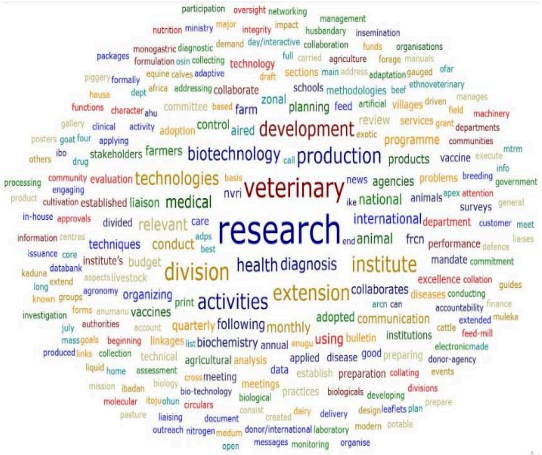

NVRI

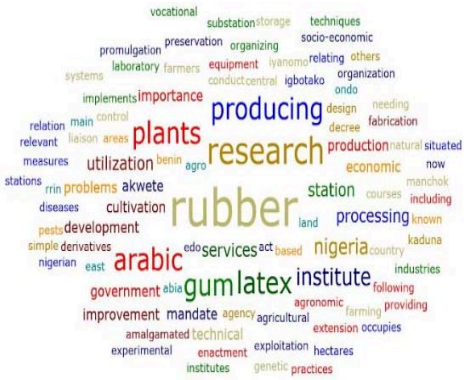

RRIN

CIFOR

Figure 1: Word Cloud of Activities of Agricultural Research Institutes

5.3 Regression Analysis of Webometric Indexes Influencing the Visibility of Websites of Agricultural Research institutes in Nigeria

The result in Table 2 shows the regression analysis of webometric indexes on the extent of visibility of websites of agricultural research institutes in Nigeria. The Semi log functional form was chosen as the lead equation based on the highest R^2 value, number of significant variables, and correct signs (+, -). The R^2 value of 0.561 indicates 56.10% variation in the extent of visibility explained by the independent variables. From table 4.6, two (2) out of the eight (8) variables used in the analysis were statistically significant. Global rank correlated positively (3.653; $P<0.05$) with visibility of the websites. The relationship was significant at 0.05 level. Visit duration correlated negatively (-21.029; $P<0.05$) with visibility of the websites. The relationship was significant at 0.05 level. The null hypothesis was therefore accepted that the webometric indexes does not influence the extent of visibility of the websites of agricultural research institutes in Nigeria.

The coefficient of global rank was found to have correlated positively with visibility of website. This implies that as the global rank increases (indicating higher global visibility or recognition), the extent of visibility of websites of agricultural research institutes in Nigeria also increases. In their research on the impact of organic traffic on user engagement and global rank of airline websites, Sakas & Reklitis (2021) found a positive correlation between user engagement and global rank, indicating that user engagement helps the airline website's global rank to increase. The coefficient of visit duration was found to have correlated negatively with visibility of websites. This suggests that as the visit duration increases (indicating longer time spent on the websites), the extent of visibility of these websites decreases. However, this does not conform to a priori expectation as visit duration should enhance visibility. According to Graus et al. (2015), longer visit duration signify that visitors are engaging with the website content and finding it beneficial. Increased user engagement measures, such as reduced bounce rates and better click-through rates, can result from users browsing a website for longer periods of time, which signals a good user experience that leads to improved visibility. In the same vein, Drivas

et al. (2020) stated that longer loading time for websites impact user experience negatively because it reduces the visit duration of website patrons thereby increasing the bounce rate.

Findings revealed that the coefficient of bounce rate had a negative correlation with visibility of websites. Although it was not significant, but it suggests that websites with lower bounce rates tend to have better visibility or higher levels of online presence. According to Ilbahar & Cebi (2017), search engines frequently give preference to websites that keep visitors engaged, resulting in improved visibility. Websites that provide relevant and valuable content, aligning with user expectations and intent, tend to have lower bounce rates. These websites may provide a seamless user experience, engaging visitors and encouraging them to explore more. Furthermore, user experience may be improved, and bounce rates can be decreased on websites with easy navigation. Visitors are more likely to remain longer and interact with the content of a website if they can easily access different areas, discover the information they need, and navigate to it. Better visibility is more likely to be given to websites that have a solid structure (Panda et al., 2015).

Table 2: Regression Analysis of Webometric Indexes Influencing the Visibility of Websites of Agricultural Research institutes in Nigeria

Variables	Parameters	Semi Log +	Double Log	Linear	Exponential
(Constant)		37.890 (0.846)*	1.985 (1.735)	40.296 (2.408)	1..513 (3.246)
Country Rank	X_1	1.762 (0.937)	0.001 (0.027)	3.345E-5 (0.541)	3.381E-7 (0.196)
Global Rank	X_2	3.653 (2.237)*	0.121 (2.907)*	1.571E-6 (1.840)***	3.912E-8 (1.645)
Total Visits	X_3	1.730 (0.192)	-0.080 (-0.349)	8.025E-5 (1.365)	1.776E-6 (1.084)
Pages per visit	X_4	-14.594 (-0.872)	-0.430 (-1.007)	0.460 (0.196)	-0.015 (-0.234)
Bounce Rate	X_5	-6.889 (-0.508)	-0.366 (-1.056)	0.010 (0.067)	-0.001 (-0.307)
Visit Duration	X_6	-21.029 (-2.709)*	-0.405 (-2.042)***	-2.274 (-3.274)*	-0.049 (-2.404)*
Speed	X_7	-0.769 (-0.054)	-0.185 (-0.512)	0.122 (0.137)	0.000 (-0.016)
Keywords	X_8	2.884 (0.558)	0.153 (1.158)	-0.001 (-0.324)	-2.041E-5 (-0.366)

Source: Field Survey Data, 2023 R^2 =0.561, F-ratio = 3.195, n = 28, + = Lead equation.
Data were available for only 28 Agricultural Research Institutes.
*Values in parentheses are t-value. * significant at 5%, *** significant at 10%*

VI. CONCLUSION

The study concluded that the visibility of agricultural research institute websites varied across different institutes, with some achieving high visibility, others moderate, and a few experiencing low visibility. The high and moderate levels of visibility were linked to the active sharing of links and content, as well as maintaining a presence on social media platforms such as Facebook, Twitter, LinkedIn, YouTube, and Instagram, which facilitated link-building and increased website traffic. Additionally, the study highlighted that the size of words in the word cloud reflected their frequency of mention, with the most prominent activities represented by words such as “research,” “development,” “food,” “capacity,” “livestock,” “agricultural,” “genetic,” “fish,” “palm,” “marine,” “soil,” and “production.” Furthermore, the findings indicated a positive correlation between global rank and website visibility, meaning that

institutes with higher global recognition had greater online visibility. However, visit duration showed a negative correlation with visibility, suggesting that websites with longer user engagement did not necessarily achieve higher visibility.

VII. RECOMMENDATIONS

The study recommended that agricultural research institutes actively utilize social media platforms such as Twitter, Facebook, and LinkedIn to promote their website content and drive traffic. Regular sharing of research findings, updates, and engaging content on these platforms can enhance visibility and attract a wider audience. Additionally, adopting search engine optimization (SEO) strategies, improving website content quality, and fostering link-building collaborations with relevant institutions can further strengthen online presence. Institutes should also monitor website analytics to assess engagement patterns and optimize their digital strategies for better visibility and accessibility.

REFERENCES

1. Akinwale, J. A., Wole-Alo, F. I., & Oluwole, B. O. (2023). Digital platforms for linking agriculture investors with smallholder farmers in Nigeria. Journal of Agricultural Extension, 27(2), 65–72. https://doi.org/10.4314/jae.v27i2.6
2. Clement, E., Emmanuel, M., Magala, D., Graceline, A., Denis, A., Patrick, K., Amos, W., Allan, T., , U., Egesa, J., & Sylvester, B. (2021). Perceptions on Liking and Disliking Public Agricultural Research Institutes in Uganda: A Case of Abi, Bulindi, Ngetta, Mbarara and Mukono ZARDIs. Journal of Resources Development and Management. https://doi.org/10.7176/jrdm/76-04
3. Davis, K., Lion, K., & Arokoyo, T. (2019). Organisational capacities and management of agricultural extension services in nigeria: Current status. *South African Journal of Agricultural Extension (SAJAE)*, *47*(2), 118–127. https://doi.org/10.17159/2413-3221/2019/v47n2a508
4. Drivas, I. C., Sakas, D. P., Giannakopoulos, G. A., & Kyriaki-Manessi, D. (2020). Big data analytics for search engine optimization. *Big Data and Cognitive Computing*, *4*(2), 5. https://doi.org/10.3390/bdcc4020005
5. Graus, M. P., Willemsen, M. C., & Swelsen, K. (2015). Understanding real-life website adaptations by investigating the relations between user behavior and user experience. In *Lecture Notes in Computer Science* (pp. 350–356). Springer International Publishing. http://dx.doi.org/10.1007/978-3-319-20267-9_30
6. Ilbahar, E., & Cebi, S. (2017). Classification of design parameters for E-commerce websites: A novel fuzzy Kano approach. *Telematics and Informatics*, *34*(8), 1814–1825. https://doi.org/10.1016/j.tele.2017.09.004
7. Kunosic, S., Ceke, D., & Zerem, E. (2019). Advantages and Disadvantages of the Webometrics Ranking System. In *Scientometrics Recent Advances* (pp. 19–44). IntechOpen.
8. Ogege, S. (2011). Nigeria's development challenges in a digitalized global economy. *African Research Review*, *4*(4). https://doi.org/10.4314/afrrev.v4i4.69213
9. Ojokoh, B. A., & Akinola, A. (2017). Enhanced Webometric Ranking of Nigerian Public Universities. *Journal of Education, Society and Behavioural Science*, *22*(3), 1–16. https://doi.org/10.9734/JESBS/2017/36136 Pant, G., & Pant, S. (2017). Visibility of Corporate Websites: The Role of Information Prosociality. S&P Global Market Intelligence Research Paper Series.
10. Patel, N. (2015). Link building strategies that actually work: A complete guide. Retrieved from https://neilpatel.com/blog/link-building-strategies-that-work/
11. Razak, S. H., Mohamed, S. E. N., Ismail, A., & Ramzi, N. (2019). An assessment of the web presence of top 10 university in Southeast Asia. *International Journal of Innovative Technology and Exploring Engineering*, *8*(9), 3316–3319. https://doi.org/10.35940/ijitee.i8746.078919

12. Rosario, M. Jr. N. D. (2021). Evaluating state universities websites visibility in one Philippine region using search engine optimization tools. *Computer Science and Information Technology*, *9*(2), 25–32. 10.13189/csit.2021.090201
13. Sakas, D. P., & Reklitis, D. P. (2021). The impact of organic traffic of crowdsourcing platforms on airlines' website traffic and user engagement. *Sustainability*, *13*(16), 8850. https://doi.org/10.3390/su13168850
14. Weideman, M. (2009). Elements of website visibility and research. In *Website Visibility: The Theory and Practice of Improving Rankings* (pp. 41–57). Elsevier.
15. Zhang, S., & Cabage, N. (2016). Search engine optimization: Comparison of link building and social sharing. *Journal of Computer Information Systems*, *57*(2), 148–159. https://doi.org/10.1080/08874417 .2016.1183447

This page is intentionally left blank

Health Risk Linked to the Consumption of Fish From Lake Tshangalele in the Sout-East of the Democratic Republic of Congo

Koya Mawazo Kaya,Nyembo wa Mwehu Eddy, Lulu Lwamba Joseph, Kitenge Mugimba Dieudonné, Anjelani Mbuyu Eugène, Kalunga Mbuba Justin, Kasongo4 Kongolo Michail, Mbuyi META Natacha, Prearo Marino & Andrea Dominici

University of Kalemie

SUMMARY

Lake Tshangalele is a reservoir formed in 1930 from the Lufira River in the south-east of the Democratic Republic of the Congo for the construction of the Mwadingusha Dam. This lake is very rich in fish. Unfortunately, for several decades, it received mining waste from the metallurgical plants in the cities of Likasi and Kambove.

To assess the health risk associated with the consumption of Lake Thangalele, fish samples were taken from the lake at the site of the locality of Kapolowe-Mission (n=21). And samples of reference fish were taken upstream of any mining activity of the Panda and Kasungwe rivers as well as of the Congo River at the level of the sections located near their sources (n=11). Then, after the sampling, a survey was carried out among 148 permanent inhabitants of Kapolowe-Mission which made it possible to understand the average quantity of fish that each of these 148 interviewed people consumed per day in their family.

Keywords: NA

Classification: LCC Code: QH545.M3

Language: English

Great Britain Journals Press

LJP Copyright ID: 925654
Print ISSN: 2631-8490
Online ISSN: 2631-8504

London Journal of Research in Science: Natural & Formal

Volume 25 | Issue 5 | Compilation 1.0

Health Risk Linked to the Consumption of Fish From Lake Tshangalele in the Sout-East of the Democratic Republic of Congo

Koya Mawazo Kaya[α], Nyembo wa Mwehu Eddy[σ], Lulu Lwamba Joseph[ρ], Kitenge Mugimba Dieudonné[Ↄ], Anjelani Mbuyu Eugène[§], Kalunga Mbuba Justin[χ], Kasongo Kongolo Michail[ν], Mbuyi META Natacha[ϴ], Prearo Marino[ζ], & Andrea Dominici[£]

SUMMARY

Lake Tshangalele is a reservoir formed in 1930 from the Lufira River in the south-east of the Democratic Republic of the Congo for the construction of the Mwadingusha Dam. This lake is very rich in fish. Unfortunately, for several decades, it received mining waste from the metallurgical plants in the cities of Likasi and Kambove.

To assess the health risk associated with the consumption of Lake Thangalele, fish samples were taken from the lake at the site of the locality of Kapolowe-Mission (n=21). And samples of reference fish were taken upstream of any mining activity of the Panda and Kasungwe rivers as well as of the Congo River at the level of the sections located near their sources (n=11). Then, after the sampling, a survey was carried out among 148 permanent inhabitants of Kapolowe-Mission which made it possible to understand the average quantity of fish that each of these 148 interviewed people consumed per day in their family.

Then, 11 Metal Trace Elements, namely Al, As, Cd, Co, Cu, Mn, Ni, Pb, Se, U and Zn, were assayed by Inductively Couple Plasma Mass Spectrometry (ICP-MS) at the Catholic University of Leuven in Belgium and by Inductively Couple Plasma Optical Emission Spectroscopy (ICP-OES) at the laboratory of the Congolese Control Office (OCC) in Lubumbashi in Democratic Republic of Congo. And finally, for 5 metal trace elements, namely Cd, Cu, Ni, Pb, Zn, the health risk was evaluated, which is expressed by the DQ hazard quote. This is calculated for the oral route on the basis of the formula DQ=FxQ x 0.208 x C/ADI x P. If DQ is greater than 1, it means that there is a good chance that it has been harmful to the health of the consumer. On the other hand, if the DQ value is less than 1, it means that there is no potential health risk associated with the consumption of fish.

This study showed that the fish from Lake Tshangalele is not suitable for human consumption since by consuming this fish 81,7% of adults and 1OO% of children have a high risk of suffering the potental of harmful effects of only 5 metal trace elements studied, which are Cu, Ni, Pb, Zn and Cd, without taking into account the other possible pollutants non.studied.

The pathologies that can be caused in humans by the different metal trace elements studied in this study have been described, to draw the attention of decision-makers, so that rigorous measures are taken to prohibit metallurgical plants from dumping their mining wastes into aquatic ecosystems, particularly those that provide fish to the population.

Author α χ§: Health Sciences Departement, University of Kalemie, DR Congo.
σ ρ: Faculty of Agricultural Sciences and Environment, University of Kalemie, DR Congo.
Ↄ:Technical Sciences Departement University of Kalemie, DR Cong.
ϴ ν: Faculty of Medecine, University of Kalemie, DR Congo.

London Journal of Research in Science: Natural & Formal

ζ: Instituto Zooprofilatico Sperimentale del Piemonte, Liguria e Valle d'Aosta, Turin, Italia.
£:. Independet Veterinarian, Turin, Italia.

I. INTRODUCTION

Lake Tshangalele is a reservoir of the Lufira River formed in 1930 for the construction of the Mwandingusha dam. For several decades it has received effluents from the Shituru hydrometallurgical complex in Likasi via the Likasi, Buluo and Panda Rivers, and wastes from the Panda Electric Smelter in Likasi also via the Panda River. And finally, it receives waste from the Kambove Concentrator via the Kabambakola, Mura and Panda Rivers (Kalenga et al., 2005). However, the effluents from the Shituru hydrometallurgical complex in Likasi contain metal trace elements (MTE) at their outlet from the plant with very high average concentrations such as Al (aliminium) with 215 µg/L, As (arsénic) with 3,9 µg/L, Cd (cadmium) with 9,9 µg/L, Co (cobalt) with 1285,1 µg/L, Cu (copper) with 816 µg/L, Mn (manganese) with1934,8µg/L, Ni (nickel) with 18,9µg/L, Pb (lead) with 20,13µg/L, Se (selenium) with 21 µg/L, U (uranium) with 8,5µg/L et Zn (zinc) with 120µg/L.

And yet, Lake Tshangalele is very rich in fish and provides a significant portion of fish consumed by the population of Likasi and Lubumbashi regions. We can therefore say that the fish of Lake Thangalele bathe in an aquatic environment heavily polluted with trace metal elements. Metal elements are necessary for life in small doses; but, they can be very harmful in excessive quantities. However, some MTEs are not necessary for life and are harmful in all cases, such as lead, cadmium and antimony. (Denayer, 2000; Miquel, 2001). Metal Trace Elements accumulate in living organisms and have short- and long-term toxic effects. Their toxicity develops through bioaccumulation (Miquel, 2001). Food remains the major source of contamination of humans with Metal Trace Element (Derache, 1986; Gérin 2003). This is why monitoring the quality of fish and its aquatic environment , in accordance with Decree N° 038/2003 (2003) of March 26, 2003 relating to Mining Regulation in its article 462, is of great importance for the protection and preservation of the health of the population who regularly consumes fish. In addition, with a view to protecting the environment, the Law N° 11/009 on the protection of the environment (2011) in its article 49, prohibits the discharge of wastewater, mine discharges, or any other contaminant into surface water. Unfortunately, despite the fact that the congolease population of the South-East of the Democratic Republic of Congo consumes fish from rivers polluted with mining waste, which is otherwise untreated, studies on the quality control of the fish are rare in our country.

When the fish of Lake Tshangalele bathe in an aquatic environment polluted with mining waste, themselves loaded with multiple pollutants including Metal Trace Elements (SNC-Lavalin, 2003 ; Kalenga, 2005), can we really believe that the consumption of these fish of the Lake is without risk to human health ? For our part, we believe that the population that buys fish from Lake Tshangalele consumes fish that is unfit for human consumption and its health is seriously exposed to a great risk from the toxic effects of the pollutants that this fish contains.

Thus, the objective of this study is to assess the health risk posed to human health by the consumption of fish from the lac Tshangalele

II. MATERIALS AND METHODS

2.1. Study Environment

Our research on the health risk associated with the consumption of fish from Lake Tshangalele was carried out in Kaplowe-Mission, in the Likasi region, in Haut-Katanga Province, in the south-east of the Democratic Republic of Congo. The lake has an area of 362,5 km² and its average depth is 2.60 m. The

lake is crossed from one end to the other by the Lufira River. It is very rich in fish and it is the main source of fish for the Likasi and Lubumbashi regions (Regrl, 2010; Infocongo, 2024). Kapolowe-Mission is a locality located on the shores of Lake Tshangalele. It has a population of 20000 habitants. In this locality, fish is one of the staple foods.

2.2 Fish Studied

The fish studied belong to a single family: Cyclidae (Tilapia baloni; T. rendalli, Tilapia sp).

2.3. Sampling and samples preparation

Fish samples were collected in March 2009 and August 2015 at the site of the locality of Kapolowe-Mission, located downstream of the mining activities (n=21) and presumed to be polluted. On the other hand, reference fish samples were taken upstream of any mining activity of the Panda, Kasungwe and Congo rivers at their sections presumed not to be polluted by mining waste and located near their sources (n=11). Fish were caught by net at the Kaoplowe-Mission site. After capture the fish samples were placed in small packing bags(28 cmx17 cm) and transported in insulated boxes to the freezer for conservation. The preparation consisted of stripping the samples of their viscera and scales using a knife. After cleaning with distilled water, put in a bucket, the samples were dried in Binder brand ovens at 70 °C for 48 hours. After drying, the samples were crushed and powdered using porcelain mortars and pestles. The samples were then sent to the laboratory.

2.4. Chemical analysis of samples

Eleven metal trace elements namely Al, As, Cd, Co, Cu, Mn, Ni, Pb, Se, U and Zn were selected and assayed using Inductively Couple Plasma Mass Spectrometry Couple (ICP-MS) at the laboratory of the Catholic University of Leuven in Belgium and Inductively Couple Plasma Optical Emission Spectroscopy (ICP-OES) at the laboratory of the Congolese Control Office (OCC) in Lubumbashi, DR Congo.

2.5. Statistical analysis

To assess and evaluate the health safety of fish from the Lake Tshangalele, the concentrations of fish samples from the lake were, by the Wilcoxon test as described by Ancelle (2002), compared with the concentrations of the reference fish samples from the Panda and Kasungwe rivers as well as from the Congo River at the level of their sections not polluted with mining wastes.

2.6. Health risk

a). Hazard quotient

It was necessary to assess the health risk to which a person regularly consuming fish from Lake Thangalele is exposed. A health risk refers to a more or less probable immediate or long-term risk to which public health is exposed (Akoto and al., 2014).

The health risk associated with fish consumption is expressed by the hazard quotient DQ. This is calculated for the oral route based on the following formula: (QD=F x Q x 0.208 x C) /ADI x P. In this formula: C represents the MTE concentrations of fish in mg/kg; F represents the frequency of exposure (F=1); Q is the quantity of fish ingested per day (kg/day). For the locality of Kapolowe-Mission, the quantity of fish ingested by an adult or a child are recorded in Table II which gives the results of the calculation of the hazard quotient (DQ) associated with the consumption of fish from Lake Tshangalele for 5 trace metal elements (TMEs). ADI is the permitted daily intake or reference dose. P represents the body weight of the consumer (Akoto et al., 2014). The average body

weight of an adult , female or male, (60kg) and that of children (28kg) were given to us by one of the health centers of Kapolowe-Mission. The daily intake allowed is 2.10^{-4}mg/kg for Cd, 410^{-2} for Cu, 210^{-2} for Ni, 3.610^{-3} for Pb and 3.10^{-1} for Zn. If the DQ value is greater than 1, it means that there is a high chance that there are harmful effects on health. On the other hand, if the DQ value is less than 1, it means that there is no potential health risk associated with the consumption of fish (Akoto et al.,2014). The higher the DQ value, the greater the probability of adverse health effects occurring (Akoto et al., 2014; Amirah et al., 2014).

b). Survey method and questionnaire

To assess the health risk associated with the consumption of fish from Lake Tshangalele, a survey was conducted. Our sample was 148 inhabitants, made up of stratified sampling and quota. This sample consisted of 50 % adults and 50% children aged 10 to 12 years.

The survey questionnaire included 3 main questions

1°) How many days a week do you consume fish from Lake Tshangalele with your family ?;
2°) How many fish does a family member consume at a meal ?;
3°) What is the number (in fishermen's language this means size, caliber...) of fish usually consumed by the family ? A certain number of fish of different « numbers » had been weighed to know their average weight. This made it possible to estimate the average weight of fish that an interviewee consumes on average per day.

c). Health risk with multiple pollutants

It has been shown that for exposure to two or more pollutants at the same time, such as metal trace elements, adverse health effects add up, and the total hazard quotient (DQ) value is equivalent to the sum of the hazard quotients of all pollutants that have contaminated fish or any other food. Thus, for the trace metal elements, we have: $DQ_{total} = D_{MTE1} + DQ_{MTE2} + DQ_{MTE3} + \ldots QD_{MTEn}$ (Akoto et al.,2014).

III. RESULTS

Table I: Concentrations of Metal Trace Elements in fish samples collected from the Lake Tshangalele at the Kapolowe-Mission locality site (mg/kg).

N°	Code	Nom scientifique	Al	As	Cd	Co	Cu	Mn	Ni	Pb	Se	U	Zn
1	KAM P10	Tilapia baloni Trewavas & Stewart	20,5	0,283	0,389	20,157	8,67	63,01	0,802	0,188	0,934	0,09	128,5
2	KAM P11	Tilapia baloni Trewavas & Stewart	54,1	0,143	0,49	15,574	16,76	53,77	0,328	0,208	1,062	0,071	134,1
3	KAM P12	Tilapia baloni Trewavas & Stewart	66,0	0,347	0,668	28,647	19,41	70,96	4,123	0,494	1,104	0,068	127,8
4	KAM P13	Tilapia baloni Trewavas & Stewart	16,5	0,138	0,31	10,381	10,23	95,13	0,466	0,53	0,668	0,106	120,9
5	KAM P15	Tilapia baloni Trewavas & Stewart	728,3	0,628	2,291	82,248	105,3	262,11	1,57	1,289	0,31	0,337	175,5
6	KAM P16	Tilapia baloni	85,8	0,206	0,555	15,607	13,47	67,91	0,601	0,27	2,291	0,114	184,1

		Trewavas & Stewart											
7	KAM P17	Tilapia baloni Trewavas & Stewart	36,9	0,212	0,44	17,178	14,48	51,92	0,469	0,237	0,555	0,17	112
8	KAM P18	Tilapia rendalii	56,4	0,125	0,611	9,602	2,63	21,87	0,291	0,533	0,44	0,018	136,9
9	KAM P19	Tilapia Sp	2,612	30,889	0,531	13,77	10,34	19,623	0,502	0,031	0,346	0,028	0,329
10	KAM P20	Tilapia Sp	23,148	46,7	0,931	12,424	31,071	11,936	0,299	0,028	0,213	0,043	0,798
11	KAM P21	Tilapia Sp	15,737	34,028	0,939	12,146	14,83	2,393	0,446	0,026	0,401	0,002	0,424
		Moyenne	100,5	10,3	0,7	21,6	22,5	65,5	0,9	0,35	0,7	0,1	101,9
		Ecart-type	209,7	17,7	0,5	20,8	28,4	71,2	1,1	0,4	0,6	0,1	68,6

The number values of concentrations above the WHO, FAO and EU thresholds are as follows: a). For Cd: OMS (1/11) et EU (11/11; b). For Cu : OMS (1/11) et EU (11/11); c). For Ni : EU (11/11; d).For Cu: OMS (0/11) et EU (4/11); e). For Zn : OMS (0/11) et EU (8/11).

3.2. Results of the statistical analysis

As a result of the statistical analysis by the Wilcoxon test, only Arsenic (As) was considered to have contaminated Lake Tshangalele.

Tableau II: Results of the calculation of the health risk related to the consumption of fish from Lake Tshangalele at the Kapolowe-Mission site for 5 TMEs (Cd, Cu, Ni, Pb, Zn, Cd).

N°	Average quantity of fish consumed by a surveyed inhabitant and number of inhabitants habitually consuming this quantity		Health risk related to the consumption of fish from Lake Tshangalele at Kapolowe-Mission for each MTE individually and total DQ for 4 MTEs (Cu, Ni, Pb, Zn)						Total health risk for 5 MTEs (Cu, Ni, Pb, Zn plus Cd)
	Quantity of fish (g)	Number of inhabitants	Cu	Ni	Pb	Zn	Total DQ for Cu, Ni, Pb, Zn)	Cd	
A Adults									
1	500	6	0,9	0,07	0,16	0,58	1,71	6,00	7,71
2	490	2	0,9	0,07	0,16	0,57	1,71	5,88	7,59
3	453	4	0,8	0,07	0,15	0,53	1,66	5,43	7,09
4	426	2	0,8	0,06	0,14	0,49	1,49	5,11	6,60
5	378	2	0,7	0,05	0,12	0,44	1,26	4,53	5,79
6	343	4	0,6	0,05	0,11	0,40	1,16	4,11	5,27
7	245	2	0,4	0,03	0,08	0,28	0,79	2,94	3,73
8	227	8	0,4	0,03	0,07	0,26	0,76	2,72	3,48
9	204	2	0,39	0,03	0,06	0,23	0,71	2,44	3,15
10	196	2	0,38	0,03	0,06	0,22	0,69	2,35	3,04

11	173	2	0,38	0,02	0,05	0,20	0,65	2,07	2,72
12	147	12	0,28	0,02	0,04	0,17	0,51	1,76	2,27
13	142	2	0,27	0,02	0,04	0,16	0,49	1,70	2,19
14	86	6	0,16	0,01	0,02	0,10	0,29	1,03	1,32
15	84	2	0,16	0,01	0,02	0,09	0,28	1,00	1,28
16	76	4	0,10	0,01	0,02	0,08	0,21	0,91	1,12
17	60	2	0,10	0,01	0,02	0,07	0,20	0,72	0,92
18	49	2	0,09	0,00	0,01	0,05	0,15	0,58	0,73
19	42	4	0,08	0,00	0,01	0,05	0,14	0,50	0,64
20	38	4	0,07	0,00	0,01	0,04	0,12	0,45	0,57
B Children									
37	250	6	1,0	0,08	0,18	0,62	1,88	6,50	8,38
	240	2	1,0	0,08	0,17	0,60	1,85	6,24	8,09
	227	2	0,9	0,07	0,1,6	0,56	1,69	5,90	7,59
	223	2	0,9	0,07	0,16	0,55	1,68	5,79	7,47
	220	2	0,9	0,07	0,15	0,55	1,67	5,72	7,32
	200	2	0,8	0,06	0,14	0,50	1,50	5,20	6,70
	180	2	0,7	0,06	0,12	0,45	1,33	4,68	6,01
	170	2	0,7	0,04, 05	0,12	0,42	1,29	4,42	5,71
	160	4	0,6	0,05	0,11	0,40	1,16	4,16	5,32
	150	2	0,6	0,05	0,11	0,37	1,13	3,90	5,03
	147	2	0,6	0,04	0,10	0,36	1,10	3,82	4,92
	142	2	0,5	0,04	0,10	0,35	1,0	3,69	4,68
	122	2	0,5	0,04	0,08	0,30	0,92	3,17	4,09
	110	4	0,4	0,03	0,08	0,27	0,78	2,86	3,64
	98	8	0,4	0,03	0,07	0,24	0,74	2,54	3,28
	90	2	0,37	0,03	0,06	0,22	0,68	2,34	3,02
	76	4	0,3	0,02	0,05	0,19	0,56	1,97	2,53
	64	6	0,26	0,02	0,04	0,16	0,48	1,66	2,14
	60	6	0,25	0,02	0,04	0,15	0,46	1,56	2,02
	56	2	0,20	0,02	0,04	0,14	0,40	1,45	1,85
	49	2	0,20	0,01	0,03	0,12	0,36	1,27	1,63
	42	4	0,20	0,01	0,03	0,10	0,34	1,09	1,43
	38	4	0,15	0,01	0,02	0,09	0,27	1,00	1,27

In the table above, we can see the following. a). Individual DQ values of Cu, Ni, Pb and Zn: none of the 4 TMEs has a DQ value greater than 1. b). Collective DQ values of Cu, Ni, Pb and Zn: the total number of DQs with values greater than 1 and resulting from the summation of the individual DQ values of Cu, Ni, Pb and Zn is 50 out of 148 i.e 33,7%; c). For Cd: the total number of DQs with values greater than 1 is132 out of 148 i.e.89,1%; d). Collective DQ values of 5 MTEs namely Cu, Ni, Pb, plus Cd : the total number of DQs with values greater than 1 is 136 out 148 i.é. 91,8%; e). For all 5 TMEs namely (Cu, Ni, Pb, Zn plus Cd): the DQs values greater than 1 range from 1,12 to 8,38.

IV. DISCUSSION

4.1. Results of the Wilcoxon test

As is the only one of the 11 measured MTEs, namely Al, As, Cd, Co, Cu, Mn, Ni, Pb, Se, U and Zn (Table 2) to have been found to contaminate Lake Tshangalele after statistical analysis by the Wilcoxon tes.

4.2. Results of the health risk assessment

4.2.1. Single-pollutant health risk

a). Cu, Ni, Pb and Zn

There is no hazard quotient value greater than 1 for individual Cu, Ni, Pb, and Zn. This suggests that an inhabitant of Kapolowe-Mission who regularly feeds on fish from Lake Tshangalelele would have very little chance of suffering adverse health effects from any of these 4 metal trace elements if this fish contained only one TME.

In very low doses, Cu is a well-known trace element. It is essential for the synthesis of hemoglobin, normal bone formation, and maintenance of myelin in the nervous system (Wright & Welbourn, 2002). However, chronic exposure can cause irritation of the affected areas, including the mucous membranes, nasal cavities, eyes. It causes headaches, stomach aches, dizziness, digestive disorders such as vomiting and diarrhea (ASEF, 2017).

In small quantities, nickel is essential but if the absorption is too great, it can pose a health risk. Chronic inhalation Ni poisoning results in changes in the nasopharynx and respiratory tract epithelium. Chronic changes may include rhinitis, polyps, asthma or pulmonary fibrosis. In addition, an increased incidence of lung cancers has been observed (Gates et al., 2023)

It should be noted that Pb is classified as one of the most toxic metal trace elements. Pb is toxic even at low concentrations and has no significant biological properties in humans and animals (Miquel 2001). Lead poisoning is manifested by renal damage characterized by discrete tubular involvement and/or a slight reduction in the glomerular filtration rate. This can sometimes lead to the development of chronic nephritis (Lauwerys, 1999). Encephalitis is the most serious manifestation of lead poisoning. In addition, lead poisoning causes anemia, high blood pressure, depression in iodine uptake by the thyroid and digestive disorders resulting in colic (Lauwerys, 1999).

Zinc is essential for normal growth, reproduction, and life expectancy in animals (Lauwerys). In chronic exposure to Zn, bone marrow and neurological effects may occur. Chronic digestion of Zn, and resulting Cu deficiency, result in sideroblastic anemia, granulocytopenia and myelodysplasmic syndrome (Angnew and Slesinger, 2022).

b). Cd

Cd has several values of the hazard quotient (DQ) greater than 1 (Table II): 132 out of 148 or 89,1% 91.9%, including 58 adults out of 148 (39.2%) and 74 children out of 148 (50%). All of this indicates that the people of Kapolowe-Mission who regularly consume fish from Lake Tshangalele are at great risk from the toxic effects of Cd. This shows that the fish from Lake Tshangalele is unfit for human consumption.

Prolonged exposure to cadmium in humans can lead to kidney damage, bone fragility, harmful effects on the respiratory system, reproductive disorders and an increased risk of cancer and especially in the occurrence of prostate and lung cancers (Lauwerys, 1999; Viala, 2005).

4.2.2. Health risk due to multiple pollutants

a). Cu, Ni, Pb and Zn

When we consider the health risk associated with the consumption of fish from Lake Tshangalele caught in Kapolowe-Mission and contaminated with Cu, Ni, Pb and Zn, the results obtained show that

the values of the hazard quotient resulting from the summation of the hazard quotients of all 4 METC combined and greater than 1 are 50 out of 148 corresponding to 50 consumers out of 148, i.e.33,7%
We have just obtained a somewhat surprising result: 50 DQ greater than 1 for metallic trace elements that individually had no DQ value greater than 1. The potential harmful effects of these 4 metallic trace elements were added together (multi-pollutant health risk principle) and 50 values of the DQ greater than 1 were obtained. Indeed, the values of the DQs ranged from 0.07 to 0.9 for Cu, from 0.00 to 0.07 for Ni, from 0.01 to 0.16 for Pb and for Zn from 0.04 to 0.58. None of the 4 metallic trace elements had a single DQ value greater than 1 individually.

This shows that the health quality of a fish depends not only on pollutants with high concentrations, but also on those with low concentrations. Indeed, the latter, even if individually they are not harmful to the consumer because of their low concentration levels, but at least their potential harmful effects added together. Thus, there is a high probability that the health of the potential consumer will be exposed to a risk of harmful effects added to several known and/or unknown pollutants. Thus, 33,7% of inhabitants of Kapolowe-Mission consuming fish from Lake Tanganyika are exposed to toxic effets of Cu, Ni, Pb and Zn together. This shows that the fish from Lake Tanganyika is not suitable for human consumption.

b). Cu, Ni, Pb, Zn plus Cd.

It can be seen that of the 148 consumers, inhabitants of Kapolowe-Mission for whom the value of the hazard quotient is greater than 1 for 5 ETMs, namely, Cu, Ni, Pb, Zn and Cd, we have 62 out of 74 adults or 81.7% and 74 out of 74 children or 100%, and a total of 136 inhabitants of Kapolowe-Mission out of 148 or 91.8 %. This means that the health of the 91.8% of the inhabitants of Kapolowe-Mission who consume the fish of Lake Tshangalele among whom the survey was carried out, are exposed to the toxic and harmful effects of Cu, Ni, Pb, Zn and Cd. This shows that the fish of Lake Tshangalele is not suitable for human consumption.

If we compare the result of statistical analysis with the method of calculating hazard quotient (DQ) to assess the health risk linked to the consumption of fish, we can notice that the second method is better. Indeed, as a result of the statistical analysis by the Wilcoxon test, only As is considered to have contaminated fish from Lake Tshangalele. But, with the assessment of the health risk linked to the consumption of fish, we observe that the health quality of a fish depends not only on pollutants with high concentrations, but also on those with low concentrations even if individually they are not harmful to the consumer because of their low concentration levels. But at least their potential harmful effects add together.

We can see that children are more exposed than adults to the pollutants contained in fish, even though they generally consume smaller quantities per person than adults. Indeed, when we examine the formula to calculate the hazard quotient i.e. DQ=(Fx0.208 xQxC)/ADIxP, we see that the weight P is in the denominator and therefore its value is inversely proportional to that of the hazard quotient. Since the average weight of children is lower than that of adults, the hazard quotient for them tends to be higher. The health risk associated with the consumption of fish contaminated with pollutants depends in particular on the weight of the consumer.

V. CONCLUSION

This study showed us that the fish from Lake Tshangalele is not suitable for human consumption since by consuming this fish 81,7% of adults and 100% of children, with a total of 136 inhabitants out of 148 or 91,8%, have a high risk of suffering from the potental of harmful effects of only 5 trace metal elements studied, which are Cu, Ni, Pb, Zn and Cd, without taking into account the other possible pollutants non measured.

We believe that this study provided a response to many inhabitants of the south-east of the Democratic Republic of Congo, who often ask themselves, if they can eat fish from Lake Tshangalele polluted by mining waste without risk to their health. The pathologies that can be caused in humans by the different metal trace elements studied in this study have been described, albeit in a succinct manner, to draw the attention of the reader, especially the consumer, so that they know whatsomebody can expect by consuming fish from the Lake Tshangalele.

We believe also that this description of some pathologies will draw the attention of decision-makers in the Haut-Katanga Province, so that rigorous measures are taken to prohibit metallurgical plants from dumping their mining wastes into aquatic ecosystems, particularly those that provide fish to the population.

BIBLIOGRAPHIC REFERENCES

1. Agnew, U.M. & Slesinger, T.L. (2022). Toxicité du zinc, https://www.ncbi.nlm.nih.govalb
2. Akoto, O., Bismark, E., Eshun,, F., Darko, G. & ADI, E. (2014). Concentrations and Health Risk Assessments of Heavy Metals in Fish from the Fosu Lagoon.(Int.J.Environ.Res. 8(2) :403-410.Spring 2014 ISSN :1735-6865,Accra, Ghana, 8(2) :403-410.
3. AMIRAH, M.N., AFIZA, A.S., FAIZAL, W.I.W., NURLIYAMA, N.H. & LAILI, S. (2013). Human health risk assessment of metal contamination through consumption of fish, University of Malaysia, Pahong, in Journal of Environment pollution and human health, pp. 1-5.
4. Ancelle, T. (2002). Statistique Epidémiologie, Paris, Maloine, pp.114-144
5. ASEF. (2017). Les métaux lourds-la synthèse de l'ASEF, http//www.asef-asso.fr.
6. Décret N° 038/2003 du 26 mars 2003 portant Règlement Minier en son article 462, Cabinet du
7. Président de la République, Journal officiel de la République Démocratique du Congo, Numéro spécial du 1 avril 2003, Kinshasa, p.177.
8. Danayer F.-O. (2000). Ecotoxicité des éléments traces métalliques chez les Bryophytes, Thèse de doctorat, Université de Metz (France).
9. Dérache, R. (1986). Toxicologie et sécurité alimentaire, Lavoisier, Paris
10. Gates, A., Jakubowski, J.A. & Régina, A.C. (20023). Toxicologie du nickel, National Library of Medecine, https://www.ncbi.nlm.nih.gov.
11. Gérin, M., Glomelin, P., Cendrier, S., Viau, CQueril, P., & De Wailly, F. 2003. Environment and Public Health. Quebec: Edisen, p. 391.
12. Infocongo (2024). L'assèchement du lac Tshangalele : un désastre écologique et social au Katanga, https ;//infocongo.net, lu le 19/12/2024)
13. KALENGA, N.M.P. FRENAX, J., KONGOLO, M., DE DONATO, P &. KANIKI T. (2006). Inventaire des sites de productions de stockage et de décharge des rejets minéraux du Katanga et évaluation des impacts environnementaux, Rapport scientifique du projet de coopération scientifique Inter-Universitaire 2005., PCSI N° 6312PS508, Université de Lubumbashi, RDC, 213p.
14. Koya M.K. (2017). Sécurité sanitaire des poissons des écosystèmes aquatiques pollués en déchets miniers au Sud-Est de la République Démocratique du Congo, these d'Agrégation, Faculté de Médecine Vétérinaire, Service de Biochimie. Université de Lubumbashi.
15. LAUWERYS, R.R. (1999). Toxicologie industrielle et intoxications professionnelles, 4eme éd., Masson, Louvain (1999).
16. Loi N°11/009 du 09 juillet 2011 portant principes fondamentaux relatifs à la protection de l'environnement en son article 49, Journal Officiel de la République Démocratique du Congo, Cabinet du Président de la République, Numéro special, p21.
17. MIQUEL, G. (2001). Les effets des métaux lourds sur l'environnement et la santé, Office parlementaire d'évaluation des choix scientifiques, Rapport 261, Senat, session ordinaire 200-2001, N° 2979,Assemblée nationale, Paris (France).

18. REYGRL, P. (2010). Né en 1993 à Lubumbashi, d'un père belge qui fut administrateur de territoire de l'administration du Congo-Belge dans plusieurs territoires du Katanga, habitant de Lubumbashi, interviewé le 10 mai 2010 près du lac Tshangalele.
19. Ouro-Sama, K., Solitoke, H. D., Gnandi, K., Afrademanyo, K. M., & Bowessidjaou, E. J. (2014). "Assessment and Health Risks of the Bioaccumulation of Heavy Metals in Fish Species of the Togolese Lagoon System." VertigO—la revue électronique en sciences de l'environnement 14 (2): 18. https://doi.org/10.4000/vertigo.15093.
20. SNC-Lavalin (2003). Etude sur la restauration des mines de cuivre et de cobalt :rapport E739,V, dossier M- 6708 (603082), Division Environnement, Lubumbashi (RDC), PP 44-130.
21. Viala A. (2005). Mécanismes et manifestations de l'action des toxiques au niveau sanguin, in Viala A. & Botta A. Toxicologie, Lavoisier, Paris, Londres, New-York, 2005.
22. WRIGHT, D.A. & WELBOURN, P. (2002). Environmental toxicology, Cambridge University Press.

Rural Poverty in the Micro-Region of Cruzeiro Do Sul – Acre

Marcondes de Lima Nicácio & Francisco Diétima da Silva Bezerra

Universidade Federal de Uberlândiay

ABSTRACT

The aim of this paper is to discuss poverty in rural areas. We intend to bring the discussion to a tangent with the dimensions of poverty characterization, with the specificities of rural poverty in Brazil and its manifestation in the micro-region of Cruzeiro do Sul - Acre. The approach uses different indicators of poverty and supports the debate in theoretical reflections built on bibliographical study and documentary research, which are protected by the qualitative approach. The bibliographic research includes consulting academic productions in journal databases and thesis and dissertation databases. Documentary research consisted of analyzing documents from official bodies and legislation on the subject. The data refers to the characterization of poverty in rural areas in the Cruzeiro do Sul micro-region, which is made up of five municipalities in the state of Acre. It shows that impoverishment cannot be understood as an isolated phenomenon, as it is shaped by unequal development processes in which rural areas reproduce a unique reality, which in the context studied is characterized by Amazonian social and environmental specificities.

Keywords: desarrollo. región amazónica. pobreza rural.

Classification: LCC Code: HN290.Z9 P6

Language: English

Great Britain Journals Press

LJP Copyright ID: 925655
Print ISSN: 2631-8490
Online ISSN: 2631-8504

London Journal of Research in Science: Natural & Formal

Volume 25 | Issue 5 | Compilation 1.0

Rural Poverty in the Micro-Region of Cruzeiro Do Sul – Acre

Pobreza Rural Na Microrregião De Cruzeiro Do Sul - Acre

Marcondes de Lima Nicácio[α] & Francisco Diétima da Silva Bezerra[σ]

RESUMO

O objetivo deste trabalho é discutir a pobreza no meio rural. Ensejamos trazer a discussão tangenciando as dimensões de caracterização da pobreza, com as especificidades da pobreza rural no Brasil e a sua manifestação na microrregião de Cruzeiro do Sul - Acre. A abordagem utiliza de diferentes indicadores de pobreza e a porta ao debate em reflexões teóricas construídas a partir de estudo bibliográfico e na pesquisa documental, as quais resguardadas pela abordagem qualitativa. A pesquisa bibliográfica abrange a consulta de produções acadêmicas em bases de dados de revistas e banco de teses e dissertações. A pesquisa documental consistiu na análise de documentos de órgão oficiais e legislações voltados para o tema estudado. Os dados remetem a caracterização da pobreza no meio rural da microrregião de Cruzeiro do Sul que é composta por 5 municípios do Estado do Acre, depreendendo que a pauperização não pode ser compreendida como um fenômeno isolado, pois é configurada por processos de desenvolvimento desiguais em que o espaço rural reproduz uma realidade singular, que no contexto estudado é caracterizada por especificidades sociais e ambientais amazônicas.

Palavras-chave: desenvolvimento. região amazônica. pobreza rural.

ABSTRACT

The aim of this paper is to discuss poverty in rural areas. We intend to bring the discussion to a tangent with the dimensions of poverty characterization, with the specificities of rural poverty in Brazil and its manifestation in the micro-region of Cruzeiro do Sul - Acre. The approach uses different indicators of poverty and supports the debate in theoretical reflections built on bibliographical study and documentary research, which are protected by the qualitative approach. The bibliographic research includes consulting academic productions in journal databases and thesis and dissertation databases. Documentary research consisted of analyzing documents from official bodies and legislation on the subject. The data refers to the characterization of poverty in rural areas in the Cruzeiro do Sul micro-region, which is made up of five municipalities in the state of Acre. It shows that impoverishment cannot be understood as an isolated phenomenon, as it is shaped by unequal development processes in which rural areas reproduce a unique reality, which in the context studied is characterized by Amazonian social and environmental specificities.

Keywords: desarrollo. región amazónica. pobreza rural.

Author α σ: Doutor em Economia pela Universidade Federal de Uberlândia. Professor do Instituto Federal de Educação, Ciência e Tecnologia do Acre. Cruzeiro do Sul. Acre. Brasil.

RESUMEN

El objetivo de este trabajo es discutir la pobreza en el medio rural. Queremos reconducir la discusión a las dimensiones de caracterización de la pobreza, con las especificidades de la pobreza rural en Brasil y su manifestación en la microrregión de Cruzeiro do Sul - Acre. El abordaje utiliza diferentes indicadores de pobreza y apoya el debate con reflexiones teóricas construidas a partir del estudio bibliográfico y de la investigación documental, que se amparan en el abordaje cualitativo. La investigación bibliográfica incluye la consulta de producciones académicas en bases de datos de revistas y de tesis y disertaciones. La investigación documental consistió en el análisis de documentos de organismos oficiales y legislación sobre el tema. Los datos muestran que la pobreza en el medio rural de la microrregión de Cruzeiro do Sul, formada por cinco municipios del estado de Acre, no puede entenderse como un fenómeno aislado, ya que está configurada por procesos de desarrollo desigual en los que el medio rural reproduce una realidad singular, que en el contexto estudiado se caracteriza por las especificidades sociales y ambientales amazónicas.

Palavrasclave: desarrollo. región amazónica. pobreza rural.

I. INTRODUÇÃO

O meio rural , mais que uma delimitação da organização de um território, é uma construção cultural composta por sujeitos e por processos que se condicionam às transformações políticas e socioeconômicas na intensificação da ação do sistema capitalista em atuação. Assim, tomando alguns elementos de discussão da pobreza com ponto de partida e com vistas à necessidade de explorar melhor o lócus deste estudo, a proposta é intensificar a reflexão das implicações das relações entre o campo e a pauperização. Nessa direção, o estudo caminhará sobre as implicações, dados e conjunturas na microrregião de Cruzeiro do Sul, Acre.

Nesse sentido, Marx (2017) indica que à medida que a riqueza social, o capital em funcionamento, o volume e o vigor de seus crescimentos aumentam, assim também aumenta a magnitude do proletariado e da força produtiva de seu trabalho e do exército industrial de reserva. A disponibilidade da força de trabalho se expande por razões similares às que impulsionam a expansão do capital. Portanto, a proporção do exército industrial de reserva está direta e proporcionalmente ligada ao crescimento das potências da riqueza. Entretanto, quanto mais numeroso for esse exército de reserva em comparação ao exército ativo de trabalhadores, maior será a quantidade de superpopulação estruturada, cuja miséria é inversamente proporcional ao sofrimento inerente ao seu trabalho. Por último, quanto mais alarmantes forem as camadas marginalizadas da classe trabalhadora e o exército industrial de reserva, maior será a incidência de pobreza oficial.

O modelo de desenvolvimento do capital, hoje configurado na tratativa neoliberal, envida uma linha de acumulação de capital onde não ocorre a distribuição de riqueza, ainda que seja a máxima de enfrentamento da pobreza ser difundida por governos e organizações internacionais. Ao contrário, a estrutura do Estado e por conseguinte destas organizações, é utilizada para garantir maior concentração de riqueza e majorar a imponência do Capital, gerando a mesma pobreza que posteriormente será conceituada, classificada e ecoada em números estatísticos por estas estruturas, ou seja, o interesse é justamente o inverso à supressão da desigualdade.

Requestando a análise dialética sobre as manifestações da pobreza no Brasil, no Acre e na microrregião de Cruzeiro do Sul, construindo gradações do objeto de estudo, refletimos, a partir dos dados consolidados, a necessidade de compormos, tanto na perspectiva unidimensional como multidimensional. Para tanto, são apresentadas informações de diferentes categorias, desde o contexto

de renda até outros dados relacionados à educação, à saúde e ao padrão de vida. A intenção é consolidar, tanto quanto possível, a totalidade que modela a pobreza.

O lócus e a análise empreendida é justificada por compor uma das vertentes que caracterizou a tese de doutoramento "Educação do campo e pauperização: implicação da agenda global sobre as políticas de educação básica no Vale do Juruá-Acre de autoria de Nicácio (2021), defendida na Universidade Federal do Amazonas (Brasil) no ano de 2021,cuja pesquisa tinha como objetivo central *analisar as políticas públicas de Educação do campo dirigidas aos jovens do Vale do Juruá – Acre e suas relações com a pobreza*.

O texto está organizado em três partes, além da introdução e das considerações finais. A primeira debate a caracterização da pobreza no Brasil; a segunda caracteriza a pobreza rural, subdividida em o que o indicadores nos mostram e caracterização Segundo Marx, e a terceira apresenta a pobreza rural na microrregião de Cruzeiro do Sul – Acre.

II. CARACTERIZAÇÃO DA POBREZA

A pobreza é um tema recorrente na literatura nacional e internacional, cujo debate se concentra enfaticamente sobre o seu caráter multidimensional. Os esforços empreendidos pelos estudiosos tem se concentrado, nos últimos anos, na superação do critério puramente econômico e de insuficiência de renda monetária que prevaleceu ao longo de décadas (Bourguignon; Chakravarty, 2003; Chakravarty; Majumder, 2005; Barros; Carvalho; Franco, 2006; Silva; Bruno; Silva, 2020).

Isso, de certo modo, implicou em mudanças qualitativas em relação à abordagem e mensuração da pobreza pela literatura especializada (ou pelo por parte dela). Atualmente, parece haver um certo consenso no meio científico sobre a necessidade de recorrer a um conjunto de dimensões econômicas, sociais e ambientais para explicar a pobreza, muito embora existam divergências a respeito das variáveis e indicadores apropriados para tal.

A complexidade da pobreza fica patente ao se analisar a evolução do pensamento científico a respeito da temática, sendo possível identificar pelo menos cinco concepções desenvolvidas ao longo do século XX. A primeira, refere-se à acepção de pobreza relacionada à *subsistência*, especificamente quando a renda dos indivíduos não seria suficiente para manter o rendimento físico no trabalho, o que pressupunha um redirecionamento dos recursos àqueles com produtividade baixa ou fraca. Em decorrência de suas limitações, a segunda concepção de pobreza está ligada às *necessidades básicas,* incialmente referente a indicadores de renda *per capita* e Produto Interno Bruto (PIB) e, posteriormente, aos serviços essenciais (saúde, educação, saneamento básico, etc.) providos por e para uma comunidade (Codes, 2008).

Codes (2008) ainda aponta na terceira concepção de pobreza à *privação relativa*, em que os pobres seriam todos os indivíduos que não podem obter recursos e condições de vida suficientes para desempenhar os papeis demandados pela sociedade em que estão inseridos, incluindo, aqui, aspectos sociais e individuais.

Amartya Sen (2000) se insere na discussão conceitual de pobreza a partir da noção de *privação de capacidades,* caracterizando-a como a impossibilidade apresentada pelos indivíduos na obtenção de liberdades substantivas (alimentação, serviços de saúde, emprego, educação, água tratada, saneamento básico, direitos civis e políticos básicos, etc.), compreendidas como o necessário para que tenham uma vida com qualidade.

Essas reformulações serviram para a ampliação da perspectiva sobre pobreza, a qual passou a ser entendida como um fenômeno mais amplo, complexo e *multidimensional*, sendo fundamental os estudos de Amartya Sen ao ampliar o horizonte para além do critério econômico predominante até então. Assim, outras dimensões para além da renda devem ser incorporadas em qualquer tentativa de mensuração da pobreza de determinada sociedade, o que torna o esforço dos pesquisadores mais dispendioso, porém necessário.

No Brasil, estudos e políticas são orientados por indicadores ou padrões de organizações multilaterais como o Banco Mundial (BM), a Organização das Nações Unidas para Alimentação e Agricultura (FAO), mas também são adotados alternativamente cálculos administrativos do Benefício da Prestação Continuada (BPC); do Cadastro Único; do Programa Bolsa Família, por exemplo.

2.1 O QUE OS INDICADORES MOSTRAM?

Um dos dados recorrentemente utilizados no Brasil para mensurar a pobreza é apresentado no Decreto nº 9.396, de 30 de maio de 2018, que foi publicado alterando os Decretos nº 5.209/2004 e nº 7.492/2011 e fixando novos valores referenciais de caracterização das situações de pobreza e de extrema pobreza e os de benefícios do Programa Bolsa Família.

De acordo com o decreto, as pessoas em situação de pobreza são caracterizadas pela relação de renda familiar *per capita* de até R$ 178,00 e as pessoas em extrema pobreza, de até R$ 89,00. Ainda que os dados sejam utilizados para orientar os cálculos da política do Bolsa Família e que estejam também configurados em variabilidade dada pela quantidade de crianças e adolescentes de até 15 anos e número máximo de benefícios para os de 16 e 17 anos, vemos claramente que isso não é suficiente para garantir um padrão mínimo de vida de uma família.

Quando analisamos a dimensão padrão de vida e distribuição de renda na exploração de dados da pobreza, chegamos ao Índice de Gini da distribuição do rendimento mensal real efetivo de todas as fontes das pessoas de 15 anos ou mais de idade. De acordo com os dados da Pesquisa Nacional por Amostra de Domicílios Contínua 2017, consolidado de primeiras entrevistas, o Brasil tem o índice de 0, 524, com CV (%) de 0,8; na região Norte, é 0, 519 e CV (%)2,1 e, no Acre, é 0, 525 e CV (%) 2,4, tudo isso considerando os rendimentos deflacionados para reais médios do próprio ano (IBGE, 2017).

O Índice de Gini da distribuição do rendimento real efetivo domiciliar *per capita*, avaliando os rendimentos deflacionados para reais médios do próprio ano, consoante à Pesquisa Nacional por Amostra de Domicílios Contínua, de 2017, também com o consolidado de primeiras entrevistas, indica que o Brasil tem o índice de 0, 549; na região Norte, é 0, 544 e, no Acre, é 0, 566. Assim, tem-se a caracterização dos rendimentos medindo a desigualdade da sua distribuição e seu valor varia de zero, que corresponde à igualdade, até um, que é a desigualdade máxima (IBGE, 2018).

Outra apreciação concernente à dimensão padrão de vida que é apresentada pelo IBGE – PNAD (2018) e que chama a atenção por dizer respeito a uma das dimensões que confirmam o estado de pobreza da população é a proporção de pessoas residindo em domicílio sem acesso aos serviços de saneamento básico (Tabela 1):

Tabela 1: Proporção de pessoas residindo em domicílios sem acesso aos serviços de saneamento básico (2017)

País, Região e Unidade da Federação	Proporção de pessoas residentes em domicílios com acesso aos serviços de saneamento									
	Total (1000 pessoas)		Deficiências							
			Ausência de coleta direta ou indireta de lixo		Ausência de abastecimento de água por rede geral		Ausência de esgotamento Sanitário por rede coletora ou pluvial		Ao menos uma deficiência	
	Absoluto	CV (%)	Proporção	CV (%)	Proporção	CV (%)	Proporção	CV (%)	Proporção	CV (%)
Brasil	207 088	-	10,0	1,5	15,1	1,4	35,9	0,8	37,6	0,8
Norte	17 655	-	20,9	3,5	41,2	2,8	80,3	0,9	82,3	0,9
Acre	817	-	23,9	6,1	48,1	4,2	68,4	2,5	77,7	1,9

Fonte: IBGE, Pesquisa Nacional por Amostra de Domicílios Contínua (2018).

Os dados confirmam a precariedade das condições de moradia da população, e mais que isso, apresenta o déficit de acesso aos serviços de saneamento básico. Variados são os agravantes de tal problema. Os principais que podem ser mencionados são: a transmissão de doenças e a poluição do meio ambiente.

Com efeito, a falta de condições domiciliares adequadas pode implicar no surgimento de diversas doenças infectoparasitárias. A Fundação de Nacional da Saúde (FUNASA, 2010, p. 65) destaca uma série de doenças relacionadas ao saneamento ambiental inadequado: "diarreia, febres entéricas, hepatite A, dengue, febre amarela, leishmanioses, filariose linfática, malária, doença de chagas, esquistossomose, leptospirose, doenças dos olhos, tracoma, conjuntivites, doenças da pele, micoses superficiais, helmintíases, teníases".

O hiato da pobreza (*poverty gap*) é calculado pela distância entre a renda das pessoas e família e a linha de pobreza. É um índice que capta a intensidade da pobreza para o conjunto da população, produzindo dado aproximado do montante necessário para erradicar a pobreza.

O IBGE, em 2017, estimou em R$ 10,2 bilhões mensais o montante de recursos que necessitariam ser alocados para que as pessoas com rendimentos inferiores à linha de pobreza, proposta pelo BM (rendimentos de até US$ 5,5 por dia, ou R$ 406 por mês), atingissem o indicador. A distância média do rendimento dos pobres em relação à linha aumentou, entre 2016 e 2017, de R$ 183 para R$ 187 reais. Quando nos referimos à linha de extrema pobreza do BM (R$ 140 por mês ou US$ 1,90 por dia), o montante a ser alcançado seria de 1,2 bilhão por mês (IBGE, 2018).

Na Tabela 2, apresentamos as medidas do hiato de pobreza em 2017. Lembramos que a pobreza é um fenômeno dinâmico, o que significa que o hiato dispõe apenas de estimativas do valor de sua erradicação no ano do cálculo.

Tabela 2: Medidas do hiato da pobreza - *poverty gap* (2017)

País, Região e Unidade da Federação	Pessoas residentes em domicílios particulares		Hiato da pobreza - BM	
	Total (1000 pessoas)	Com rendimento real efetivo domiciliar *per*	Massa de rendimento para que todos alcancem a	Hiato médio (2)

			capita até US$ 1,9 PPC 2011 (1)		linha de pobreza (R$ milhões)			
	Absoluto	CV (%)	Percentual	CV (%)	Rendimento	CV (%)	Percentual	CV (%)
Brasil	207 004	0,0	7,4	1,5	1 171	1,7	4,0	1,7
Norte	17 647	0,0	11,8	3,6	140	4,1	5,6	4,1
Acre	816	0,0	17,4	6,5	10	6,9	8,3	6,9

Fonte: IBGE. Pesquisa Nacional por Amostra de Domicílios Contínua (2018), consolidado de primeiras entrevistas.

Notas: Inclusive as pessoas cuja condição no domicílio era pensionista, empregado doméstico ou parente do empregado doméstico. Rendimentos deflacionados para reais médios de 2017 (IBGE).

Na tabela, a taxa de conversão de paridade de poder de compra para consumo privado é de R$ 1,66 para US$ 1,00 PPC, considerando valores diários tornados mensais e deflacionados pelo IPCA para anos recentes. Tal fato é ainda mais destacado por representar a quantia da renda necessária que deve ser transferida aos pobres para fazer com que as pessoas alcancem os valores das linhas estabelecidas. Na análise dos dados, outra questão que também deve ser considerada na tabela é que o cálculo é feito com a soma das distâncias das rendas dos pobres na linha de pobreza, medidas em proporção ao valor da linha e o resultado é divido pelo total da população.

A proporção de pessoas pobres no Brasil, em 2017, pela linha proposta pelo BM, era de 26,5% da população, um total de 54,8 milhões de pessoas na pobreza. Enquanto o número de pessoas em extrema pobreza era de 15,2 milhões, ou seja, 7,4% população (IBGE, 2019).

Na dimensão educação, destaca-se a taxa de analfabetismo da população de 15 anos ou mais de idade como um dos reflexos da pobreza (Tabela 3):

Tabela 3: Taxa de analfabetismo da população de 15 anos ou mais de idade, com indicação do coeficiente de variação, segundo Grandes Regiões e características selecionadas (2017)

Grandes Regiões e características selecionadas	Taxa de analfabetismo da população de 15 anos ou mais de idade	
	Taxa	CV (%)
Brasil	**7,0**	**0,9**
Norte	8,0	2,6
Situação do domicílio		
Urbana	5,2	1,2
Rural	17,7	1,2
Sexo		
Homem	7,1	1,1
Mulher	6,8	1,1
Cor ou raça (1)		
Branca	4,0	1,7
Preta ou parda	9,3	1,0
Grupos de idade		
15 a 19 anos	0,6	6,7
20 a 24 anos	1,1	6,1
25 a 34 anos	1,9	2,9
35 a 44 anos	4,6	2,1

45 a 54 anos	7,7	1,8
55 a 64 anos	11,4	1,6
65 anos ou mais	22,3	1,2
Quintos de rendimento mensal domiciliar *per capita* nacional		
Até 20%	11,1	1,5
Mais de 20% até 40%	9,1	1,5
Mais de 40% até 60%	8,3	1,7
Mais de 60% até 80%	6,6	1,9
Mais de 80%	1,3	4,0

Fonte: IBGE. Pesquisa Nacional por Amostra de Domicílios Contínua (2018), segundo trimestre.
Nota: (1) Não são apresentados resultados para amarelos, indígenas e pessoas sem declaração de cor ou raça.

A taxa de analfabetismo (pessoas que ainda não sabem ler e escrever) da população com 15 anos ou mais de idade no Brasil, em números absolutos, é de 11,5 milhões. Duas incidências nos chamam a atenção. A primeira é a taxa da característica rural, que é 17,7, e a segunda é a relação de quintos de rendimento mensal domiciliar *per capita* nacional de até 20%, que tem uma taxa de analfabetismo de 11,1%, ambas proporcionalmente muitíssimo elevadas (IBGE, 2018).

Os dados ou estatísticas produzidas nas abordagens da pobreza aponta que não existe um modo único de dimensionar os pobres e numerar seus indicadores sociais. Existe uma variabilidade que está ligada aos conceitos, perspectivas e métodos utilizados para a mensuração de pobreza. Nessa confluência, o que importa em definitivo não são as representações do problema, e sim efetivamente a condição de vida das pessoas.

Consolidando esta discussão, é significativo que independente dos métodos, à identificação conjetural da pobreza no Brasil, quando olhamos a representação da evolução (Gráfico1), temos a noção do quão preocupante se constitui o quadro de pobreza,

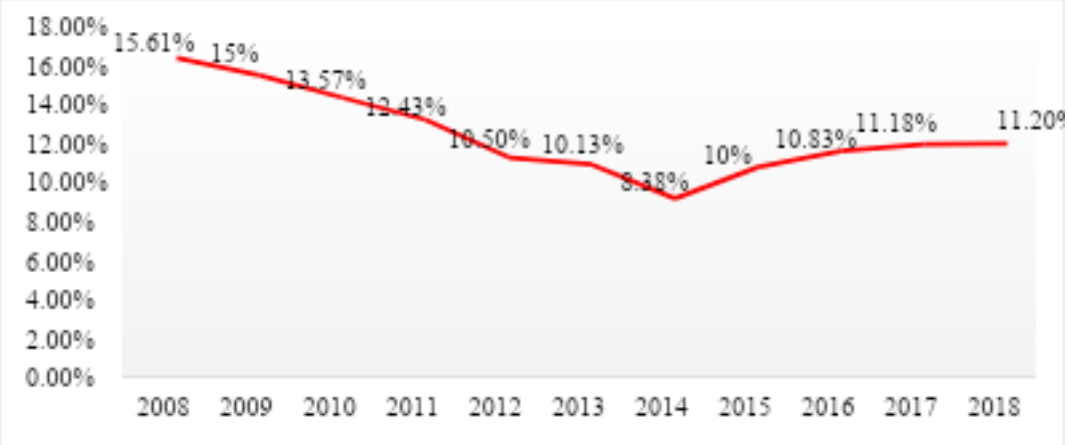

Fonte: FGV Social/CPS a partir de Microdados da PNAD/IBGE (2019).

Gráfico 1: Evolução da Pobreza %

Os dados da pobreza devem ser dialeticamente analisados para compreendermos a realidade socioeconômica e histórica que faz com que 26,5%, em dados reais, 54,8 milhões de pessoas, (IBGE, 2018) da população brasileira, vivam abaixo da linha da pobreza (critérios do BM).

Deveria fazer uma comparação com o Acre, porque o estado da arte do seu trabalho caracteriza uma região que não está sendo evidenciada até o presente momento.

2.2 Caracterização Segundo Marx

Encontra-se na expectativa de um endossamento crítico, o exame da pobreza a partir da teoria da necessidade. Um olhar marxista para a realidade que, para ser compreendida, precisa apoiar-se em elementos outros que não se limitem a uma relação meramente fenomênica. Ressaltando o imperativo de Marx na construção dialética, evoca-se a base material para as reflexões e fundamenta-se uma crítica que tem orientado múltiplas percepções da natureza humana e da economia política e nos conduzido para uma condição de mediação e compreensão das necessidades, dadas pelo desenvolvimento histórico. Estas são construções dispostas em diferentes produções de Marx, identificadas como categoria primordial para a sociabilidade humana e suscitantes do ideal de emancipação.

Marx, nos *Manuscritos econômico-filosófico,* produz uma crítica à economia política ao identificar a visão da burguesia do proletário, que é rebaixado à condição de mero fazedor de vontade de seus dominadores. Não tendo capital, não tendo renda, seu trabalho não se finda na augura do seu fazer diário, mas assume uma condição que se manifesta nas suas necessidades, no seu subjugamento aos meios de produção e de vida, na venda da sua força de trabalho como sua única mercadoria. O trabalho abstrato é a atuação alienada imposta ao trabalhador na subserviência ao patrão, que é convertida na exploração do trabalho assalariado (Marx, 2008).

Portanto, suas necessidades são utilizadas como mecanismos de controle da força produtiva e são acentuadas em processo de asseveramento da exploração, que no curso histórico vem tomando proporções cada vez mais perversas, sendo múltiplos os métodos utilizados para a manutenção ou continuidade de tais condições.

A pobreza, nesse figurativo, é também convertida como um imperativo de controle e, quando são estabelecidas linhas de mensuração, classificação, teórica, justificativas ou métodos, parece haver uma desvinculação da problemática com as bases da economia política imperante. Como se a pobreza, a miséria, a fome não fossem reflexo da exclusão daqueles que não são aptos à relação trabalho e mercadoria. O capital, ao tempo em que nos conduz para um processo de esvaziamento da nossa condição humana e utiliza-se da nossa qualidade natural para o trabalho, vale-se das necessidades para sustentar as modernas condições trabalhistas.

A sustentação da engenharia teórica do capital firma-se pelo processo que é produzido intrínseco e avesso à pessoa humana. Os trabalhadores pobres são movidos por suas necessidades, que também são configuradas e reconfiguradas pelos interesses do capitalismo. Esta sustentação mencionada baseia-se na motriz produtiva da necessidade que se processa no trabalho estranhado.

A atividade estranhada que encurrala os pobres é produzida dinamicamente e perpetuada numa espécie de anestesia coletiva que faz com que o trabalhador não perceba que o produto de seu trabalho é separado da sua condição individual e é transformado em objeto que sai de seu controle, torna-se alheio, lhe é estranho. O trabalhador, ao finalizar um produto ou participar de sua produção, não consegue vislumbrar sua efetiva colaboração naquilo, porque foi convencido de que o trabalho é uma atividade externa a ele. Nesse sentido, é possível dizer que a pobreza é uma forma de manifestação da deformação e unilateralização dos indivíduos, que é produzida pelo trabalho estranhado.

Nisso, privilegiamos, na próxima parte, a discussão sobre pobreza rural, apontando-a com suas relações, características e com seus dados conjunturais.

III. POBREZA RURAL

A definição de rural é tão complexa quanto a de pobreza, como debatida anteriormente. No Brasil, a definição oficial de rural é um problema, seja pela sua controvérsia repartição de tributos (zona urbana – imposto total do município; zona rural- imposto dividido com a União), seja em razão de que é o governo municipal que define, (Soares et al, 2016).

Para fundamentar a análise o meio rural pode ser definido como

1. Domicílios agrícolas: definidos como qualquer domicílio no qual pelo menos um membro está empregado no setor agrícola e 67 por cento ou mais da renda domiciliar advém de atividades agrícolas.
2. Domicílios pluriativos: definidos como aqueles em que pelo menos um membro está empregado no setor agrícola, mas menos de 67 por cento da renda domiciliar vem da agricultura.
3. Domicílios rurais não agrícolas: definidos como aqueles que vivem em áreas oficialmente rurais, mas sem qualquer membro do domicílio trabalhando na agricultura.
4. Domicílios urbanos não agrícolas: definidos como aqueles que vivem em áreas oficialmente urbanas, com nenhum membro domiciliar empregado na agricultura (Soares *et al*, 2016, p. 3).

São dimensões que ajudam na definição de rural, mas que estão sujeitas às dinâmicas dos espaços e das construções sociais.

A pobreza, no contexto rural, caminha no curso da história, paralela ao ideário de desenvolvimento produtivo agrícola, um processo marcado pelo corolário de que o campo naturalmente é o lugar de atraso, numa relação que torna mais amena e menos relevante as condições multidimensionais atenuantes da pobreza no meio rural.

A pobreza rural não pode ser conjeturada da mesma forma que nas áreas urbanas, embora seja o mesmo problema, elas são realidades diferentes numa variabilidade de aspectos.

As características específicas da pobreza no meio rural são resultado do agravamento e precariedade da atuação do poder público. Abordando com maior exatidão, os desafios no campo diz respeito à falta de estradas para o escoamento da produção, falta de crédito rural, secas que levam à fome, falta de água adequada ao consumo humano, precariedade dos serviços de saúde (Sawaya et al, 2003).

Assim, pode-se somar aos problemas apresentados, outros agravantes, como a desnutrição, baixa escolaridade, gravidez na adolescência, violência, isolamento social, uso de drogas ilícitas, condições de moradia e saneamento básico inadequado (Sawaya et al, 2003), que são descritos como problemas urbanos e são situações que permeiam os espaços rurais.

No entanto, o processo produtivo para autoconsumo não se constitui como modo de organização característica do capitalismo, pois não visam ao lucro com a produção e é considerada uma atividade antieconômica. Numa caracterização da pobreza no meio rural, especialmente da ruralidade acreana, a produção para o próprio consumo se faz presente na agricultura familiar e deve também ser considerada, o que não é comum por não ser do interesse do capital, pois representa uma possibilidade de independência do mercado no que se refere à alimentação (Cavalcante Filho et al, 2018).

O estado do Acre está, localizado na região norte brasileira, na Amazônia, tem área territorial de 164.173,525km², população residente de 830.018 pessoas, densidade demográfica de 5,06hab/km², Índice de Desenvolvimento humano de 0,71 (IBGE, 2023).

Na comparação paralelamente apresentada, expõem-se dados da pobreza no meio rural no Brasil, retratando o índice em recortes geográficos e demográficos (Gráfico 2 A/B).

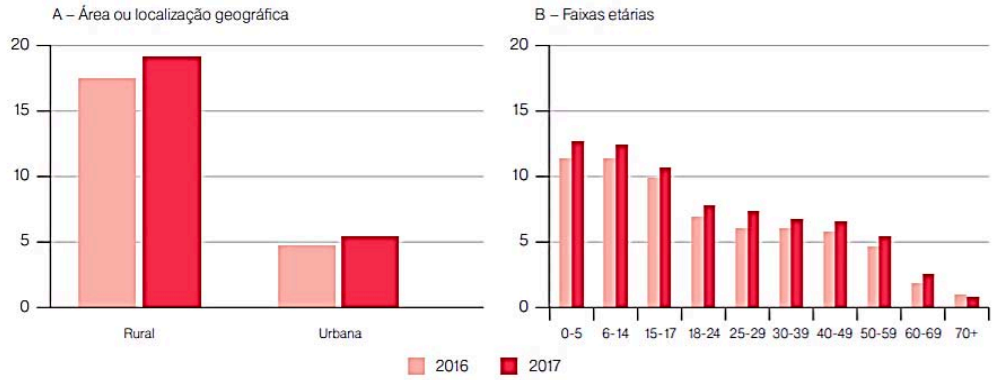

Fonte: Plataforma ODS (IBGE, 2019).

Gráfico 2 – A/B: Incidência da pobreza para a linha de US$ 1,90 *per capita* por dia para desagregações selecionadas – Brasil (2016-2017) (Em %)

No gráfico A, em relação a áreas ou localização geográfica, fica explícita a robustez da pobreza nas áreas rurais e também demonstra que a pobreza cresceu de um ano para o outro, já estando acima de 19%, ainda que também tenha ocorrido um crescimento também nas áreas urbanas. O número total de pobres extremos no Brasil que moram em áreas rurais é de 5,6 milhões e corresponde a 37% do total de pobres no país e constituem-se em significativa proporção em razão de que ao todo menos de 15% da população brasileira vive no campo (IPEA, 2019).

No gráfico B, no intervalo de idade, a pobreza extrema apresenta-se com perfil etário muito expressivo. As crianças se apresentam como o grupo mais afetado, no entanto, ainda que ocorra um gradativo decrescimento, os jovens superam taxas de 10%. Independentemente da faixa etária, observa-se um crescimento representativo entre os anos de 2016 e 2017 (IPEA, 2019).

O Gráfico 3 reúne os dados que definem a porcentagem da população vivendo com menos de $5.50 por dia aos preços internacionais de 2011, feita de acordo com a paridade do poder de compra (PPP) de 2011 e segundo o Programa de Comparação Internacional (ICP) do Banco Mundial.

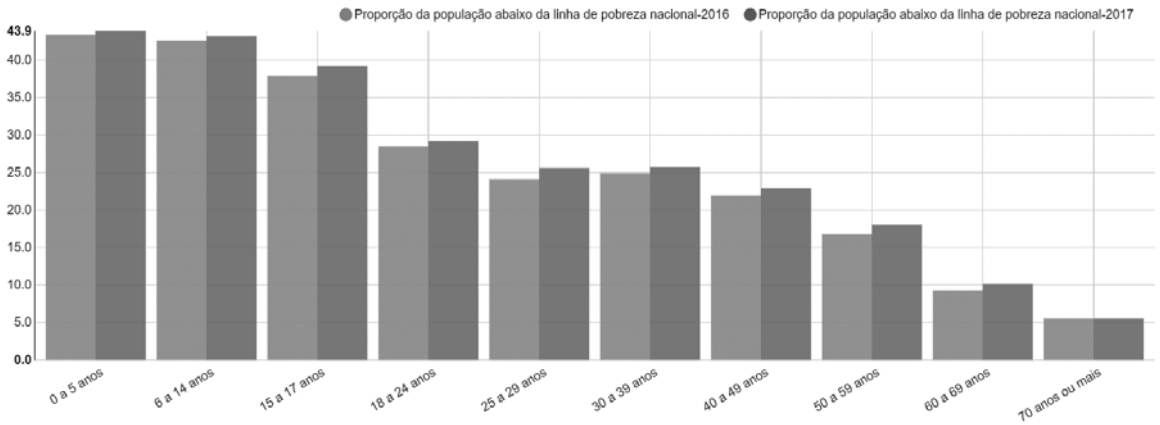

Fonte: IBGE, Pesquisa Nacional por Amostra de Domicílios Contínua (PNAD Contínua).

Nota: Fórmula de Cálculo: H = (Q/N). 100, onde N é o total da população e Q é o total de pessoas vivendo abaixo da linha de pobreza Z. Z é dada por $5.50 de 2011 convertidos pela PPP de 1.66 e corrigidos pela inflação ao consumidor, seguindo a metodologia utilizada na PNAD Contínua.

Gráfico 3: Proporção da população vivendo abaixo da linha de pobreza nacional, por idade, condição perante o trabalho – Brasil

A proporção da população abaixo da linha de pobreza nacional em percentual, considerando o sexo: Homens, em 2016 (25,6) e 2017 (26,5); Mulheres, em 2016 (25,8) e 2017 (26,4). Em relação à situação de domicílio: Rural, em 2016 (50) e 2017 (50,3); Urbana, em 2016 (21,6) e 2017 (22,5). Em se tratando da proporção da população ocupada abaixo da linha de pobreza nacional, também em percentual, quanto à variável sexo: Homens, em 2016 (17) e 2017 (17,3); Mulheres, em 2016 (13,3) e 2017 (13,8). No quesito situação de domicílio: Rural, em 2016 (39,7) e 2017 (39,1); Urbana, em 2016 (11,9) e 2017 (12,6) (IBGE, 2019).

Numa especificação ampliada, o perfil das famílias rurais de baixa renda é apresentado a partir das seguintes constatações: "prevalência da agricultura familiar (74%), concentração na região Nordeste (65%), forte presença de crianças e jovens até 17 anos (41%) e maioria da população constituída por negros (78% somando pretos e pardos)" (Mello, 2018).

O Acre, de acordo com a distribuição de pessoas por UF e Grandes Regiões, segundo o tipo de público (2015), possui os seguintes números do meio rural de baixa renda: Agricultura Familiar - 61.348; Reforma Agrária - 68.502, e Inclusão Produtiva Rural - 5.612, num total de 135.462 pessoas de acordo com a Base Geral Rural de 2011-2015 (Mello, 2018).

A pauperização rural carece de ser compreendida, não como um fenômeno isolado, mas que se configura pela ação do capital e se dá por processos de desenvolvimento geográficos desiguais. Esse aspecto será aprofundado no próximo segmento, quando se discute a sua manifestação na microrregião de Cruzeiro do Sul, Acre.

IV. POBREZA RURAL NA MICRORREGIÃO DE CRUZEIRO DO SUL - ACRE

O espaço rural no Acre é marcado por extensões territoriais compostas por terras indígenas, unidades de conservação, projetos de assentamento, polos agroflorestais em propriedades privadas. Além desses, existem porções territoriais cortadas por ramais ou estradas vicinais, rodovias federais (BR 364, BR 307 e BR 317), rodovias estaduais diversas e por uma extensa rede de rios e cursos d'água. Esses espaços são ocupados por agricultores familiares, grupos tradicionais (ribeirinhos, seringueiros, indígenas, pescadores, extrativistas), famílias de assentados, enfim, por trabalhadores do campo e pecuaristas, por exemplo.

Este espaço rural é uma dimensão de uma realidade singular que se caracteriza pelas especificidades sociais e ambientais como parte da região amazônica. Em sua diversidade, se edifica de modo que:

> Das diversas formas que os espaços rurais assumem no território do país, talvez as menos conhecidas estejam na Amazônia. Aqui, a associação direta e necessária entre área rural e produção agrícola se rompe: existe o foco na conservação da biodiversidade (o caso das Áreas de Preservação Ambiental) ou de culturas – por exemplo, áreas indígenas e quilombolas. Mesmo a produção agrícola assume características próprias, respeitadoras do tempo e dos caminhos das águas (Loschi, 2017, p. 9).

Um espaço ocupado por uma população extremamente diversificada, mas, em sua maioria, são pequenos produtores que residem em lugares isolados, desenvolvem uma agricultura para consumo próprio e só vendem o excedente no comércio local. Os barcos estão entre os principais meios de transporte e são usados para garantir o acesso à escola e aos produtos da cidade (Loschi, 2017).

O governo do Brasil, em 2003, propôs o Programa Nacional de Desenvolvimento Sustentável de Territórios Rurais (PRONAT), criando os Territórios Rurais e da Cidadania. No Acre, foi organizado o desenvolvimento da política em três territórios: Alto Acre e Capixaba – AC, Baixo Acre e Vale do Juruá - AC.

A microrregião de Cruzeiro do Sul é composta pelos mesmos municípios que integram o Território do Vale do Juruá: Cruzeiro do Sul, Mâncio Lima, Marechal Thaumaturgo, Porto Walter e Rodrigues Alves. Sua área total é de 31.948,77 km², com população total de 153.948 habitantes (IBGE, 2022). É formado por áreas naturais protegidas (Unidades de Conservação e Terras Indígenas), que ocupam 64% da área, e 38 projetos de assentamento e polos agroflorestais, de diversas categorias. A população rural é de 55.822 pessoas, isto é, 42.45% (2010). O número de família assentada é de 6.505, dispõe ainda de 5.922 estabelecimentos de agricultura familiar, 21.420 pessoas são ocupadas com agricultura familiar e 4.221 pescadores (2010) (Brasil, 2011).

Na microrregião existem quatro unidades de conservação (Parque Nacional da Serra do Divisor, Reserva Extrativista do Riozinho da Liberdade, Reserva Extrativista do Alto Juruá e ARIE Japiim Pentecostes) e 9 terras indígenas (Katukina do Campinas, Jaminawa do Igarapé Preto, Nukini, Poyanawa, Kampa do Rio Amonea, Kaxinawa-Ashaninka do Rio Breu, Jaminawa-Arara do Rio Bajé, Arara do Rio Amônia e Arara do Igarapé Humaitá). As áreas protegidas são divididas em unidades de conservação e proteção integral e unidades de conservação de uso sustentável (Brasil, 2011).

Na análise sobre renda e pobreza na microrregião de Cruzeiro do Sul, alguns indicadores devem ser considerados. O Produto Interno Bruto (PIB) é um desses.

No Brasil, em 2018, o PIB foi de R$ 6,8 trilhões. O IBGE, em 2016, indica que o PIB do Acre foi de 13.751.126 milhões a preços correntes. Dentre os municípios que compõem a região, Cruzeiro do Sul é o que tem o maior PIB *per capita*, no valor de R$ 13.263,80; seguido de Mâncio Lima, com PIB de R$ 10.796,46; Marechal Thaumaturgo, com R$ 10.084,48; Rodrigues Alves, com R$ 10.084,48, e Porto Walter, com R$ 9.853,18. Importante destacar que Marechal Thaumaturgo e Porto Walter são municípios isolados geograficamente, só tendo acesso por via fluvial e por meio aéreo de pequeno porte.

Em síntese, os dados são resultados do baixo crescimento urbano e industrial, assim como por um histórico cenário resultante da economia primária-exportadora promovida pelos migrantes nordestinos dentro floresta Amazônica, de modo que estes mercados fragmentados regionalmente e a exploração dos trabalhadores não repercutiu num padrão econômico de desenvolvimento local.

Sem uma verdadeira inserção e valorização dos trabalhadores da floresta nas benesses produtivas, isolaram-se os trabalhadores e reafirmou na atualidade condições de pauperização. Com o declínio produtivo da borracha, novos setores econômicos foram se instalando no Acre, entre eles, a agropecuária e a indústria; os trabalhadores da floresta passam a se integrar a estes setores, ainda que este processo não tenha se dado de forma tão intensa.

A microrregião de Cruzeiro do Sul, nos setores de agropecuária, indústria e serviços, tinha valor adicionado bruto, no ano de 2016, muito semelhantes entre Mâncio Lima, Thaumaturgo e Rodrigues Alves. Percebe-se, no geral, que o setor da administração, defesa, educação e saúde públicas e seguridade social, em 2016, era o principal responsável pelo dinamismo da economia local. No período recente, o setor de serviços é o principal setor, seguido da administração pública. Nos demais municípios da microrregião de Cruzeiro do Sul permanece a administração pública como a principal atividade (Tabela 4).

Tabela 4: Setores da Economia da microrregião de Cruzeiro do Sul em valores adicionado bruto a preço corrente (2016)

Unidade da Federação	Setores da economia			
	Agropecuária	Indústria	Serviços, exclusive administração, defesa, educação e saúde públicas e seguridade social	Administração, defesa, educação e saúde públicas e seguridade social
Cruzeiro do Sul	73.289,43	72.949,87	470.363,17	495.630,73
Mâncio Lima	43.325,51	5.962,75	34.712,58	110.598,30
Marechal Thaumaturgo	41.691,36	4.257,36	16.115,10	111.532,28
Rodrigues Alves	48.582,05	4.736,26	18.411,76	109.619,09
Porto Walter	21.355,82	2.469,59	11.464,31	70.278,62
Total	228.244,17	90.375,83	551.066,92	897.659,02

Fonte: IBGE, 2019 (organização dos autores).

No cômputo total, o setor de serviços, exclusive a administração, defesa, educação e saúde públicas e seguridade social, consiste na segunda maior participação no valor adicionado bruto na microrregião de Cruzeiro do Sul. Todavia, quando se analisa os municípios individualmente, à exceção de Cruzeiro do Sul, todos os demais têm a agropecuária como a segunda atividade principal.

A constituição do setor privado no Acre choca-se com as correntes neoliberais do estado mínimo, o serviço público instituiu-se como extremamente necessário, no entanto, no Acre, a questão social foi condicionada historicamente a mero caso de política. O que repercutiu e repercute nos indicadores de desenvolvimento.

A análise do Índice de Desenvolvimento Humano Municipal (IDHM) também é importante indicador para compreensão das manifestações das relações de renda e pobreza na microrregião de Cruzeiro do Sul. Especificamente na observação das mudanças das condições sociais que podem ser percepcionadas pelas três dimensões do IDHM, ou seja, nas configurações do IDHM Renda; IDHM Educação e IDHM Longevidade (Tabela 5).

Tabela 5: Índice de Desenvolvimento Humano Municipal (IDHM – 2010)

Município	População rural	População total	População de 15 a 17 anos	População de 18 anos ou mais	Subíndice de escolaridade – IDHM Educação	Subíndice de frequência escolar - IDHM Educação	IDHM	IDHM Educação	IDHM Longevidade	IDHM Renda
Cruzeiro do Sul	23181	78507	5403	44782	0,479	0,642	0,664	0,582	0,776	0,648
Mâncio Lima	6456	15206	1062	8251	0,447	0,604	0,625	0,546	0,77	0,58

Marechal Thaumaturgo	10258	14227	1178	6343	0,246	0,438	0,501	0,361	0,726	0,479
Porto Walter	5853	9176	629	4070	0,298	0,459	0,532	0,397	0,726	0,521
Rodrigues Alves	10074	14389	1070	7109	0,339	0,565	0,567	0,477	0,736	0,518

Fonte: IPEA/IBGE (2019).

No geral, existem, mesmo dentro da regional, disparidades em relação às dimensões de desenvolvimento dos municípios. Em 2010, o maior IDHM Educação na região era Cruzeiro do Sul, seguido por Mâncio Lima e Rodrigues Alves. Esses municípios também são, entre os cinco, os maiores IDHM Longevidade. De modo diferente, no IDHM Renda, Porto Walter ultrapassa Rodrigues Alves.

A FIRJAN, no interesse do monitoramento das nuances da economia, desenvolveu um índice de desenvolvimento municipal, uma metodologia em que o "índice varia de 0 (mínimo) a 1 ponto (máximo) para classificar o nível de cada localidade em quatro categorias: baixo (de 0 a 0,4), regular (0,4 a 0,6), moderado (de 0,6 a 0,8) e alto (0,8 a 1) desenvolvimento. Ou seja, quanto mais próximo de 1, maior o desenvolvimento da localidade" (FIRJAN, 2019).

Na Tabela 6, fazemos o recorte do índice para a microrregião de Cruzeiro do Sul, considerando o ano base de 2016, último ano com disponibilidade dos dados.

Tabela 6: Índice FIRJAN de Desenvolvimento Municipal (2016)

Índice FIRJAN de Desenvolvimento Municipal		AC		IFDM	Emprego & Renda	Educação	Saúde
		IFDM BRASIL		0,6678	0,4664	0,7689	0,7655
		Mediana dos Municípios		0,5395	0,3624	0,6515	0,5865
		Máximo dos Municípios		0,7390	0,6486	0,7770	0,7915
Ano Base 2016		Mínimo dos Municípios		0,3570	0,2377	0,4347	0,3316
Ranking IFDM Geral		UF	Município	IFDM	Emprego & Renda	Educação	Saúde
Nacional	Estadual						
3430º	2º	AC	Cruzeiro do Sul	0,6427	0,4332	0,7363	0,7586
5096º	13º	AC	Mâncio Lima	0,5140	0,2377	0,6790	0,6252
5251º	14º	AC	Porto Walter	0,4889	0,3913	0,5082	0,5671
5291º	17º	AC	Rodrigues Alves	0,4797	0,2790	0,6562	0,5040
5373º	19º	AC	Marechal Thaumaturgo	0,4564	0,2655	0,5395	0,5642

Fonte: FIRJAM, 2019.

O ranking estabelecido pelo FIRJAN mantém algumas diferenças mínimas nos indicadores, mas mesmas posições do IDHM do IPEA, embora a metodologia de mensuração seja diferente. Dos municípios da microrregião sob análise, Cruzeiro do Sul lidera os dados, seguido por Mâncio Lima. As

diferenças se dão especificamente na conjuntura analítica de Porto Walter e Rodrigues Alves, já que as indicações individuais dos municípios em suas posições coincidem.

Analisando o desenvolvimento da microrregião de Cruzeiro do Sul por meio da metodologia das médias convergentes[1] verifica-se que, à exceção do IFDM emprego e renda, todos os demais componentes do índice evidenciaram crescimento no período de 2010 a 2016, refletindo melhora desses indicadores nesse intervalo temporal. Nota-se que foi exatamente o IFDM Emprego e Renda o único a apresentar média de convergência negativa e crescimento acentuado do coeficiente de variação (Tabela 7). Portanto, os municípios que integram essa microrregião apresentaram convergência em relação às variáveis saúde e educação, enquanto se mostraram divergentes no tocante ao emprego e renda, o que corrobora os dados apresentados na Tabela 6.

Tabela 7: Médias Convergentes do Índice FIRJAN de Desenvolvimento Municipal da microrregião de Cruzeiro do Sul - Acre (2010-2016)

VARIÁVEL	2010	2016
IFDM Geral		
Média	0,5	0,5
Desvio Padrão	0,1	0,1
Coeficiente de Variação	10,9	12,7
Média Convergente (MC)	-2,8	
IFDM Saúde		
Média	0,4	0,6
Desvio Padrão	0,1	0,1
Coeficiente de Variação	17,6	14,3
Média Convergente (MC)	3,1	
IFDM Emprego e Renda		
Média	0,5	0,3
Desvio Padrão	0,1	0,1
Coeficiente de Variação	13,5	23,8
Média Convergente (MC)	-12,8	
IFDM Educação		
Média	0,5	0,6
Desvio Padrão	0,1	0,1
Coeficiente de Variação	18,4	13,8
Média Convergente (MC)	4,2	

Fonte: FIRJAM, 2023.

Outro importante indicador das condições sociais é a distribuição de renda e a taxa de pobreza. Na avaliação da desigualdade da renda domiciliar *per capita* entre os indivíduos, temos o Índice de Gini, que mede a concentração ou desigualdade, em que o valor vai de 0 a 1. Quanto menor a desigualdade, mais próxima de zero, quanto maior a desigualdade, mais aproximada de um. Utilizando ainda dados do último censo (2010), vemos que os municípios apresentam um Índice de Gini muitíssimo próximo,

[1] Para uma descrição dessa metodologia, ver: Williamson e Fleming (1977); Souza e Lima (2023).

variando de 0,59 a 0,64, portanto, dentre os municípios, o que apresenta menor desigualdade é Marechal Thaumaturgo, e a maior é de Cruzeiro do Sul, apesar de este ser o que em todos os outros indicadores anteriores mencionados o que melhor se apresenta.

Comparando os dados do Índice de Gini já apresentados com o levantamento de Sistemas Básicos de Produção Familiar Rural do Estado do Acre (ASPF), acompanhamos a evolução dos indicadores de desigualdade de renda na mesorregião do Vale do Juruá, a qual abrange a microrregião de Cruzeiro do Sul (Tabela 8).

Tabela 8: Evolução dos indicadores de desigualdade de renda do Vale do Juruá (2006/2007)

Descrição	Vale do Juruá	Evolução (%) **
Índice de Gini	0,49	-6,6
% renda 10+	29%	10,37
% renda 50-	32%	-4,29
10% rico/ 50% pobre	0,89	15,32

Fonte: CAVALCANE FILHO et al, 2018; ASPF (2017).
*Nota: ** Relativo ao período 1999/2001.*

No conjunto da região, é possível dizer que os municípios apresentam um alto índice de desigualdade que pode ser relacionado com as condições de desenvolvimento socioeconômico. Estes dados refletem, principalmente, nas condições de vida dos pobres e extremamente pobres.

O gráfico 4, apresenta um consolidado de informações sobre as condições sociais da Microrregião de Cruzeiro do Sul de acordo com dados do IBGE (2010). Chama a atenção nos municípios os números da pobreza, de modo geral destacam-se, o elevadíssimo número dos extremamente pobres de Porto Walter (34,9%) e o pareamento aproximado entre Marechal Thaumaturgo (39,31%) e Rodrigues Alves (40,9%), o pior indicador entre os municípios estudados.

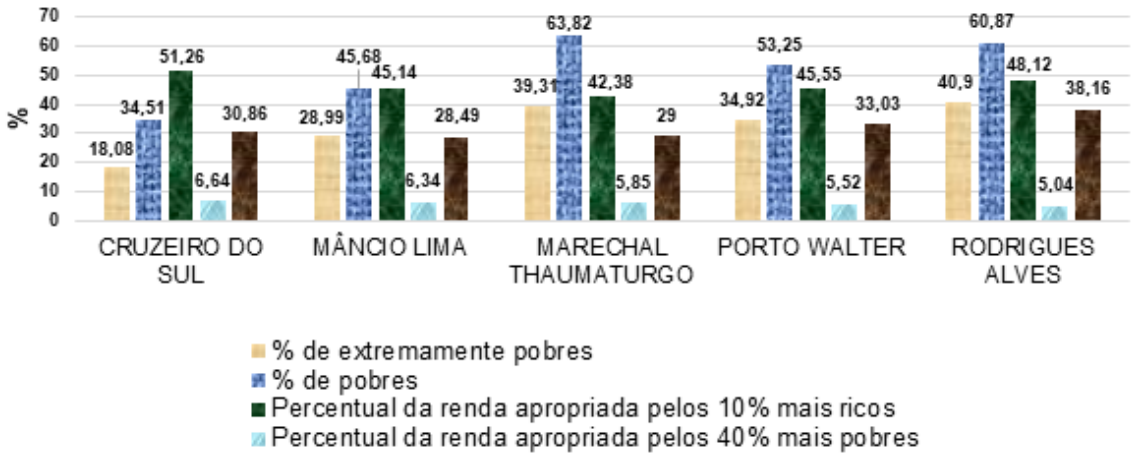

Fonte: Fonte: IPEAGEO, 2019 (Organização dos autores).

Gráfico 4: Dados socioeconômicos da microrregião de Cruzeiro do Sul (2010)

A concentração de riqueza é exorbitante, os 10% mais ricos, dentre os cinco municípios, concentram percentual superior a 42% de riqueza. Sendo que Cruzeiro do Sul é a apropriação maior, 51,25% das riquezas, ao passo que os seus 40% mais pobres concentram apenas 6,64% da renda.

Em 2010, a renda *per capita* dos municípios segmentava-se em: Cruzeiro do Sul (R$ 450,06), Mâncio Lima (R$ 295,50), Marechal Thaumaturgo (R$ 157,27), Porto Walter (R$ 204,19) e Rodrigues Alves (R$ 200,58). A renda *per capita* dos pobres distribui-se em: Cruzeiro do Sul (R$ 62,43), Mâncio Lima (R$ 57,45), Marechal Thaumaturgo (R$ 52,77), Porto Walter (R$ 49,19) e Rodrigues Alves (R$ 52,57). No que corresponde à renda *per capita* dos extremamente pobres, o quadro é: Cruzeiro do Sul (R$ 23,66), Mâncio Lima (R$ 27,22), Marechal Thaumaturgo (R$ 22,31), Porto Walter (R$ 20,63) e Rodrigues Alves (R$ 26,12) (IPEAGEO, 2019).

Tratando dos percentuais relacionados à educação na microrregião de Cruzeiro do Sul, a renda *per capita* dos pobres distribui-se em: Cruzeiro do Sul (R$ 62,43), Mâncio Lima (R$ 57,45), Marechal Thaumaturgo (R$ 52,77), Porto Walter (R$ 49,19) e Rodrigues Alves (R$ 52,57). No que corresponde à renda *per capita* dos extremamente pobres, o quadro é: Cruzeiro do Sul (R$ 23,66), Mâncio Lima (R$ 27,22), Marechal Thaumaturgo (R$ 22,31), Porto Walter (R$ 20,63) e Rodrigues Alves (R$ 26,12) (IPEAGEO, 2019). Quando se considera o percentual de pessoas de 18 anos ou mais sem ensino Fundamental completo e em ocupação informal, as informações são claramente chocantes, pois Cruzeiro do Sul tem 45,81%, Mâncio Lima coloca-se com 52,45%, Marechal Thaumaturgo reúne 72,42%, Porto Walter tem 68,56% e Rodrigues Alves tem 63,44% (IPEAGEO, 2019).

Em 2017, o salário médio mensal nos municípios da microrregião sob análise variava de 1,5 a 1,8 salários mínimos, sendo que os menores são os de Marechal Thaumaturgo e Porto Walter, que se apresentam iguais. A proporção de pessoas ocupadas em relação à população total de toda a região era de 34,1%, na comparação, Cruzeiro do Sul tem a maior proporção, com 11,2%, e Rodrigues Alves tem a menor, com 4,7; Porto Walter e Mâncio Lima são iguais, têm 5,5% e Marechal Thaumaturgo era de 7,2% (IBGE, 2018).

Considerando domicílios com rendimentos mensais de até meio salário mínimo por pessoa, Cruzeiro do Sul tinha 44.2% da população nessas condições; Mâncio Lima tinha 48,7%; Marechal Thaumaturgo ficava com 50,6%; Rodrigues Alves situava-se com 51,9% e; Porto Walter tinha 48,9% das pessoas nessas condições (IBGE, 2018).

Nas dimensões da produção familiar rural, é uma dimensão importante para a região e compõe a sua renda bruta (Tabela 9). Nesta composição da renda bruta das famílias do Vale do Juruá, mesorregião que engloba a microrregião de Cruzeiro do Sul, no período entre 1999/2001 e 2006/2007, temos, na produção da macaxeira, a sua mais importante cultura, especificamente no seu subproduto, que é a farinha de mandioca, sendo responsável por mais de 70% da renda gerada (Cavalcante Filho et al, 2018).

Tabela 9: Evolução de Renda Bruta por Linha de Exploração no Vale do Juruá (2006/2007)

Linhas de Exploração	Geração de Renda Bruta (%)	
	Vale do Juruá	
	2006/2007	Evolução
Criações	29,31	8,85
Criações de Bois	23,52	12,93
Criação de Porcos	-*	-*
Criação de Aves	-*	-*
Outros	5,79	-4,08
Agricultura	74,18	9,74
Café	-*	
Macaxeira	57,68	18,92
Banana	-*	-*

Melancia	-*	-*
Feijão	-*	-*
Arroz	4,82	-8,34
Milho	-*	-*
Outros	11,68	-0,84
Extrativismo	2,19	-12,91
Castanha	-*	-*
Borracha	1,16	-5,71
Madeira	1,03	-5,28
Outros	-*	-*

Fonte: CAVALCANE FILHO et al, 2018; ASPF (2017).

A criação de boi também é uma das potencialidades econômicas na composição da receita dos sistemas de produção do Vale do Juruá, apresentando um percentual e 29.31% da geração de renda (CAVALCANTE FILHO et al, 2018).

No conjunto dos indicadores econômicos das famílias do Vale do Juruá (2006/2007), chega-se à evolução apresentada na Tabela 10.

Tabela 10: Evolução dos indicadores econômicos das famílias rurais do Vale do Juruá (2006/2007)

Indicadores	Unidade	Vale do Juruá	Evolução (%) **
Renda Bruta	R$/mês	452,07	-28,53
Renda Bruta Total	R$/mês	835,64	15,94
Margem Bruta Familiar	R$/mês	368,49	-14,74
Custo Real da Força	R$/mês	663,56	112,97
Custos Variáveis	R$/mês	183,88	11,11
Valor dos Bens de Consumo Comprado no Mercado	R$/mês	2.110,28	544,17
Linha de Dependência do Mercado	R$/mês	1.976,38	180,7
Autoconsumo	R$/mês	240,29	-66,65
Nível de Vida	R$/mês	735,21	-43,62
Índice de Remuneração da Mão de Obra Familiar	R$/mês	29,21	44,62
Índice de Eficiência Econômica	Und.	0,55	-55,28

Fonte: CAVALCANTE FILHO et al, 2018; ASPF (2017).

Notas: Resultados mediados por UFP; Relativo ao período de 1999/2001; Atualização monetária até abril de 2018 (INPC/IBGE).

Na tabela, é possível observar um desequilíbrio evolutivo entre a renda e custo da produção. Esta oscilação dá-se em razão de o crescimento da renda não estar acompanhando as proporções de crescimento dos custos. Estes indicadores de renda em evolução não compatível agravam a situação das condições de vida das famílias rurais, especialmente das famílias mais pobres. A preocupação também recai sobre a piora das condições de vida das famílias do Juruá, uma vez que a produção para o autoconsumo está em decrescimento, o que impacta diretamente em razão do aumento da dependência do mercado. Todos estes dados conjunturais são colaborativos para o aumento da pobreza (Cavalcante Filho et al, 2018).

O enfrentamento deste quadro pode ser atenuado por via de três elementos essenciais, como nos é colocado, não que eles sejam a solução ao nosso olhar. De acordo com Pochmann, Amorin e Aldrin (2007, p. 66), elas seriam:

1. A necessidade de encontrar arranjos sociais e modelos produtivos que permitam rápido crescimento econômico;
2. S construção de um Estado forte, capaz de regular, planejar e mesmo atuar produtivamente fornecendo um norte para os arranjos sociais e modelos produtivos;
3. A construção de um Estado forte, capaz de atuar na redistribuição secundária da renda fornecendo não só amparo aos mais fracos, mas principalmente regulando as relações de trabalho e fornecendo bens públicos universais de qualidade como escolas de alto nível, saúde e segurança.

As perspectivas apresentadas devem ser objeto de luta dos trabalhadores e não serão efetivas se forem modeladas pelo meio político econômico atual, elas devem ser protagonizadas pelos próprios trabalhadores, rompendo-se a lógica de cumplicidade entre capital produtivo com o interesse do capital monetário internacional.

A evolução produtiva da microrregião de Cruzeiro do Sul também pode ser acompanhada através dos dados da agricultura, pecuária e extrativismo reunidos, apresentados na Tabela 11. Como já fora destacado, o cultivo de macaxeira é a maior linha produtiva.

Tabela 11: Produção Agropecuária e extrativista da microrregião de Cruzeiro do Sul (2017)

Linhas de Exploração	Cruzeiro do Sul	Marechal Thaumaturgo	Mâncio Lima	Porto Walter	Rodrigues Alves
Pecuária					
Bovinos	30.072	10.424	12.881	7.151	15.708
Suínos	2.878	1.692	4.719	884	2.717
Aves (Galináceos e outros)	144.654	52.006	63.029	19.553	43.741
Outros	2.875	759	1.020	241	1.767
Agricultura					
Cana-de-açúcar toneladas	1.226,265	393,988	179,750	179,750	271,400
Agricultura					
Feijão	47,7740	81,8040	15,6810	87,3000	8,6250
Macaxeira	39.270,959	13.247,705	11.074,547	10.445,935	16.280,385
Banana	2.565,008	696,191	175,680	276,002	227,185
Melancia	635,075	953,292	240,480	135,310	102,775
Arroz	185,315	131,690	21,130	53,140	206,880
Agroflorestal					
Pupunha Fruto	-	-	-	-	-
Açaí	270	99	210	121	75
Cupuaçu	-	-	-	-	-
Palmito	-	-	-	-	-

Café	-	-	-	-	-
Outros	-	-	-	-	-
Extrativismo					
Castanha	-	-	-	-	-
Borracha	-	-	-	-	-
Madeira	3000	3100	3000	1000	1900
Outros	-	-	-	-	-

Fonte: CENSOAGRO (IBGE, 2018) – Resultados preliminares (2019); IBGE – Produção da extração vegetal e da silvicultura (organização dos autores).
Nota: Agricultura, Agroflorestal e Extrativismo - medidas em toneladas, exceto madeira – metros cúbicos; Pecuária - cabeças.

Na conjuntura maior do estado Acre, tem-se 124.894 pessoas ocupadas em estabelecimentos agropecuários, distribuídas entre 37.342 estabelecimentos. Desse total de pessoas ocupadas, 80% dos produtores são do sexo masculino, 67% têm de 30 a menos de 60 anos de idade; 83% possuem laço de parentesco com o produtor, e 69% são trabalhadores temporários (CENSOAGRO, 2018).

A concentração fundiária, noutra dimensão, também se constitui como fator de elevação da pobreza no Brasil. Daí a importância de voltarmo-nos para a caracterização da estrutura fundiária do Acre.

O Módulo Fiscal (MF) do Vale do Juruá corresponde, de acordo com o Sistema Nacional de Cadastro Rural (SNCR) do Instituto Nacional de Colonização e Reforma Agrária (INCRA), a 100 hectares.

É evidente a concentração de terras no Acre. De acordo com o SNCR (2018), 0,05% dos imóveis estão na faixa de 100.000 e mais hectares, o que corresponde à concentração de 34,78% da área total na estrutura fundiária do Acre. Enquanto 42,7% dos imóveis situam-se na faixa de 50 a menos de 100, tendo apenas 7% da área total do território em hectares. No geral, 1% dos imóveis situa-se na faixa que vai de 5.000 a 100.000 e mais hectares e suas áreas totais conferem mais de 80% do território total.

O espaço rural do Vale do Juruá é caracterizado por elementos sócio-históricos reproduzidos pelas relações dos indivíduos, suas famílias e o ambiente que estão inseridos, dados por processos de ocupação e disputas territoriais de grupos humanos incentivados pelos ciclos de mobilidade; pela resistência e permanência dos povos originários e das relações que ambos estabelecem com a natureza, e pelas transformações socioeconômicas da região.

Seu meio rural é marcado também pelo modo precarizado das relações de trabalho e pelas relações sociais das famílias que experimentam historicamente as desigualdades de renda. Uma representação que não foge da conjuntura imperante do meio rural no Brasil, que enfrenta um processo de injustiça social ao longo dos tempos, que se tem agravado cada vez mais em razão dos quantitativos de trabalhadores sem rendimentos e em extremas condições de pobreza.

Concorre com este cenário uma representação intensificadora do quantitativo de pessoas ocupadas com os efeitos da renda sobre o trabalho em relação à escolaridade. Se por um lado existe uma discussão em torno do aumento da renda em razão da escolaridade mais elevada, o comportamento do mercado é que dita estas relações, haja vista que a mão de obra qualificada compete com o baixo nível de escolaridade. Isso nos faz perceber que a baixa demanda de mão de obra também leva os profissionais com educação elevada a se submeterem a postos que exigem menor qualificação ou ainda a falta de experiência conduz para essa mesma situação. Por outro lado, o sistema produtivo, mesmo que aumente a produtividade no trabalho em razão da maior formação do trabalhador, não repassa os

benefícios desse processo para este. Em outra dimensão, a redução de renda dos trabalhadores com formação maior e o aumento dos rendimentos dos menos qualificados, em certa medida, geram a diminuição da desigualdade de rendimentos (Rocha, 2006).

Ao analisar a relação entre pauperização, segurança alimentar e autoconsumo familiar rural no Acre, se separa com uma realidade extremamente particular, pois existe uma concentração altíssima de rios, muitas áreas de difícil acesso, as estradas não apresentam condições de tráfego adequado durante todo o ano, o que produz implicações diretas sobre os indicadores socioeconômicos da produção agrícola e das condições de vida das pessoas do campo. Um conjunto de condições que interfere também na economia em razão das dificuldades e escoamento da produção nos centros de comercialização, o que faz com que não haja geração de renda e de desenvolvimento no campo (Cavalcante Filho *et al*, 2018).

No Vale do Juruá, de acordo com os Sistemas Básicos de Produção Familiar Rural do Estado do Acre (ASPF), nos anos agrícolas de 2006/2007, 70% da renda gerada nos sistemas produtivos está relacionada diretamente com a produção de macaxeira, mais especificamente da farinha de mandioca. Na análise do nível de vida das famílias rurais, em termos monetários (2006/2007), 1% tem faixa de renda maior que 4 salários mínimos por mês; 11% têm renda entre 2 e 4 salários mínimos por mês, e 61% situam-se na faixa de ½ e 2 salários mínimos por mês. Na linha da pobreza, 17% são pobres, tendo renda de ¼ e ½ de salário mínimo por mês, e10% são considerados extremamente pobres, com nível de vida menor que ¼ de salário mínimo por mês (Cavalcante Filho *et al*, 2018).

Nesse sentido, é preocupante o número de famílias rurais do Vale do Juruá que estão em situação de pobreza e indigência. Chama a atenção ainda mais o crescimento do número de pobres em 223% e de indigentes, em 394% no período de 1999-2001/2006-2007. Este cenário é caracterizado por uma exacerbada redução da produção para autoconsumo e, como consequência, faz com que muitas famílias saiam de suas propriedades em busca de melhores condições de vida, uma perspectiva dificilmente alcançada em razão, dentre outros fatores, pelo baixo nível de escolaridade e pela inexistência de qualificação profissional. (Cavalcante Filho *et al*, 2018).

Avaliando o impacto do nível educacional sobre o desempenho econômico da agricultura familiar acreana, enveredamos por alguns apontamentos sobre a relação educação e pobreza a partir da realidade do Vale do Juruá. Quando se relaciona escolaridade com desempenho econômico nos arranjos produtivos das famílias rurais do Vale do Juruá, identificamos que as pessoas com formação de nível médio ou mais, se comparadas com as que têm somente o Ensino Fundamental incompleto no âmbito do desenvolvimento econômico, possuem um desempenho inferior (Maciel; Bezerra; Cavalcante, 2018) (Gráfico 5).

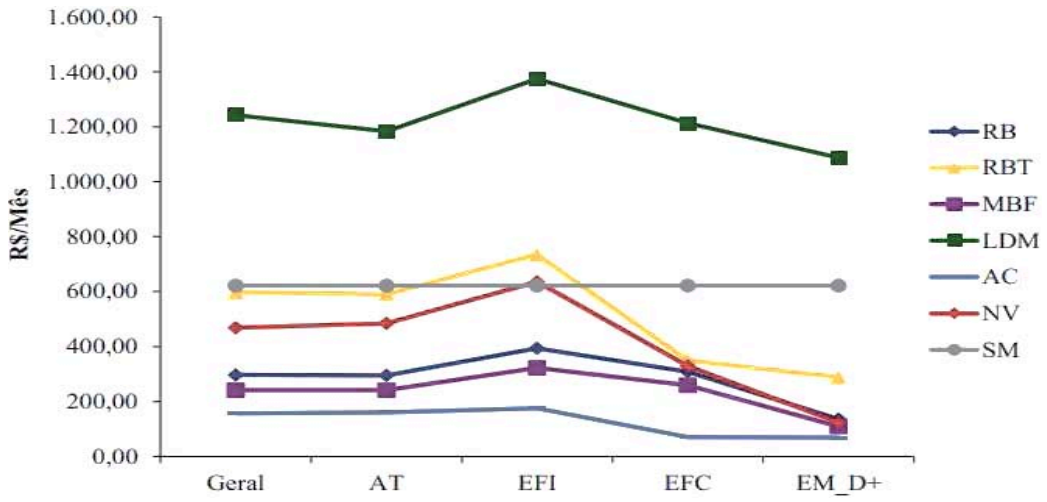

Fonte: Maciel; Bezerra; Cavalcante, 2018; ASPF (2015).

Nota: Valores medianos por UPF, atualizados pelo INPC Março de 2014. AT ± Analfabeto Total; EFI ± Fundamental Incompleto Total; EFC ± Fundamental Completo; EM_D+ - Escolaridade a partir do ensino médio; Renda Bruta (RB); Renda Bruta Total (RBT); Margem Bruta Familiar (MBF); Linha de Dependência do Mercado (LDM); Autoconsumo (AC); Nível de Vida (NV); Salário Mínimo (SM).

Gráfico 5: Desempenho Econômico por nível de escolaridade da produção familiar rural, Vale do Juruá, 2006-2007, Acre ± Brasil

No gráfico, o desempenho econômico no Vale do Juruá das famílias com Ensino Fundamental incompleto possui Renda Bruta Total (RBT), que se aproxima ao valor do salário mínimo do Brasil em 2014, mas, a partir do Ensino Fundamental, ocorre decrescimento considerável no nível de renda pela produção familiar (Maciel; Bezerra; Cavalcante, 2018).

Em outra perspectiva de avaliação da relação educação e pobreza no Vale do Juruá, é constatado que, se considerar que a educação é apenas uma dimensão para a ascensão social, não existe diretamente uma relação propositiva de interpretação da realidade da região, dada sua constituição socioeconômica e as condições laborais dos trabalhadores do campo.

Quando o nível de escolaridade das pessoas da família aumenta, constata-se que é comum que as pessoas passem a atuar fora da unidade de produção. O trabalhador mais qualificado não tem maior remuneração em razão de sua formação pelas suas atividades no espaço de produção local (Maciel; Bezerra; Cavalcante, 2018).

Este quadro é constituído pelas características produtivas da região, já que a oferta de trabalho é incipiente em relação à quantidade de pessoas que querem ser assalariadas, o que acaba por também interferir no nível de renda na unidade de produção, já que as pessoas com melhor formação também enxergam uma incompatibilidade entre a formação mais elevada e o trabalho produtivo no campo (Maciel; Bezerra; Cavalcante, 2018).

A análise dos indicadores econômicos do Vale do Juruá, considerando o índice de remuneração da mão de obra familiar (MBF/Qh/d) e nível educacional, é apresentada no gráfico 6.

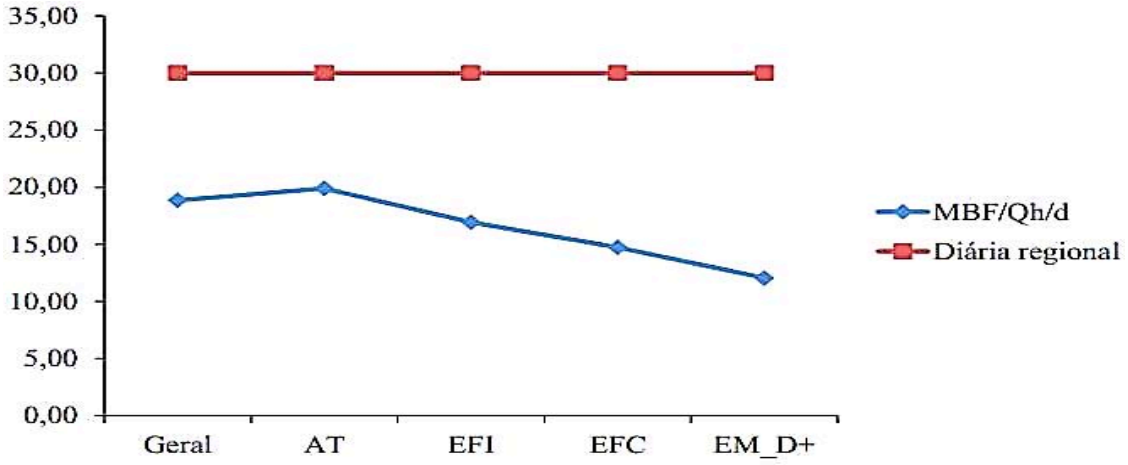

Fonte: (Maciel; Bezerra; Cavalcante, 2018); ASPF (2015).

Notas: Valores medianos por UPF, atualizados pelo INPC Março de 2014. AT – Analfabeto Total; EFI – Fundamental Incompleto Total; EFC – Fundamental Completo; EM_D+ - Escolaridade a partir do ensino médio.

Gráfico 6: Análise da relação MBF/Qh/d e o nível educacional do Vale do Juruá

Diferente de outro contexto em que a renda tende a crescer em razão da elevação no nível de educação para as atividades produtivas no meio rural, os dados apresentados pelo ASPF (2006/2007) do Vale do Juruá indicam que a maior formação não produz diretamente efeitos no processo de produção. Contraditoriamente evidencia-se que quanto maior a formação maior a incidência de declínio no índice de remuneração da mão de obra familiar.

Estas expressões apontam que o caminho de avaliação na relação pobreza e educação não pode ser traçado apenas com o mecanismo de comparação. Para além dessas dimensões, é necessário insistir nos mecanismos mais específicos de promoção da educação. O objetivo é constituir, portanto, um processo mais estreito que venha nominar mais especificamente os interlocutores e os principais sujeitos dos processos educativos. Todavia, uma análise comparativa também é importante, mas não é o único processo a ser cumprido para alcançar efetivamente à realidade que se consolida a relação pobreza e educação e suas manifestações nos espaços do campo.

V. CONSIDERAÇÕES FINAIS

Da conjuntura apresentada, depreende-se que o capital, com seus organismos de composição, produz, nos espaços, construções geográficas favoráveis à sua reprodução e consequente evolução. Este vai se embrenhando, modelando e, ao atuar na formação do mundo, garante que seus processos de acumulação infinita no tempo e no espaço se propaguem numa organização ativa através do Estado.

A natureza dinâmica do capital atua nos espaços rurais e, por conseguinte, é também configurador dos quadros de pobreza à medida que gera desenvolvimento geográfico desigual e suas contradições. O capital, ao se reinventar, vai ampliando suas atividades. O espaço rural, que antes se confirmava com o desenvolvimento agrícola e outras configurações correlatas, hoje se tangenciou para outros interesses, a exemplo, a ideia de desenvolvimento ancorada em perspectivas de defesa do meio ambiente, da cultura dos povos tradicionais, etc.

Uma dinâmica micro e macro ao mesmo tempo, pois a proposta do capital para as economias periféricas é permeada por projetos e programas setoriais específicos dados por realidades que são particulares e alinham-se a uma conjuntura maior, uma realidade econômica desejável de maneira que

as economias regionais formam um conjunto diversificado e pouco coeso de desenvolvimento geográfico desigual, onde as áreas mais afluentes tendem a acumular ainda mais riqueza, ao passo que as regiões menos favorecidas acabam se aprofundando na pobreza (Harvey, 2016).

Só olhando a verdadeira natureza do capital, libertos das camuflagens do desenvolvimento geográfico, como nos leciona Harvey (2016), em qualquer uma de suas dimensões que poderemos entender a pobreza rural dentro de um complexo dinâmico bem maior que é o capital.

Destarte, fica explicitamente compreendida a necessidade da reflexão dialética sobre as condições dos pobres no meio rural com suas especificidades. Enxergando a pobreza em suas múltiplas dimensões e construindo teoricamente conceitos que não se limitem a indicadores estatísticos, mais que isso, que também envolvam aspectos sociológicos, políticos e/ou filosóficos, que são caracteristicamente construídos e vividos na ruralidade das pessoas e de seus espaços. Isso permitirá melhor compreensão a vida da população do campo em seus territórios.

REFERÊNCIAS

1. BARROS, R. Paes.; CARVALHO, Mirela de.; FRANCO, Samuel. Pobreza multidimensional no Brasil. Rio de Janeiro: IPEA, 2006.
2. BRASIL. Plano Territorial de Desenvolvimento Rural Sustentável do Vale do Juruá (AC). Brasília: MDA/SDT, 2011.
3. BOURGUIGNON, Francois; CHAKRAVARTY, Satya R. The Measurement of Multidimensional Poverty. The Journal of Economic Inequality, Netherlands, v. 1, n. 1, p. 25-49, 2003.
4. CAVALCANTE FILHO, Pedro Gilberto et al. Pobreza rural e desigualdade de renda na Amazônia: um estudo da produção familiar rural do Estado do Acre. Revista de Estudos Sociais, [S.l.], v. 20, n. 40, p. 161-178, jul. 2018. ISSN 2358-7024. Disponível em: http://periodicoscientificos.ufmt.br/ojs/index.php/res/article/view/6482. Acesso em: 25 jul. 2019.
5. CHAKRAVARTY, Satya. R.; MAJUMDER, Amita. Measuring human poverty: a generalized index and an application using basic dimensions of life and some anthropometric indicators. Journal of Human Development, Londres, v. 6, n. 3, p. 275-99, 2005.
6. CODES, Ana L. M. A trajetória do pensamento científico sobre pobreza: em direção a uma visão complexa. Brasília: IPEA, 2008.
7. FIRJAN. Índice FIRJAN de Desenvolvimento Municipal (IFDM) 2016. Rio de Janeiro: FIRJAN, 2019.
8. BRASIL. Fundação Nacional de Saúde. Impactos na saúde e no sistema único de saúde decorrentes de agravos relacionados a um saneamento ambiental inadequado. Brasília: Fundação Nacional de Saúde, 2010.
9. HARVEY, David. 17 contradições e o fim do capitalismo. Tradução de Rogério Bettoni. São Paulo: Boitempo, 2016.
10. IBGE. Instituto Brasileiro de Geografia e Estatística. Censo Agropecuário 2017. Rio de Janeiro, 2018. Disponível em: https://sidra.ibge.gov.br/pesquisa/censo-agropecuario/censo- agropecuario-2017. Acesso em: out. 2018.
11. IBGE. Síntese de Indicadores Sociais: indicadores apontam o aumento da pobreza entre 2016 e 2017. 05 maio 2018. Disponível em: https://agenciadenoticias.ibge.gov.br/agenciasaladeimprensa/2013agenciadenoticias/releases/23298sintesedeindicadoressociaisindicadoresapontamaumentodapobreza-entre-2016-e-2017. Acesso em: 19 jul. 2019.
12. IBGE. Síntese de Indicadores Sociais: uma análise das condições de vida da população brasileira: 2019. Rio de Janeiro: IBGE, 2019. Disponível em: liv101678.pdf (ibge.gov.br). Acesso em: 2 dez. 2020.

13. BRASIL. Censo Demográfico de 2022. Disponível em: https://sidra.ibge.gov.br/pesquisa/censo-demografico/demografico-2022/primeiros-resultados-populacao-e-domicilios. Acesso em: 20 ago. 2023.
14. IPEA. ODS1 - Acabar com a pobreza em todas as suas formas, em todos os lugares: o que mostra o retrato do Brasil? Brasília: IPEA, 2019. Disponível em: http://www.ipea.gov.br/portal/images/stories/PDFs/livros/livros/190524_cadernos_ODS_objetivo_1.pdf. Acesso em: 22 jul. 2019.
15. IPEAGEO. Bases. 2019. Disponível em: http://www.ipea.gov.br/ipeageo/bases.html. Acesso em: 02 ago. 2019.
16. LOSCHI, Marília. Rural Amazônico. Retratos a revista do IBGE, Rio de Janeiro, n. 4, p. 8-11, out, 2017. Disponível em: https://agenciadenoticias.ibge.gov.br/media/commediaibge/arquivos/4bce2919090cf0f2e94f46fa59a4f485.pdf. Acesso em: 3 ago. 2019.
17. MACIEL, Raimundo Cláudio Gomes; BEZERRA, Francisco; CAVALCANTE, Pedro. Agricultura Familiar, sustentabilidade e educação na Amazônia: considerações a partir do Estado do Acre. Saarbrucken, Deutschland: Novas edições acadêmicas, 2018.
18. MARX, Karl. Manuscrito econômico-filosóficos. Tradução de Jesus Ranieri. São Paulo: Boitempo, 2008.
19. MARX, Karl. O capital: crítica da economia política. Livro I: o processo de produção do capital. Tradução de Rubens Enderle. 2. ed. São Paulo: Boitempo, 2017.
20. MELLO, Janine. Estratégias de superação da pobreza no Brasil e impactos no meio rural. Rio de Janeiro: IPEA, 2018.
21. NICÁCIO, Marcondes de Lima. Educação do campo e pauperização: implicação da agenda global sobre as políticas de educação básica no Vale do Juruá-Acre. 2021. 374 p. Tese (Doutorado em Educação) – Universidade Federal do Amazonas, Manaus, 2021.
22. ROCHA, Sonia. Pobreza e indigência no Brasil: algumas evidências empíricas com base na PNAD 2004. Nova econ, Belo Horizonte, v. 16, n. 2, p. 265-299, Ago. 2006. Disponível em: http://www.scielo.br/scielo.php?script=sci_arttext&pid=S0103-63512006000200003&lng=en&nrm=iso. Acesso em: 15 jul. 2019.
23. SAWAYA, Ana Lydia et al. Os dois Brasis: quem são, onde estão e como vivem os pobres brasileiros. Estud. av., São Paulo, v. 17, n. 48, p. 21-44, ago.2003. Disponível em:http://www.scielo.br/scielo.php?script=sci_arttext&pid=S0103401420030002000003&lng=en&nrm=iso. Acesso em: 10 jul.2019.
24. SEN, Amartya. Desenvolvimento como Liberdade. São Paulo: Companhia das Letras, 2000.
25. SILVA, J. Jaime.; BRUNO, M. A. Pinho.; SILVA, D. B. Nascimento. Pobreza multidimensional no Brasil: uma análise do período 2004-2015. Revista de Economia Política, São Paulo, v. 40, n. 1, p.138-160, jan./mar., 2020.
26. SOARES, Sergei; SOUZA, Laetícia de; SILVA, Wesley; SILVEIRA, Fernando Gaiger; CAMPOS, Áquila. Perfil da pobreza: norte e nordeste rurais. Brasília: IPC-IG, 2016.
27. SOUZA; Kennedy J. de C., LIMA, Jandir F. de. Amazônia legal: uma análise da convergência do crescimento e do desenvolvimento econômico. Geosul, Florianópolis, v. 38, n. 88, p. 398-422, 2023.
28. BOURGUIGNON, F.; CHAKRAVARTY, s. R.The Measurement of Multidimensional Poverty. The Journal of Economic Inequality, Netherlands v. 1, n. 1, p. 25-49, abr. 2003.
29. CHAKRAVARTY, S. R.; MAJUMDER, A. Measuring human poverty: a generalized index and an application using basic dimensions of life and some anthropometric indicators. Journal of Human Development, Londres v. 6, n. 3, p. 275-99, nov.2005.
30. WILLIAMSON, J. B.; FLEMING, J. Convergence theory and the social welfare sector. International Journal of Comparative Sociology, Romênia, v. 18, n. 3-4, p. 242-253, jan. 1977.